

(NASA-TM-85052) GREAT MICROWAVE BURSTS AND
HARD X-RAYS FROM SOLAR FLARES (NASA) . 112 p
HC A06/MF A01 CSCL 03B

N83-34876

Unclas

G3/92 36600



Technical Memorandum 85052

GREAT MICROWAVE BURSTS AND HARD X RAYS FROM SOLAR FLARES

Herbert J. Wiehl, David A. Batchelor,
Carol Jo Crannell, Brian R. Dennis and
Phillip N. Price

JUNE 1983



National Aeronautics and
Space Administration

Goddard Space Flight Center
Greenbelt, Maryland 20771

Great Microwave Bursts and Hard X Rays from Solar Flares

Herbert J. Wiehl^{*}, David A. Batchelor[†], Carol Jo Crannell, Brian R. Dennis
and Phillip N. Price

NASA Goddard Space Flight Center
Laboratory for Astronomy and Solar Physics

*Swiss National Science Foundation Fellow from the University of Berne.

†Also Energy/Environmental Research Group, Incorporated, Tucson, Arizona, and
Department of Physics & Astronomy, University of North Carolina, Chapel Hill.

ABSTRACT

The microwave and hard X-ray characteristics of 13 solar flares that produced microwave fluxes greater than 500 Solar Flux Units have been analyzed. These Great Microwave Bursts were observed in the frequency range from 3 to 35 GHz at Berne, and simultaneous hard X-ray observations were made in the energy range from 30 to 500 keV with the Hard X-Ray Burst Spectrometer on the Solar Maximum Mission spacecraft. The principal aim of this analysis is to determine whether or not the same distribution of energetic electrons can explain both emissions. The temporal behaviors of the microwaves as a function of frequency and the X rays as a function of energy were tested for correlations, with results suggesting that high-frequency (> 5 GHz) microwaves usually come from the same electrons that produce the X-rays, while low-frequency microwaves do not. Other properties of the two emissions were found to be correlated, such as the microwave peak frequency and the X-ray spectral index. A single-temperature and a multi-temperature model from the literature were tested for consistency with the coincident X-ray and microwave spectra at microwave burst maximum. A source area derived on the basis of the single-temperature model agrees to within the uncertainties with the observed area of the one burst for which spatially resolved X-ray images are available. Four events are inconsistent with both of the models tested, and neither of the models attempts to explain the high-frequency part of the microwave spectrum. We propose a model in which the emissions above and below the peak frequency originate in two different parts of a diverging magnetic loop. With this model we explain the entire microwave spectrum of all but 1 of the events.

Subject headings: Plasmas - Sun: Bursts - Sun: Microwaves - Sun: X-Rays

1. INTRODUCTION

The association of impulsive microwave and hard X-ray bursts from solar flares has been known since the first observation of an impulsive hard X-ray burst (Peterson and Winkler 1959). Close time correlation of these emissions was established (Kundu 1961) and later improvements in the time resolution of the observations revealed common time structures on a scale as short as 1 s (Frost 1969; Kane and Anderson 1970; McKenzie 1972; Kane 1972; Crannell et al. 1978; Wiehl and Matzler 1980). The microwave emission is believed to be gyro-synchrotron radiation from energetic electrons gyrating along the magnetic field lines that thread solar plasmas; the hard X rays are electron-ion collisional bremsstrahlung produced by electrons of comparable energy. The close time correlation and similar electron energy ranges suggest that both emissions come from the same population of electrons. Because the X-ray yield and microwave emissivity are sensitive to physical conditions in the flare plasma, comparison of associated hard X-ray and microwave emissions, event-by-event, provides a critical test of competing flare models (cf. Takakura and Kai 1966; Holt and Ramaty 1969; Takakura 1972; Matzler et al. 1978; Kane et al. 1980; Kundu and Vlahos 1982).

Two crucial issues remain to be settled concerning the physics of these emissions. The first is whether both are produced by the same distribution of electrons. The second is whether thermal or nonthermal electrons produce the emissions.

Regarding the first question, only analysis of coincident hard X-ray and microwave images can give a conclusive answer. Only one flare with 2 dimensional mapping in both microwaves and hard X rays has been described in the literature (Hoyng et al. 1983). They concluded that a single power-law dist-

tribution of electrons could have produced both emissions, with the X rays originating near the footpoints and the microwaves coming from the top of a single loop. Statistical uncertainties in the data were large, however, and more complex models could not be excluded. While some other flare X-ray images place the sources at the footpoints of loops (Hoyng et al. 1981a, b; Duijveman, Hoyng and Machado 1982), there are observations of impulsive X-ray sources at the tops of flare loops or filling one leg (Ohki et al. 1982; Tsuneta et al. 1982; Takakura et al. 1982; Kawabata et al. 1982). In some cases, 1-dimensional interferometric microwave observations were also made, suggesting that the microwaves and X-rays usually come from the same location (Takakura et al. 1982; Kawabata et al. 1982). Because the question of source locations remains unsettled, and particularly because time resolution and spectral coverage are sacrificed in present imaging observations, it is worthwhile to exploit to the fullest the available data obtained without spatial resolution. Observations with fine time resolution and broad spectral coverage but without spatial resolution have recently been made, and some important inferences about the structure of flares can be drawn from their analysis. Spectral analysis of these observations also allows deductions of the source electron distributions to be made, which may settle the second question.

In this paper we present the results of a study of 13 flares observed with the Berne Radio Observatory and with the Hard X-Ray Burst Spectrometer (HXRBS) on the Solar Maximum Mission spacecraft (SMM). The dynamic spectra of both emissions were compared, on an event-by-event basis, and properties of the spectra at the time of maximum microwave flux were compared from event to event. The results were analyzed in an effort to address the issues stated above. Concerning the first issue, we find new evidence for a close connect-

ion between the source electrons for the hard X rays and the microwaves. Interpretation of the microwave spectra is a complex process, however, because gradients in the magnetic field strength and in the electron distribution within the source both contribute to the observed microwave spectral properties (Schochlin and Magun 1979). This complexity may explain the results of Marsh et al. (1981), who concluded that no single-temperature or single power-law electron spectrum could be the sole source of both the hard X-ray and microwave spectra of a flare observed with HXRBS and the Very Large Array (VLA). Our results also contain evidence for important thermal contributions to impulsive microwave and hard X-ray emissions. A thermal origin is not widely attributed to impulsive microwave bursts. However, the hypothesis that a common, single-temperature electron distribution dominated the hard X-ray and microwave emissions allowed us to deduce an X-ray source area of one of the flares in agreement with the area measured by the Solar hard X-ray Telescope (SXT) aboard the Hinotori spacecraft (Ohki et al. 1982). This is the only flare for which such a comparison could be made.

The selection criteria for the present study were designed to take optimum advantage of the broad spectral coverage at microwave frequencies available for the first time for a large sample of solar flares. The events analyzed in this work were selected because of their large microwave peak fluxes. Their peak fluxes were > 500 SFU, thus qualifying them as Great Microwave Bursts (GMBs) according to the standard criteria of solar radio astronomy (Solar Geophysical Data 1982). Attention was restricted to events which exhibited a relatively simple microwave time structure at low frequency, and to events observed with the HXRBS.

Of the many flare models in the literature, we chose to test the single-

temperature interpretation of Crannell et al. (1978) and a multi-thermal model developed by Dulk and Dennis (1982). Our interest in thermal models is spurred by several recent observations and theoretical developments. First, one of the primary predictions of the popular nonthermal beam model (Brown 1971, 1975) is a strong brightening of the observed hard X rays with energy greater than 300 keV from flares near the solar limb; this limb brightening has been searched for in observations with the Gamma Ray Spectrometer on SMM and found to be absent (Zolcinski et al. 1982). This result is consistent with a source electron distribution which is isotropic, such as in thermal models. Anisotropic emission has also been sought in single flares by comparing observations made from widely separated points in space (Kane 1980; Wiehl and Desai 1983), with negative results to date.

Secondly, the results of theoretical and experimental studies of proposed impulsive-phase flare energy release mechanisms suggest that heating of the flare plasma to temperatures of order 10^8 K occurs, rather than acceleration of large numbers of particles. It is generally agreed that release of energy stored in magnetic fields is the only process capable of supplying the energy released in flares. Known mechanisms of release of the stored energy via magnetic field reconnection are only capable of depositing 10% or less of the energy released into kinetic energy of accelerated particle beams, with the remaining 90% or more appearing as heat (cf. Smith 1980; Spicer and Brown 1981). The thermalization of electrons is much faster than would be expected from Coulomb self-collision time considerations because the heating is due predominantly to plasma turbulence. Therefore, strong thermal contributions to the emissions are to be expected. Thermal models have been developed by Brown (1974); Matzler et al. (1978); Matzler (1978); Smith and Lilliequist

(1979); Brown, Melrose and Spicer (1979); Brown, Craig and Karpen (1980) and others.

It should be noted that the common observation of power-law X-ray spectra is not adequate to establish the nonthermal distribution of flare electrons. Multi-thermal electron populations can give rise to power-law X-ray spectra (Chubb et al. 1966; Brown 1974; Colgate 1978). Exponential spectra which can be fitted by a single-temperature thermal bremsstrahlung function are also common (Crannell et al. 1978; Elcan 1978). Such exponential spectra may originate in a single-temperature plasma, but nonthermal processes are capable of producing them as well (cf. Kaplan et al. 1974). We have tested the X-ray spectra of the events of the present study for acceptable fits to both the thermal and power-law forms, but the significance of the spectral parameters so derived is model-dependent.

The multi-thermal model of Dulk and Dennis (1982) attempts to explain both the power-law X-ray spectrum and the microwave spectrum at frequencies below the peak frequency by means of a plausible distribution of temperatures and magnetic fields. We will show that its predictions are inconsistent with the properties of most of the events in this study. This may be because the particular geometry chosen for the source region is not appropriate. We show how the geometry can be changed to correspond with that of the leg of a flaring loop. Some VLA observations are suggestive of such a source region (e.g. Kundu, Schmahl and Velusamy 1982). The modified geometry can account for all but one of the microwave spectra.

In §2, details of the event selection, microwave and hard X-ray instrumentation and calibration, and hard X-ray spectral deconvolution are set forth. Techniques of temporal and spectral analysis which were applied to

the microwave data are described in §3. The hard X-ray analysis is described in §4. In §5, the derivation of source parameters is presented based on the assumption that both the X-ray and microwave emissions originate in a common thermal source with temperatures of the order of 30 keV. The predictions of the hemispherical thermal model of Dulk and Dennis involving plausible non-uniformities in the temperature and magnetic field within the source are also compared with the observations, possible absorption processes are discussed, and a new nonuniform model employing diverging magnetic fields is developed. In §6, the temporal behaviors as functions of microwave frequency and X-ray photon energy of the respective emissions are parameterized for each event and compared from event to event. Spectral parameters and other derived parameters are also correlated. The correlations found in §6 are interpreted in §7, yielding numerous model-independent and model-dependent results. In §8, overall conclusions of the study are summarized.

2. DATA

2.1 Event Selection

Solar cycle 21, which began in 1976 June, peaked in late 1979 at a smoothed sunspot number of 165. This is well above the mean peak number of 105 for cycles 8 through 20 (Coffey 1982). From the many hundreds of microwave bursts recorded at Berne during the period of peak sunspot number, we selected all events having a flux in excess of 500 SFU ($1 \text{ SFU} = 10^{-22} \text{ W m}^{-2} \text{ Hz}^{-1}$) in at least one of the frequency bands in our operating range of 3.2 to 92.5 GHz. This flux threshold corresponds to the definition of a GMB (SGD 1982). During the interval from 1980 January until 1981 December, the Berne Radio Observatory recorded observations of 61 GMBs in digital form. We found that 26 of these 61 GMBs were also observed with the HXRBS on SMM.

These 26 events were examined to determine whether or not their microwave time histories were dominated by a single rise and fall in emission during each event, and each event was labelled "simple" or "complex", accordingly. In the present work we chose to concentrate on the "simple" flares in the hope that they would be easier to understand. Of the above 26 events, 13 had time histories which were dominated in the frequency range from 3 to 8 GHz by a single peak with possible superposed fluctuations of $< 10\%$ of the peak flux. In some of these events, there was evidence for complexity at high frequencies, but even at those frequencies a single peak dominated the emission at the time of maximum flux. These 13 events were labeled "simple", and time histories of them at representative frequencies are shown in Figures 1 through 13, together with time histories of the hard X-ray flux and effective electron temperature computed from the X-ray spectra (see §4.2).

TABLE 1: GMBs WITH SIMPLE TIME PROFILES

EVENT NUMBER	DATE	TIME OF MAX. EMISSION (UT)	H α FLARE ^(a) POSITION	RADIO ^(b) SPECTRAL TYPE	PARTICLES ^(c) EVENTS		GRS ^(d) EVENTS >0.3 MeV
					e-	p+	
1	1980 Mar 27	13:00	N29E70 ^(e)	NONE	N	N	N
2	1980 Mar 29	09:18	N27E38	IIIGG	N	N	Y
3	1980 Mar 29	09:55	N12W13	IIIGG	N	N	Y
4	1980 Jun 4	06:55	S13E59	NONE	N	P	Y
5	1980 Jun 29	10:42	S27W90	IIIGG	P	P	Y
6	1980 Jul 1	16:27	S12W38	II	N	N	Y
7	1980 Nov 6	06:51	N09E08	NONE	N	P	N
8	1981 Apr 15	06:44	N20W65	IIIG	N	N	Y
9	1981 Apr 18	10:51	NO FLARE OBSERVED	IIIG	N	N	Y
10	1981 Apr 26	11:16	N12W74	IIIG	-	P	N
11	1981 Apr 26	11:54	N16W75	IIIG,IV	-	P	Y
12	1981 Aug 10	06:59	S13W15	IIIG	N	N	Y
13	1981 Dec 7	14:51	S06E90 ^(f)	NONE	N	N	Y

(a) Flare positions: SGD reports; Helen E. Coffey, NOAA, private communication.

(b) Radio spectral type: SGD prompt Reports, NOAA
GG indicates Large group of > 10 bursts, G indicates small group of < 10 bursts.

(c) Particle events: Solar Maximum Year Flare List, Rust *et al.* (1982)
N indicates No, P indicates Possible, Y indicates Yes, and "-" implies no observations available.

(d) SMM/Gamma Ray Spectrometer (GRS) Data, courtesy D.J. Forrest

(e) indicates three events in progress at the same time

(f) SGD Preliminary Report, 1981 December 15

The analysis and interpretation of these 13 "simple" bursts are the subject of the present work. The associated H α , radio, particle and γ -ray observations are summarized in Table 1. The 13 GMBs are, in most cases, associated with Type III radio bursts and with γ rays above 0.3 MeV, but were not associated with large particle events. Of the 13 events studied, 4 events had associated H α flares in the eastern hemisphere of the Sun, making it unlikely that prompt particle events could be observed. Seven events had flare sites in the western hemisphere, making it likely that the Earth was well connected magnetically, and, therefore, probable that any prompt particle events could have been observed. Of those 7 events, 4 flares were definitely not associated with particle events. For the other 3 flares, particle events could not be ruled out entirely, but any that were produced must have been relatively weak. Consequently, we believe that these bursts were produced in confined sources in which most of the particles remain trapped.

On the basis of the microwave time profiles and the adopted selection criteria we regarded events No. 10 and 11 as two separate bursts. The X-ray observations, however, indicate flare emission starting with event No. 10 and continuing through event No. 11, without returning to the background level. On this basis, therefore, event No. 10 might be considered as the impulsive phase and event No. 11 as a second stage of a single event.

2.2 Microwave Instrumentation and Calibration

The facilities and instrumentation of the Berne Radio Observatory are described by Magun et al. (1981). The following is a summary of those facts pertinent to an understanding of the analysis presented in this paper.

The temporal resolution changes from 1 s before a flare to 0.1 s during

the flare. Absolute timing with an accuracy of 100 μ s is derived from a standard frequency reference transmitted from Prangins, Switzerland.

During the observations of the first three simple events, microwave intensities were measured at 8.4, 10.4, 11.8, 19.6 and 35.0 GHz. After the 3rd event, the 10.4 GHz radiometer was replaced by the 5.2 GHz polarimeter. In addition to the intensities measured at these different frequencies, circular polarization was also recorded with all receivers except those at 10.4 GHz and 11.8 GHz. Starting in early 1981, an additional polarimeter at 3.2 GHz was put into operation. In order to supplement our observations at lower microwave frequencies, for events prior to the implementation of our 3.2 and 5.2 GHz polarimeters, we used the time profiles at 2.8 GHz published in the Ottawa monthly reports.

The 92.5-GHz polarimeter was in operation during the entire interval, but did not indicate any flux above quiet-Sun levels for any of the simple events. No spatial information was obtained for the present work since the beam width at all frequencies except 92.5 GHz was greater than the diameter of the solar disk.

The absolute fluxes were determined in the following manner: the microwave flux was recorded as a percentage of the quiet Sun flux at each frequency with three automatic calibrations daily. For the days of burst activity, absolute quiet-Sun fluxes were obtained at 2.8 GHz from Ottawa; at 1.0, 2.0, 3.75 and 9.4 GHz from Toyokawa; at 1.47 and 9.5 GHz from Berlin; and at 17 GHz from Nobeyama. These values were then used to construct a spectrum of the quiet-Sun flux in the range from 1 to 17 GHz for each day of interest. The interpolated quiet Sun values at our frequencies were used to determine the absolute flux levels from the original relative Berne values. The quiet-

Sun flux at 35.0 GHz was assumed to be constant at 2400 SFU.

2.3 Hard X-Ray Instrumentation and Spectral Analysis

The hard X-ray data were obtained with the HXRBS on the SMM spacecraft. This instrument is described in detail by Orwig, Frost, and Dennis (1980). Count rates were recorded for fifteen channels distributed over the instrument's energy range, which has varied slowly and monotonically since launch. In 1980 March the energy range was 26 to 456 keV, and in 1981 December it was 30 to 531 keV. A description of this behavior and a listing of events observed with HXRBS are available in Dennis et al. (1983).

X-ray data used in this study were collected with a time resolution of 0.128 s. We used count rates averaged over 1 s intervals or longer in the spectral analysis of this study in order to reduce uncertainties in the fitting parameters due to photon counting statistics to less than ~ 10%.

Representations of the incident hard X-ray spectra were obtained from the measured count rates by the use of a software model of the HXRBS response function. Physical properties of the detector and characteristics of the pulse-height analyzer were employed to compute the instrument response to various assumed incident spectra. The response of the instrument is complex because of the numerous types of interactions which are possible in the CsI(Na) crystal, the aluminum window, and the dead layer on the crystal. The most probable type of photon interaction is photoelectric over most of the applicable energy range; but K-escape, Compton scattering, and rejection of counts by the anticoincidence shield can change the detector's sensitivity significantly. The energy resolution of the detector causes spreading of counts into a given channel from its neighbors and vice versa. Another complicating factor at high count rates is pulse pile-up, which occurs when

several counts arrive within the shortest time (2 μ s) resolvable with the pulse-height analyzer. The pulse pile-up effects are artifacts of the pulse counting system of the instrument and were modeled using the statistical techniques of Datlowe (1975, 1977). The spectra we present are corrected for all of these effects.

The following two types of incident spectra were assumed: the power-law form

$$I(E) = K_{\gamma} (E/50)^{-\gamma} \quad (1)$$

and the thermal bremsstrahlung function

$$I(E) = K_T E^{-1} T^{-0.5} G_E \exp[-(E-50)/T], \quad (2)$$

where K_{γ} , γ , K_T and T are fitting parameters, E is the photon energy in keV, T is the temperature in keV, and $I(E)$ is the X-ray flux in photons $\text{cm}^{-2} \text{s}^{-1} \text{keV}^{-1}$.

The thermal emission measure, EM, can be calculated from T and K_T as follows:

$$EM = 9.3 \cdot 10^{41} K_T \exp(50/T) \text{ cm}^{-3}. \quad (3)$$

The total effective Gaunt factor, $G_E (= \overline{G Z^2})$, was determined for temperatures less than 5×10^8 K from Groenschild and Mewe (1978) and Mewe (private communication) assuming solar abundances giving the average value of $Z^2 = 1.355$. For temperatures greater than 5×10^8 K, the Gaunt factor was calculated using the expressions given by Matteson (1971). For the power-law and the thermal forms, tables of convolved spectra were constructed for various K , γ and T values using the software model mentioned above. The values were chosen so that interpolation could be used to obtain spectra for intermediate K_{γ} , γ or K_T , T pairs, with $\approx 10\%$ accuracy. To find a least-squares representation of the incident spectrum, the following iterative method was

used: initial values of (K_γ, γ) or (K_T, T) were chosen and the corresponding convolved spectrum was computed from the table. For each of the 15 channels, a conversion factor was found to convert observed counts s^{-1} into incident photons $cm^{-2} s^{-1} keV^{-1}$. Each observed count rate (minus the pre-flare background rate) was divided by this ratio to estimate the true incident flux. Finally, the result was fitted to a power-law or thermal function to obtain new (K_γ, γ) or (K_T, T) pairs such that χ^2 was minimized. These new parameters were then used to generate the convolved spectrum in the next iteration. This procedure was found to converge rapidly, usually in two or three iterations.

It should be noted that we have excluded data in Channel 1 from all spectral fits on the grounds that its calibration is poorly known.

The resulting fitted parameters are believed to be accurate to within 10%. Deconvolved HXRBS flare spectra have been compared with spectra obtained from simultaneous observations with an X-ray detector on ISEE-3 resulting in agreement to better than 20% (Kane, private communication).

3. MICROWAVE OBSERVATIONS

In this section we present values of parameters that characterize the microwave temporal behavior and the microwave spectra at the time of maximum microwave flux. These parameters are used in the correlation analysis of §6.

3.1 Temporal Structures

Three time histories of each event at different microwave frequencies are shown in Figures 1 through 13, together with the corresponding hard X-ray time histories. Three times were computed to characterize each time history: the rise time, fall time and characteristic time. For both microwave and hard X-ray events, the rise and fall times are the times taken for the flux to change from 25% to 100% of the peak flux. In Tables 2 and 3 the microwave rise ($\tau_{\mu r}$) and fall times ($\tau_{\mu f}$) measured in this way are given for all 13 events.

Because of the spikiness of some events, particularly at high frequencies, the above definition of rise and fall times can sometimes give misleading results. To avoid this problem we also computed a characteristic time, $\tau_{\mu c}$, for each event defined by the following expression:

$$\tau_{\mu c} = S_{\max}^{-1} \sum S(t) \Delta t \quad (4)$$

where S_{\max} is the maximum flux, $S(t)$ is the measured flux as a function of time, t , and the sum is taken over all time intervals, Δt , for which there was significant flux above pre-flare levels. This is approximately equivalent to the full width at half maximum of the event. Table 4 gives $\tau_{\mu c}$ for each event at different frequencies.

Examination of Tables 2 through 4, shows that the rise and fall times, as well as the characteristic times, generally decrease with increasing fre-

ORIGINAL PAGE IS
OF POOR QUALITY

TABLE 2: MICROWAVE RISE TIMES, $\tau_{\mu r}$, IN SECONDS

EVENT NUMBER	FREQUENCY (GHz)							
	2.8	3.2	5.2	8.4	10.4	11.8	19.6	35.0
1	459	-	-	136	136	112	-	-
2	-	-	-	8	7	8	5	4
3	-	-	-	10	10	11	9	10
4	-	-	29	36	-	35	35	33
5	-	-	36	29	-	34	24	-
6	43	-	42	29	-	32	29	29
7	-	-	50	18	-	15	13	≈ 14
8	-	25	26	25	-	20	15	-
9	-	93	84	70	-	60	59	58
10	77	62	93	92	-	98	98	-
11	843	512	470	-	-	463	482	584
12	-	16	14	14	-	12	9	≈ 10
13	-	-	-	10	-	13	10	9

TABLE 3: MICROWAVE FALL TIMES, $\tau_{\mu f}$, IN SECONDS

EVENT NUMBER	FREQUENCY (GHz)							
	2.8	3.2	5.2	8.4	10.4	11.8	19.6	35.0
1	951	-	-	843	898	930	-	-
2	-	-	-	13	9	8	6	6
3	-	-	-	31	28	25	19	23
4	-	-	81	56	-	28	23	12
5	-	-	28	23	-	18	22	-
6	121	-	130	122	-	109	80	35
7	-	-	102	30	-	28	31	≈ 33
8	-	81	77	55	-	19	25	-
9	-	128	112	104	-	76	74	83
10	181	176	171	135	-	128	81	-
11	991	997	1021	-	-	1085	1061	908
12	-	158	69	56	-	43	31	≈ 33
13	-	-	-	35	-	37	35	31

TABLE 4: MICROWAVE CHARACTERISTIC TIMES, $\tau_{\mu\text{C}}$, IN SECONDS

EVENT NUMBER	FREQUENCY (GHz)						
	3.2	5.2	8.4	10.4	11.8	19.6	35.0
1	-	-	426	435	524	≈ 300	-
2	-	-	24	20	16	10	-
3	-	-	31	29	27	21	21
4	-	77	66	-	56	48	-
5	-	50	42	-	44	-	-
6	-	102	96	-	94	67	41
7	-	136	74	-	83	40	-
8	85	83	68	-	26	≈ 30	-
9	281	270	195	-	154	175	238
10	217	229	211	-	203	165	-
11	1203	1187	-	-	1203	1177	1323
12	123	83	66	-	51	≈ 59	-
13	-	-	29	-	36	22	12

quency. This is shown graphically in Figure 14. This result is a quantitative statement of something that has long been known only qualitatively (Takakura 1975).

3.2 Spectral Parameters

The microwave spectra taken at the peak of each of the 13 simple events are shown in Figures 15 to 27. They were constructed from the calibrated Berne data and from additional microwave observations given in Solar Geophysical Data Comprehensive Reports (Coffey 1980-1981; Coffey 1981-1982). These spectra are classified as C-type (Guidice and Castelli 1975). Each spectrum has a frequency of maximum emission, f_{peak} , and can be described by two power laws, one above f_{peak} , with a spectral index, α_{H} , the other below f_{peak} with an index, α_{L} . The good spectral coverage of our data from 3 to 35 GHz allows us to measure α_{L} for all 13 events, and f_{peak} and α_{H} for all but two of the events. The transition frequency f_{t} , below which the flux rises again in the decimeter domain, was estimated from other radio data. It was found to be as low as 0.4 GHz in one event. This compares to the lowest value previously reported of 1.0 GHz (Batchelor, Benz and Wiehl 1983). At the high frequency end of the spectrum we can estimate the frequency, f_{h} , at which the flux has decreased to 10% of the flux at f_{peak} . These spectral parameters are graphically defined in Figure 15. The values of the spectral parameters obtained for each event are listed in Table 5.

3.3 Polarization

The Stokes parameters V and I were measured at the following frequencies: 3.2, 5.2, 8.4, 19.6 and 35.0 GHz. (V is the excess of left circular polarized flux over right and I is the sum of left and right.) For each event, at the time of maximum flux, we plot in Figure 28 the circular polarization, ρ_{c} ,

TABLE 5: MICROWAVE SPECTRAL PARAMETERS

EVENT NUMBER	α_L	α_H	f_t (GHz)	f_{peak} (GHz)	f_h (GHz)	$S(f_{\text{peak}})$ SFU
1	1.4	-4.5	1.0	8.4	18	900
2	2.0	-1.7	1.7	11.8	> 50	1100
3	1.4	< -0.6	3.5	19.6	> 50	580
4	1.7/3.1	-0.5	\approx 1.0	11.8	> 50	1200
5	0.9	-1.4	0.8	8.4	45	780
6	0.5/1.1	-	\leq 0.9	\geq 35.0	> 50	\geq 3100
7	2.7	-2.0	\approx 2.0	11.8	40	1400
8	1.7	-3.7	0.8	10.7	33	820
9	2.1	-0.5	1.5	11.8	> 50	690
10	0.4	-1.0	\leq 0.4	2.8	36	510
11	2.1	-0.9	\approx 0.5	5.2	> 50	12000
12	0.8	-1.9	0.6	11.8	50	780
13	1.2	-	\leq 8.4	\geq 35.0	> 50	\geq 770

as a function of frequency, where ρ_c is defined by the relation

$$\rho_c = (V-V_0)/(I-I_0), \quad (5)$$

and V_0 and I_0 are the values of the Stokes parameters prior to the burst. At low frequencies the circular polarization is small, as expected for optically-thick sources. At higher frequencies ρ_c is sometimes higher, 10 to 20%, as expected for optically-thin sources (Dulk and Marsh 1982). In 5 cases the sense of circular polarization is right handed only, in 4 cases it is left handed only, and in 3 cases it changes sense from one frequency to another during the flare.

4. HARD X-RAY OBSERVATIONS

In this section we present values of parameters that characterize the X-ray temporal behavior and the X-ray spectra at the time of maximum microwave flux. Because the relationship between the X-ray and the microwave maxima is of interest in constructing flare models, we also characterize the X-ray spectrum at both the time when it is most intense and at the time when it is hardest. In all cases, the spectrum was hardest near the time of maximum intensity so that each event exhibited a soft-hard-soft spectral evolution.

4.1 Temporal Parameters

Two hard X-ray time profiles (Channels 3 and 7) of each event are shown in Figures 1 through 13, together with three microwave time profiles. The X-ray fluxes used in the time profiles are the estimated photon fluxes obtained from the best-fit power-law spectra. The rise and fall times were measured from these time profiles in the same manner as that used for the microwave parameters, i.e. from a quarter peak to peak value. The hard X-ray rise times, τ_{xr} , for channels 1 through 7 are given in Table 6, and the fall times, τ_{xf} , are given in Table 7. We also computed the hard X-ray characteristic times, τ_{xc} , according to Equation (4), substituting the measured X-ray flux I for S. These are given in Table 8 and are plotted as a function of energy in Figure 29 for each of the 13 events.

4.2 Spectral Parameters

For analytic simplicity, two different functional forms were assumed for the incident X-ray spectra. First the spectrum was assumed to be that expected for thermal bremsstrahlung and second it was assumed to be a single power law (Section 2.3). As noted in §1, the results should not necessarily

ORIGINAL PAGE IS
OF POOR QUALITY

Table 6: HARD X-RAY RISE TIME, τ_{xr} , IN SECONDS

EVENT NUMBER	CHANNEL NUMBER						
	1	2	3	4	5	6	7
1	466	440	405	69	69	103	69
2	7	7	6	5	5	-	4
3	8	8	7	9	10	8	8
4	13	15	13	10	11	9	10
5	15	15	15	11	9	22	35
6	34	37	33	30	30	30	29
7	~ 15	~ 15	~ 15	~ 15	-	-	-
8	23	17	15	15	13	9	~ 11
9	112	112	123	53	53	45	45
10	118	97	46	46	39	39	-
11	247	258	220	220	240	240	240
12	10	11	10	7	5	5	5
13	11	8	8	8	8	8	5

ORIGINAL PAGE IS
OF POOR QUALITY

Table 7: HARD X-RAY FALL TIME, τ_{xf} , IN SECONDS

EVENT NUMBER	CHANNEL NUMBERS						
	1	2	3	4	5	6	7
1	~ 371	~ 328	~ 345	~ 336	~ 310	~ 284	~ 200
2	5	5	5	4	4	-	4
3	10	10	10	8	5	5	5
4	38	34	31	33	32	31	31
5	51	47	39	37	39	24	11
6	136	123	65	63	62	62	20
7	~ 24	~ 24	~ 24	~ 24	-	-	-
8	7	7	7	7	6	6	7
9	>54	>54	33	22	25	27	20
10	>72	>72	72	72	51	51	-
11	>360	>345	>345	>330	>300	>300	>300
12	33	28	20	14	13	29	28
13	18	12	7	6	5	8	4

ORIGINAL PAGE IS
OF POOR QUALITY

TABLE 8: HARD X-RAY CHARACTERISTIC TIME, τ_{xc} , IN SECONDS

EVENT NUMBER	CHANNEL NUMBER								
	1	2	3	4	5	6	7	8	9
1	505	401	304	262	252	270	172	184	151
2	14	14	11	11	10	-	9	8	8
3	13	14	12	12	11	11	11	9	10
4	40	37	28	26	24	22	21	20	20
5	51	45	37	35	34	33	31	29	25
6	99	88	56	47	44	43	41	36	35
7	47	37	26	24	26	24	26	18	-
8	19	18	13	12	11	9	7	11	7
9	92	86	65	56	48	45	42	38	25
10	124	107	85	78	86	70	72	80	53
11	406	397	376	381	368	365	378	362	353
12	33	29	21	18	18	21	19	16	19
13	18	18	12	12	10	12	10	12	-

be taken to imply that the electron distributions are thermal or nonthermal, because multi-thermal electron populations can give rise to power-law X-ray spectra (Chubb et al. 1966; Brown 1974) and nonthermal processes can give rise to exponential X-ray spectra (cf. Kaplan et al. 1974). Fitted temperatures and power-law indices for the two assumed spectral forms are given for each event in Table 9. Plots of the spectra determined at the times of maximum microwave emission for the two assumed functional forms are shown in Figures 30 through 42 for each of the 13 events. Again, it should be noted that the data in channel 1 has been excluded from the fitting routine.

One can decide whether one or both of the two assumed spectral types give acceptable fits to the observations, or whether neither is acceptable, on the basis of the value of χ^2 obtained from the least squares fitting procedure. The relevant parameter is $P(>\chi^2)$, defined as the probability that random fluctuations in the count rates plus uncertainties in the instrument response function would result in a value of χ^2 greater than or equal to the value obtained, if the true incident spectrum is of the assumed functional form and if the estimated uncertainties accurately represent the actual deviations. Taking into account uncertainties of $\pm 10\%$ in the conversion factors from count rate to photon flux, we adopted the criterion for an acceptable fit of $P(>\chi^2) > 0.1$. With this criterion, it can be seen from Table 9 that, at the time of maximum microwave emission, t_{max} , there are 3 events that give acceptable fits to a thermal bremsstrahlung function (Equation (2)) but not to a power-law function (Equation (1)), and there are 4 that give acceptable fits to a power law but not to a thermal function. There are 3 cases in which both functions are acceptable representations of the spectra, and 3 in which neither function is.

TABLE 9: TEMPERATURES AND POWER LAW SPECTRAL INDICES

EVENT NUMBER		1	2	3	4	5	6	7	8	9	10	11	12	13
Time of Maximum X-ray Intensity t_{xmax}	T(keV)	31	44	61	39	44	61	24	40	29	20	54	27	50
	$P(>\chi^2)$	0.08	<u>0.73</u>	<u>0.10</u>	0.00	0.02	0.00	0.00	<u>0.31</u>	0.00	<u>0.12</u>	0.00	<u>0.39</u>	<u>0.49</u>
	γ	4.0	3.5	3.1	3.8	3.5	3.2	4.5	3.7	4.3	4.8	3.6	4.3	3.3
	$P(>\chi^2)$	0.00	0.00	0.00	0.04	0.0	0.04	<u>0.42</u>	0.00	<u>0.33</u>	<u>0.47</u>	0.00	<u>0.17</u>	0.04
Time of Hardest X-Ray Spectrum t_{xh}	T(keV)	46	45	68	48	51	61	26	40	38	21	75	27	64
	$P(>\chi^2)$	0.02	<u>0.19</u>	<u>0.99</u>	0.00	0.01	0.00	0.00	<u>0.31</u>	0.00	0.02	0.00	<u>0.39</u>	0.09
	γ_{min}	3.3	3.5	3.0	3.5	3.4	3.2	4.5	3.7	3.9	4.7	3.1	4.3	2.9
	$P(>\chi^2)$	<u>0.81</u>	0.00	0.00	<u>0.39</u>	<u>0.30</u>	0.04	0.03	0.00	0.00	<u>0.37</u>	<u>0.63</u>	<u>0.17</u>	<u>0.75</u>
Time of Maximum Microwave Intensity $t_{\mu max}$	T_x (keV)	40	45	61	46	44	61	24	40	38	21	74	27	56
	$P(>\chi^2)$	<u>0.14</u>	<u>0.19</u>	<u>0.10</u>	0.00	0.02	0.00	0.00	<u>0.31</u>	0.00	0.02	0.00	<u>0.11</u>	<u>0.78</u>
	γ	3.5	3.5	3.1	3.5	3.5	3.2	4.5	3.9	3.9	4.7	3.1	4.3	3.1
	$P(>\chi^2)$	<u>0.10</u>	0.00	0.00	<u>0.43</u>	0.00	0.04	<u>0.42</u>	0.02	0.00	<u>0.37</u>	<u>0.82</u>	<u>0.17</u>	<u>0.26</u>
$t_{xmax} - t_{\mu max}$ (s)		-19.5	-0.5	0	-6	0.6	0	-5	-1.3	-4	-44	-330	-3	-1.5
Uncertainty (s)		± 15	± 0.5	± 0.5	± 1	± 1	± 1	± 5	± 1	± 2.5	± 6.5	± 10	± 1	± 0.5
$t_{xh} - t_{\mu max}$ (s)		44	0.3	0.7	-1.5	2.6	0	5	-1.3	1	-3.8	-54	-0.5	2.5
Uncertainty (s)		± 15	± 0.5	± 0.5	± 1	± 1	± 1	± 5	± 1	± 2.5	± 6.5	± 10	± 1	± 0.5
$t_{xh} - t_{xmax}$		64	0.8	0.7	4.5	2.0	0	10	0	5	40	276	2.5	4.0
Uncertainty (s)		± 15	± 0.5	± 0.5	± 1	± 1	± 1	± 5	± 1	± 2.5	± 6.5	± 10	± 1	± 0.5

N.B. Underscored values of $P(>\chi^2)$ correspond to acceptable fits.

Table 9 also shows that there is a significant delay in most events between the time of peak X-ray flux, $t_{x\max}$, and the time of peak microwave flux, $t_{\mu\max}$. A time difference is also common between $t_{x\max}$ and t_{xh} , the time of hardest X-ray spectrum. There is a tendency for t_{xh} and $t_{\mu\max}$ to be closer than $t_{x\max}$ and $t_{\mu\max}$, but such is not always the case; the significance of this is discussed in §7.

As is shown in Table 9, during the course of a given event the X-ray spectrum is sometimes better represented by a thermal function, sometimes by a power law, sometimes represented acceptably by both forms, and sometimes by neither. The thermal function tends to fit more spectra at $t_{x\max}$, and the power law to fit more spectra at t_{xh} . For comparison, we note that similar flare observations made with OSO-7 indicated that 28 of 38 events were better characterized by a thermal function at $t_{x\max}$ (Elcan 1978).

In §5.1, we make use of the fit parameters of the X-ray spectrum and the microwave spectrum at $t_{\mu\max}$ in deriving source parameters.

5. DERIVED PARAMETERS

In this section we discuss the parameters that can be derived from the microwave and hard X-ray measurements under the assumption that the source of both types of radiation is plasma in thermal equilibrium. In other words, we assume that the microwaves are gyrosynchrotron radiation and the X rays are bremsstrahlung from a common thermal source. In §5.1 we derive the area of emission at the peak frequency and the corresponding magnetic field for the 6 events in which a single-temperature interpretation of the X-ray spectrum is possible. In §5.2 we discuss a hemispherical model developed by Dulk and Dennis (1982) involving nonuniformities in the temperature and magnetic field to explain the low-frequency part of the microwave spectrum. In §5.3 we discuss possible absorption processes affecting the low-frequency spectrum. In §5.4 we propose a diverging loop model for the microwave source to explain the complete microwave spectrum, both the high- and the low-frequency parts.

For the sake of simplicity, we use the following nomenclature and units in this discussion: T for temperature in units of keV, f for frequency in GHz, n for density in 10^8 cm^{-3} , L or r for length in 10^8 cm , A for area in 10^{18} cm^2 , S for microwave flux in solar flux units ($1 \text{ SFU} = 10^{-22} \text{ W m}^{-2} \text{ Hz}^{-1}$), I for hard X-ray flux in photons $\text{cm}^{-2} \text{ s}^{-1} \text{ keV}^{-1}$, B for magnetic field strength in gauss, ED for energy density in erg cm^{-3} , U for thermal energy in 10^{27} ergs , and EM for emission measure in 10^{45} cm^{-3} .

5.1 Single-Temperature Source Parameters

At $t_{\mu\text{max}}$, the area of the microwave source and the magnetic field strength in the source can be estimated from the microwave and X-ray spectral

data under the assumption that both emissions originate in a common single-temperature region. In order to determine the area, we first consider the microwave spectrum at frequencies $< f_{\text{peak}}$. The microwave source is generally believed to be optically-thick in this range, and the spectrum for a uniform, single-temperature source is given by the relation

$$S = 0.16 f^2 A T \quad (6)$$

(Crannell et al. 1978). Thus, the source area at a given time and frequency can be determined from measurements of S and T . Table 5 shows that the microwave spectrum usually doesn't have this dependence on f (i.e. $\alpha_L \neq 2$). A possible explanation for this is discussed below, but for the present we assume that the flux S_{peak} at f_{peak} is dominated by such a single-temperature source. The assumption that the X rays originate in the same source allows us to substitute the temperature derived from the X-ray spectra at $t_{\mu\text{max}}$ (T_x in Table 9) for T in Equation (6). This substitution is valid only when the thermal function is an acceptable representation of the X-ray spectrum at $t_{\mu\text{max}}$, i.e. for events 1, 2, 3, 8, 12 and 13. The area can then be calculated from the following relation derived from Equation (6):

$$A_{\text{peak}} = 6.26 S_{\text{peak}} T_x^{-1} f_{\text{peak}}^{-2} = 10^{-2} \pi r_{\text{peak}}^2 \quad (7)$$

Dulk and Marsh (1982) have provided simplified expressions characterizing the microwave emission which are applicable to those events under consideration. The magnetic field strength was determined using the following expression for f_{peak} obtained from Dulk and Marsh with the numerical constant adjusted for the units used here:

$$f_{\text{peak}} = 4.9 \cdot 10^{-3} (n L)^{0.1} (\sin \theta)^{0.6} T_x^{0.7} B^{0.9} \quad (8)$$

where θ is the angle between the magnetic field and the line of sight, and L is the characteristic length of the source. Because of the small power of

nL , the peak frequency is not very sensitive to the values of n and L . For typical values of density of $5 \times 10^8 \text{ cm}^{-3}$ and length of $\approx 10^9 \text{ cm}$, we obtain $(nL)^{0.1} \approx 1.5$. We will use this value in what follows, without incurring significant errors. Because the emissivity is proportional to the 6th power of $\sin\theta$, only regions with large θ contribute significantly to the observed radiation. For example, when $\theta \approx 70^\circ$, the magnetic field can be determined from the following relation:

$$B = 244 f_{\text{peak}}^{1.11} T_x^{-0.78} \quad (9)$$

We will assume $\theta \approx 70^\circ$ in what follows.

For those events for which the single-temperature model is applicable, the electron densities can be calculated from the X-ray thermal emission measure and the area of microwave emission, using the following relationship:

$$n^2 = 100 \text{ EM } A_{\text{peak}}^{-3/2} \quad (10)$$

(cf. Crannell et al 1978). These and other parameters of the source can be determined under the assumption of a common thermal source for microwaves and hard X rays, and these are given in Table 10. The other derived parameters are as follows:

- (a) The energy density at τ_{max} calculated from the following expression under the assumption that the ions and the electrons have the same temperature and number density:

$$ED = 0.48 n T \quad (11)$$

- (b) The total thermal energy of the flare plasma at τ_{max} calculated from the following expression under the same assumption:

$$U \approx 2 \cdot 10^{-3} r_{\text{peak}}^3 n T \quad (12)$$

The volume of the source was assumed to be $4/3 \pi r_{\text{peak}}^3$.

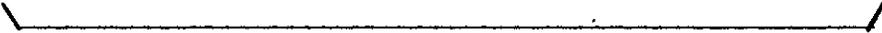
- (c) The value of β , the ratio of gas to magnetic pressure, obtained

TABLE 10: SINGLE-TEMPERATURE OBSERVED AND DERIVED PARAMETERS

Event Number	EM	T_X	S_{peak}	f_{peak}	A_{peak}	r_{peak}	B	n	ED	U	β	B_1	f_m
1	0.13	40	897	8.4	2.0	8.0	150	2.1	41	85	0.05	32	0.36
2	4.0	45	1079	11.8	1.1	5.9	190	19	410	350	0.27	100	1.1
3	1.4	61	576	19.6	0.15	2.2	270	49	1400	64	0.50	190	2.1
8	1.3	40	656	8.4	1.5	6.8	150	8.5	160	210	0.19	64	0.72
12	5.3	27	779	11.8	1.3	6.4	290	19	250	270	0.08	80	0.9
13	0.61	56	771	35	0.07	1.5	550	57	1500	22	0.13	200	2.2



Measured Values



Derived Values

from the previously determined temperature and field strength using the relation

$$\beta = 12 n T B^{-2}. \quad (13)$$

The values of β are in the range from 0.05 to 0.50, implying that the magnetic field is capable of confining the plasma.

- (d) The minimum magnetic field strength, B_1 , required to confine the source, i.e. for the plasma β to be unity:

$$B_1 = 3.5(n T)^{1/2}. \quad (14)$$

- (e) The minimum frequency, f_m , at which the radiation is expected to be gyrosynchrotron:

$$f_m \approx 1.1 \cdot 10^{-2} B_1. \quad (15)$$

This expression was derived assuming that the 4th harmonic of the gyrofrequency is the lower limit of the spectrum. Below the 4th harmonic, gyroresonance absorption is expected to attenuate the emission (Ramaty and Petrosian 1972).

The derived parameters for events with thermal X-ray spectra are of the same order of magnitude as those found for simple impulsive events by Crannell et al. (1978), and are all reasonable for the corona in an active region.

5.2 A Multi-Temperature Source Model

From Equation (6) we see that for a single-temperature source of constant area, $S \propto f^2$ or $\alpha_L = 2$. Examination of Table 5 shows that the observed values of α_L deviate significantly both above and below this predicted value of 2. Of the 13 events studied, 9 have $\alpha_L < 2$, 2 have $\alpha_L > 2$, and 3 have $\alpha_L \approx 2$. Event number 4 is a special case in that $\alpha_L > 2$ for $1 < f < 3$ GHz but $\alpha_L < 2$ for $3 < f < 10$ GHz. The average value of α_L

for the 13 events is 1.4 ± 0.4 , a value similar to that found from studies of other events (Schöchlin and Magun 1979; Dulk and Dennis 1982, hereinafter DD).

In thermal models, a value of $\alpha_L < 2$ can arise only from nonuniformities in the source. A value of $\alpha_L > 2$ may result from free-free and gyroresonance absorption in regions outside the source, as is discussed in §5.3.

In this section we describe the model developed by DD to parameterize possible source nonuniformities in the temperature and magnetic field that can give rise to values of $\alpha_L < 2$. DD developed a model involving a hemisphere in which the temperature and magnetic field decrease with distance, r , from the center according to the following power-law relationships:

$$T = T_{\max} (r/r_{\min})^{-\alpha_T}; B = B_{\max} (r/r_{\min})^{-\alpha_B}; r > r_{\min}, \quad (16)$$

where r_{\min} is the radius of the hottest core. T_{\max} was assumed to be 86 keV (10^9 K) because the X-ray spectrum suggests the presence of components with the temperature this high. This structure was intended to model a nest of loops in an active region. Having adopted this geometry, DD showed that a formula due to Brown (1974) could be used to derive the differential emission measure, a power-law in T , which would be required to produce a power-law X-ray spectrum with a given γ . The two parameters, α_T and α_B , were then derivable from the hard X-ray power-law spectral index, γ :

$$\alpha_T = 6/(2\gamma - 3), \text{ and} \quad (17)$$

$$\alpha_B = (7\alpha_T \alpha_L - 24\alpha_T - \alpha_L + 22)/(18 - 9\alpha_L), \quad (18)$$

where it should be noted that α_L was called m in the notation of DD.

This analysis was only applicable for events in which a power-law was an acceptable fit to the X-ray spectrum, and for $\alpha_T < 2$, which corresponds to $\gamma > 3$. A source with $\alpha_T > 2$ is one in which the temperature falls off very

rapidly with distance outside the core producing relatively little emission there. Hence, the source can be considered to be uniform at a single temperature, T_{max} . The model of DD, then, is only realistic for $0.1 < \alpha_T < 2$, and $0.1 < \alpha_B$.

In order to predict the frequency dependence of the microwave flux, the variation in the area of the source with frequency was found. Because the optical depth, d_f , depends strongly on the temperature and the magnetic field, radiation at any given frequency comes primarily from a very thin layer near the level at which $d_f = 1$. The radius, r_1 , of this layer varies with frequency according to the following relation derived by DD:

$$r_1 \propto f^{-10/(7\alpha_T + 9\alpha_B - 1)} . \quad (19)$$

The area of emission in Equation (6) was assumed to be circular, so that we can use Equation (19) to obtain the following frequency dependence of the source area, A:

$$A = \pi r_1^2 = A_0 (f_0/f)^{\alpha_A}, \quad (20)$$

where

$$\alpha_A = 20/(7\alpha_T + 9\alpha_B - 1). \quad (21)$$

Support for this model comes from recent observations with the VLA indicating that the area of emission commonly decreases with increasing frequency, sufficiently strongly that spectra with α_L much smaller than 2 (even $\alpha_L < 0$) can be explained (Marsh and Hurford 1982). A magnetic structure in which the high-frequency microwave radiation originates in smaller, lower and probably denser areas of increased magnetic field strength is consistent with this situation.

We can now express the frequency dependence of the microwave flux by taking into account the frequency dependence of the area of emission through

Equation (20) and of the temperature through Equations (16) and (19).

The resulting expression is as follows:

$$S \propto A_0 T_{\max} f^{\alpha_L}, \quad (22)$$

where

$$\alpha_L = (24\alpha_T + 18\alpha_B - 22)/(7\alpha_T + 9\alpha_B - 1). \quad (23)$$

Again, note that this analysis is realistic only for α_T , α_B in the range from approximately 0.1 to 2.

Following the procedure described in part III of DD, we can calculate α_T (Equation 17), α_B (Equation 18), B_{\max} (Equation 9 with T_x replaced by T_{\max}), and r_{\min} (Equations 7 with r_{peak} replaced by r_{\min}). T_{\max} is assumed to be 86 keV. The derived electron density of each source was calculated using the following expression given by DD and adjusted for the present system of units:

$$n^2 = 6.8 \alpha_T K_\gamma 50^\gamma T_{\max}^{-3/\alpha_T} r_{\min}^{-3} \{\Gamma(\gamma - 1)\}^{-1} \quad (24)$$

where Γ is the gamma function.

Examination of Table 9 (§4.2) reveals that the hemispherical model developed by DD is applicable to only 7 of the 13 events at the time of maximum microwave flux. These are events 1, 4, 7, 10, 11, 12, and 13, the events for which a power law is an acceptable fit to the X-ray spectrum. In Table 11 we present the observed parameters of these 7 GMBs and the source parameters derived from the model of DD. We also have included in Table 11 the maximum plasma β derived using Equation (13). Events 7 and 11 have values of α_L which are incompatible with the model (>2); absorption effects are required in this model to explain the spectrum (see §5.3). Events 1 and 13 cannot be explained because of negative values of α_B , inconsistent with the assumed behavior of B. Only events 10 and 12 can be explained fully with this approach. In Event 4, the part of the spectrum with $\alpha_L = 3.1$

must be attributed to absorption, but the part for which $\alpha_L = 1.7$ can be explained. Events 10 and 12 are unusual because of their large values of α_A , 2.9 and 2.6, respectively. For example, event 12 was observed to produce a constant α_L from

TABLE 11: DULK & DENNIS MODEL TEST

EVENT NUMBER	γ	α_L	α_T	α_B	α_A	K_γ	r_{\min}	n	B_{\max}	β_{\max}
1	3.5	1.4	1.5	-0.13†	-	-	-	-	-	-
4*	3.5	1.7	1.5	0.8	1.2	4.2	4.6	6.3	120	0.45
7	4.5	2.7†	-	-	-	-	-	-	-	-
10	4.7	0.4	0.94	0.12	3.0	0.45	12	0.16	24	0.29
11	3.1	2.1†	-	-	-	-	-	-	-	-
12	4.3	0.8	1.1	0.09	2.7	3.2	3.6	4.5	120	0.012
13	3.1	1.2	1.9	-1.2†	-	-	-	-	-	-

† Indicates a value inconsistent with this parametric approach.

* α_L applies to $3 < f < 10$ GHz, only.

1.5 to 10 GHz. If this model applies, the microwave source at 1.4 GHz was ~ 140 times as large in area as at 10 GHz. There is no report of such a drastic change in source size with frequency, but no observations of source size are available at such widely-separated frequencies for a single event. This type of analysis could be compared with microwave images at well-separated frequencies to decide whether the model is compatible with observations.

Of the events that can be explained by the model of DD, only event 12 is also explained by the single-temperature model (Table 10). In the DD model, the derived density n is a factor of 4 smaller, the value of B_{\max} is 2.4 times smaller and β is ~7 times smaller. These differences are due to the

choice of $T_{\max} = 86$, $T_x = 27$.

It may be that an inappropriate geometry is assumed in the multi-thermal model of DD. Optically-thick radiation is assumed to be emitted from a continuum of single-temperature sources with peak frequency and peak flux which decreases as the distance from the central core increases. Thus, such a model is inherently limited to adjusting only one spectral slope, either the low side or the high side of the microwave spectrum, but not both simultaneously. Gradients in T and B could be used, however, to explain the spectrum both above and below the peak frequency. In §5.4, therefore, we examine a two-component, diverging loop model in which separate parts of the loop explain the low- and high-frequency portions of the microwave spectrum. In this geometry, the peak flux decreases with distance from the region of maximum temperature, but the peak frequency increases below and decreases above the altitude of temperature maximum.

5.3 Flares for which $\alpha_L > 2$

Two of the events (No. 4 and No.7) exhibit a low-frequency spectral index, α_L , significantly larger than 2 (cf. Table 5). For an optically-thick thermal source, this must be due to an absorption process operating outside the source (Wiehl, 1980). There are three possible absorption processes that could be operating: the Razin effect, gyroresonance absorption, and free-free absorption.

To decide which absorption process might be involved, we calculate the frequency below which each process is operative. The Razin effect (also known as medium suppression) attenuates the flux below

$$f_R = 2 n/B_{\perp} \quad (25)$$

(Ginzburg & Syrovatskii 1965) while gyroresonance absorption is important

below $f_G = 4 f_B$, where $f_B = 2.8 \times 10^{-3} B$ is the gyrofrequency (Ramaty and Petrosian 1972). Free-free absorption is important below f_{FF} given by the following expression:

$$f_{FF} = 8 \cdot 10^{-3} n L^{0.5} T^{-0.75} \quad (26)$$

where the numerical constant is uncertain by $\pm 25\%$ (Ramaty and Petrosian 1972). Values of these limiting parameters are given in Table 12 for the two events with $\alpha_L > 2$. The frequency, f_A , denotes the highest frequency for which $\alpha_L > 2$. In order to calculate f_G , f_R and f_{FF} we have derived A_{peak} , B and n as in §5.1, making use of the fitted T_x . We have then set $L \approx r_{peak}$. For free-free absorption, we give in Table 12 both the value of f_{FF} assuming coronal temperatures ($2 \times 10^6 K$ or 0.17 keV) and, also the value of the temperature, T_{FF} , assuming $f_{FF} = f_A$.

TABLE 12. ABSORPTION PROCESSES

EVENT NUMBER	α_L	f_A	f_R	f_G	$(T=2 \times 10^6 K)$	$(f_{FF}=f_A)$
					f_{FF}	T_{FF}
				(GHz)		($10^6 K$)
4	3.1	4	0.1	2.4	0.7	0.2
7	2.7	3	0.1	3.3	1.6	1.0

Based on this analysis of the possible absorption processes that could explain values of $\alpha_L > 2$, we conclude that

- 1) The Razin effect is not important in either of the two events since $f_R \ll f_A$ in both cases.
- 2) Gyroresonance absorption is the most probable process responsible for values of $\alpha_L > 2$ in these two events since $f_G \sim f_A$ in both cases.

- 3) Free-free absorption can be ruled out for event number 4 since T_{FF} calculated with $f_{FF} = f_A$ is significantly lower than typical coronal temperatures. Free-free absorption cannot be ruled out, however, for event number 7 since T_{FF} is of the same order as coronal temperatures.

5.4 A Diverging Loop Model for the Microwave Source

In this section we study a diverging loop model which might explain the observed microwave spectrum, both the low frequency and the high-frequency part. We assume that the emission at any particular frequency is dominated by the optically-thick radiation at that frequency (Matzler 1978). The cross-section of the loop increases rapidly with height above the chromosphere up to the region of maximum temperature, and then increases more gradually with altitude above that level. This behavior of the cross-section is believed to be characteristic of the leg of the loop near the footpoint (Spruit 1981). We further assume that magnetic flux is conserved along the loop. The strongest field is found near the footpoint of the loop where it approaches sunspot values ≈ 1000 G, and the lowest field near the top. Because microwave radiation at high frequencies originates from regions of high magnetic field, there exists an inverse relationship between the surface area of the emission region and the frequency. Such a frequency-area relationship is commonly observed (Marsh and Hurford 1982). To make the calculations simple, we assume the same power-law form for the area as in Equation (20), but now we have the following two values of α_A : α_{A1} corresponding to the region above the temperature maximum and α_{A2} to the region below the temperature maximum.

Because the radiation at a frequency, f , originates mainly from the region in which the optical thickness $d_f = 1$, the temperature of that region is

derived from the expression for the peak frequency (Dulk and Marsh 1982), solved for T and adjusted for the present units:

$$T = 1936 f^{1.43} (nL)^{-0.14} B^{-1.29} . \quad (27)$$

Assuming conservation of magnetic flux for a diverging flux tube and a frequency dependence of the source area as in Equation (20), we find

$$T \propto f^{(1.43 - 1.29\alpha_A)} \quad (28)$$

The radiation below the peak frequency originates from areas above the temperature maximum. In order to have a localized temperature maximum, a positive correlation between temperature and frequency is required in this part of the loop. According to Equation (28) this constrains the fanning parameter $\alpha_{A1} < 1.11$. Observations of spatially resolved microwave sources at two or more frequencies in the range 5 to 15 GHz indicate $\alpha_A \approx 1$ (Marsh and Hurford 1982). This value is consistent with the above calculated range for α_A on the low-frequency side of the spectrum.

At altitudes below the temperature maximum, we require an anticorrelation between T and f, and this then restricts $\alpha_{A2} > 1.11$ in this region.

With the aid of Equations (16), (20) and (28) we find

$$S \propto f^\alpha \quad \text{where } \alpha = 3.43 - 2.29\alpha_A . \quad (29)$$

The fanning parameters, α_{A1} and α_{A2} , are each obtained from Equation (29)

with α set to α_L and α_H respectively. Thus

$$\begin{aligned} \alpha_{A1} &= (3.43 - \alpha_L)/2.29 \text{ and} \\ \alpha_{A2} &= (3.43 - \alpha_H)/2.29 . \end{aligned} \quad (30)$$

Table 13 gives the values of α_{A1} and α_{A2} obtained for all 13 events. (Again, events 4 and 7 cannot be explained without absorption effects - cf. §5.3). Only for event number 10 is $\alpha_{A1} > 1.11$ which would result in

$T \propto f^{-0.13}$. This is only a small violation of the required positive correlation. For all other events we find $\alpha_{A1} < 1.11$ and $\alpha_{A2} > 1.11$, insuring a decrease of the temperature with increasing distance from the region of maximum temperature.

For $\alpha_A = 1.5$ we obtain $\alpha_L = 0$, corresponding to a flat spectrum, sometimes observed during microwave bursts (Hachenberg and Wallis 1961).

TABLE 13

EVENT NUMBER	1	2	3	5	6	8	9	10	11	12	13
α_{A1}	0.89	0.62	0.89	1.10	1.02	0.76	0.58	1.32	0.58	1.15	0.97
α_{A2}	3.46	2.24	1.76	2.11	-	3.11	1.72	1.93	1.89	2.33	-

In the lower part of the loop the temperature must decrease rapidly with increasing frequency and, therefore, must increase with altitude above the photosphere. For $T \propto f^{-2}$, $T_{\max} \approx 70$ keV. At the lower extremity of the source, there must be a high-frequency break in the spectrum; above this frequency the source is optically-thin, and the spectrum is steep ($S \propto f^{-8}$). Assuming that the peak frequency is 15 GHz and the high frequency break is at 35 GHz, we find the temperature of the 35 GHz level to be approximately 13 keV, and, by using Equation (9), we obtain $B \approx 1700$ G. This value is consistent with observations of photospheric fields obtained for the 13 events which varied between 1100 and 2500 G (Coffey, 1980, 1981).

By assuming a simple diverging loop model in which the lower part fans out more rapidly than the upper part, we are able to explain the observed microwave spectra in terms of two fanning parameters, α_{A1} and α_{A2} .

The values of α_{A1} are in accord with commonly observed source properties. The values of α_{A2} are, however, higher than the observed rate of change of area with frequency reported from direct imaging measurements. These values of α_{A2} are consistent with the observations of Kundu et al. (1982) in that they attribute significant emission to regions of relatively low altitudes as well as the loop legs above the temperature maximum. Observations of dynamic microwave spectra obtained in coincidence with microwave images over the same range of frequencies would provide a more critical test of this diverging loop model.

6. CORRELATIONS

In searching for a possible relationship between any pair of parameters (x,y) , we first obtained a new pair $(\log x, \log y)$ and then tested for evidence of a linear correlation between the two logarithms. Correlation coefficients, r , between the various pairs of observed and derived parameters have been calculated together with the probability, $P_c(r,N)$, that any random sample of uncorrelated data points would yield a linear correlation coefficient greater than or equal to the value obtained for r (Equation 7.8 of Bevington 1969). All correlation coefficients (r) refer to this linear dependence in log-log space of N data points. Because the number of data points, N , is not the same for each of the parameter pairs, the probability, $P_c(r,N)$, rather than the correlation coefficient, r , is the figure of merit for the significance of the correlations. All those pairs for which $P_c(r,N) \geq 40\%$ are considered as "not correlated". Pairs for which $5\% < P_c(r,N) < 40\%$ are considered "correlated" and all pairs for which $P_c(r,N) < 5\%$ are "well correlated".

Considered as a member of this set, event No. 11 is anomalous. Not only is it less impulsive and of longer duration than all other flares in the group of 13 studied, but the ratio of its microwave to hard X-ray peak fluxes is greatest and its microwave emission is delayed the longest. Taking all the available data into account, we have chosen to regard this event as the second stage of event No. 10 and have omitted event No. 11 from the correlation analysis.

6.1 Model-Independent Parameters

In order to determine how the characteristic times, $\tau_{\mu C}$, of the micro-

TABLE 14: FREQUENCY DEPENDENCE OF THE MICROWAVE CHARACTERISTIC TIME $\tau_{\mu c}$

EVENT NUMBER	D_{μ}	g_{μ}	r	N	$P_c(r, N)$
1			-0.71	4	0.28
2	188	-0.97	-0.99	4	0.005
3	59	-0.31	-0.94	5	0.014
4	139	-0.36	-0.99	4	0.003
5			-0.85	3	0.35
6	268	-0.50	-0.93	5	0.021
7			-0.94	4	0.06
8			-0.86	5	0.059
9			-0.47	6	0.33
10			-0.83	5	0.081
11			-0.60	5	0.28
12	178	-0.43	-0.90	5	0.037
13			-0.91	4	0.088

r = correlation coefficient

N = number of points

TABLE 15: ENERGY DEPENDENCE OF THE HARD X-RAY CHARACTERISTIC TIME τ_{xc}

EVENT NUMBER	D_x	ξ_x	r	N	$P_c(r,N)$
1	3160	-0.56	-0.96	9	<0.001
2	40	-0.31	-0.98	8	<0.001
3	29	-0.21	-0.93	10	<0.001
4	130	-0.35	-0.98	10	<0.001
5	142	-0.31	-0.98	10	<0.001
6	566	-0.53	-0.98	10	<0.001
7	169	-0.40	-0.89	8	0.0028
8	74	-0.40	-0.88	10	<0.001
9	719	-0.57	-0.97	10	<0.001
10	361	-0.32	-0.89	9	0.0012
11	581	-0.10	-0.82	12	0.0012
12	113	-0.37	-0.86	10	0.0014
13	46	-0.28	-0.87	8	0.0051

r = correlation coefficient, N = number of points

wave bursts depend on the frequency, we performed such a correlation analysis for each GMB. Table 14 shows that a power-law relation of the form $\tau_{\mu c} = D_{\mu} f^{g_{\mu}}$ for the frequency dependence of $\tau_{\mu c}$ is a valid description in 5 of the 13 cases (i.e. $P_c(r,N) \leq 5\%$). In Figure 14 we plot the values of $\tau_{\mu c}$ as a function of frequency for all 13 events. Straight lines indicate cases in which a power law approximation is valid. Even in those cases for which this approximation is not acceptable at the 5% confidence level, there is a general decrease of $\tau_{\mu c}$ with increasing frequencies. Similar relationships exist for the rise and fall times of the microwave events, $\tau_{\mu r}$ and $\tau_{\mu f}$.

The characteristic time, τ_{xc} , for the hard X rays also exhibits a power-law energy dependence of the form

$$\tau_{xc} = D_x E^{g_x} . \quad (31)$$

We found a correlation of τ_{xc} with the mean photon energy at a confidence level of $P_c(r,N)$ better than 0.5% in all 13 events (Table 15). The time τ_{xc} , is a measure of the burst duration. The values of g_x are in the range from -0.56 to -0.10, the average being -0.35. In Figure 29 the measured values of τ_{xc} are shown as a function of photon energy together with the correlation curves. Similar relationships hold for the rise and fall times, as well. For the rise time τ_{xr} , the average exponent was -0.5 with only 7 events correlated at the 1% confidence level. For the fall time τ_{xf} , the average exponent was -0.4 with all but one event correlated at the 5% confidence level.

In Table 16 we summarize the results of the correlation analysis of the time parameters of the hard X-ray and microwave bursts. The hard X-ray bursts exhibit a good correlation between rise and fall times at all energies.

TABLE 16

	MICROWAVE											X-RAY														
	Rise Times					Fall Times						Rise Times							Fall Times							
	R3	R5	R8	R11	R19	R35	F3	F5	F8	F11	F19	F35	R1	R2	R3	R4	R5	R6	R7	F1	F2	F3	F4	F5	F6	F7
Microwave Rise Times	R3	N	N	N	N		N																			
	R5		C	C	C	N		N																		
	R8			W	W	W			C					W	W	W	W	W	W	C		W		C		C
	R11				W	W				C																
	R19					W						C														
	R35											C		C	C	C	C	C	C	C	C		C		C	C
Microwave Fall Times	F3							N	N	N	N															
	F5								C	C	C	N														
	F8									W	W	C	W		W		W		N	C		C		C		C
	F11										W	C														
	F19											W														
	F35												C		C		C		C	C	C		N		N	
X-Ray Rise Times	R1																			W						
	R2																				W					
	R3																					W				
	R4																						W			
	R5																							W		
	R6																								W	
	R7																									W

"R" indicates rise time, "F" indicates fall time. For the microwave times, the numbers refer to frequency in GHz; for the X-ray times, the numbers indicate channel number. The goodness of the correlation is indicated by "N" for pairs which are not correlated ($P > 40\%$), by "C" for correlated pairs ($5\% < P < 40\%$) and by "W" for well correlated pairs ($P < 5\%$).

The microwave bursts exhibit a less significant correlation between rise and fall times, and there is evidence for a second component at low frequencies which is not correlated with the bursts at high frequencies.

We have searched for correlations between other measured and derived parameters and summarize below the most important findings of the correlation analysis.

The microwave rise and fall times at all frequencies are not correlated with the corresponding maximum flux at any particular frequency. We also computed the rate of increase RI, defined as the maximum microwave flux at a given frequency divided by the rise time at that frequency, and the rate of decrease RD, defined as the maximum flux at a given frequency divided by the fall time at that frequency. It was found that the values of RI, are well correlated with the values of RD, at all microwave frequencies except at 3 GHz. The hard X-ray peak flux is not correlated with the microwave flux at the peak frequency or with the maximum flux at 11 GHz. The transition frequency, f_t , is correlated with the peak frequency, confirming a result found by Guidice and Castelli (1975). However, the high frequency cutoff, f_h , is not correlated with the peak frequency. Also, a measure of the width of the microwave spectrum, $f_h - f_t$, is not correlated with f_{peak} .

As mentioned in §4, at $t_{\mu\text{max}}$ a power-law function was an acceptable representation of the X-ray spectrum for only 7 of the events. However, the best fit γ can be used to parameterize the hardness of the spectrum even when the fit is not acceptable, provided that the values of γ are regarded only as rough indicators of the spectral hardness. If the microwave source electrons are the same as (or closely related to) the X-ray source electrons, some relation between γ and the microwave spectral parameters is expected. The ex-

cellent microwave and X-ray spectral coverage available in this study enabled us to search for such correlations for the first time. It was found that, at $t_{\mu\max}$, the values of γ and f_{peak} are correlated at the 6% confidence level, a correlation that has not been reported previously. The relation is $f_{\text{peak}} \propto \gamma^{-2.6}$. The expected correlation between γ and α_{H} is not found, however; we discuss possible explanations in §7.

No correlation was found between g_{X} and the microwave spectral parameters f_{peak} , α_{H} , α_{L} and S_{peak} , when all 13 events were considered. However, when attention was limited to events 1, 2, 3, 8, 12 and 13, which had X-ray spectra that were well represented by single-temperature bremsstrahlung functions, it was found that g_{X} and α_{H} were correlated at the 1% confidence level and that g_{X} and f_{peak} are correlated at the 9% confidence level. For this subset of the events, f_{peak} and α_{H} are also correlated at the 0.6% confidence level.

6.2 Model-dependent Parameters

We first discuss the results of tests for correlations involving parameters derived assuming a single-temperature source. A thermal energy density, ED, defined by equation (11), was derived from each of events 1, 2, 3, 8, 12 and 13, the events for which a single-temperature bremsstrahlung function was an acceptable fit to the X-ray spectrum at $t_{\mu\max}$. The values of ED and g_{X} given by equation (31) were correlated at the 0.3% confidence level. We found $g_{\text{X}} \propto \text{ED}^{-0.58}$. The parameter g_{X} and the density, n , were correlated at the 0.7% confidence level with $g_{\text{X}} \propto n^{-0.25}$. A_{peak} was also correlated with g_{X} , at the 6% confidence level. Other parameters derived in a single-temperature model (B , U , β) are not correlated with g_{X} .

Both ED and A_{peak} were correlated with α_{H} to better than 1.5% con-

confidence. There were slight correlations of B and β with α_H , to 10% and 15% confidence, respectively.

As noted in §4, at $t_{\mu\max}$, a thermal function was not an acceptable representation of the X-ray spectrum for 6 of the 13 events. However, the best fit EM and T can be used to parameterize the spectrum even when the fit is not acceptable, as long as their values are regarded only as rough indicators of the intensity and hardness of the spectrum. The curve in the EM-T plane which is generated as the spectrum evolves in time is a useful constraint on any thermal model that is proposed to explain the flare. Therefore, we studied the EM-T correlation for all 13 events.

The 13 events can be grouped into 3 different classes as far as the EM-T correlation is concerned and typical examples of each class are shown in Figure 43. The first class exhibits a relatively flat EM-T correlation in which the emission measure remains approximately constant while the temperature first increases and then decreases (e.g. event 2). Six events exhibit such a behavior. The second class (4 events) shows anticorrelation between EM and T (represented by events 7 and 10). Such a relation was reported earlier for two events of 1972 May 18 (Wiehl et al., 1980). They ascribed this anticorrelation to expansion of the source. The third class (e.g. event 12) can be described by a positive correlation between EM and T (3 events). The power-law index of T in this correlation is different from the value $3/2$ which would be expected from the adiabatic model (Matzler et al. 1978). Also, these curves exhibit a considerable amount of hysteresis: T remains large while the EM decreases during the decline of the event. Hence none of these events are compatible with a reversible, adiabatic process.

7. DISCUSSION

7.1 Model-independent Results

We draw several conclusions about whether the same electrons produce both the hard X-rays and microwaves. In §6.1, the microwave temporal parameters ($\tau_{\mu r}$, $\tau_{\mu f}$ and $\tau_{\mu c}$) were tested for correlations with their X-ray counterparts. While the temporal parameters for frequencies above 5 GHz are correlated from event to event with the X-ray parameters, the low-frequency parameters are not. This may be evidence that the electrons responsible for the low-frequency emission are not the same as those that produce the X rays and high-frequency microwaves. The peaks in the time histories for $f < 5$ GHz suggest that they are closely related, however. This difference in low-frequency time behavior may also indicate a different source region in space. The correlations of high-frequency parameters with X-ray parameters are consistent with a common source.

The correlation of γ and f_{peak} (§6.1) is evidence that the same electrons produce the X rays and the microwaves near f_{peak} . This is expected whether a thermal or nonthermal interpretation is made (cf. Dulk & Marsh 1982). A correlation between γ and α_H is to be expected if the electron spectrum dominates the microwave spectrum, but this is not found. The fact that the high-frequency temporal parameters and X-ray temporal parameters are correlated, but the spectral parameters are not suggests that gradients in the magnetic field of the microwave emission region dominate the high-frequency portion of the microwave spectrum.

Next we consider the relationships among the time of maximum microwave flux, $t_{\mu\text{max}}$, the time of maximum X-ray flux, $t_{x\text{max}}$, and the time of

hardest X-ray spectrum, t_{xh} . All of the X-ray events exhibited a soft-hard-soft spectral evolution, implying that a corresponding evolution of the source electron distribution occurred. The microwave emissivity of an electron distribution increases rapidly with the relative number of high-energy electrons. Hence, if the same electron distribution is the source of both hard X-rays and microwaves, it is to be expected that $t_{\mu\max} = t_{xh}$. This is often not the case (cf. Table 9). B also has a strong effect on the microwave emissivity, however (Dulk and Marsh 1982). The difference between t_{xh} and $t_{\mu\max}$ can be explained by changes in B during the event. On the average, $t_{\mu\max}$ is closer to t_{xh} than to $t_{x\max}$.

The events that had X-ray spectra which were fit acceptably by a thermal function seem to represent a distinct class of flares in other respects. For these 6 events, f_{peak} was correlated with g_x , the parameter which characterized the variation of τ_{xc} with energy. A value of g_x near -1 corresponds to an event in which there was a large change in γ during the event, while $g_x \approx -0.1$ indicated that γ was relatively constant. The X-ray spectral evolution in each event followed a soft-hard-soft pattern; therefore, if $|g_x|$ was small, the X-ray spectrum was relatively hard for a relatively longer time during the event. The events with small $|g_x|$ tended to have higher f_{peak} , in agreement with expectations but why the correlation of g_x and f_{peak} breaks down when the spectrum does not fit a thermal function at $t_{\mu\max}$ is not apparent.

We have observed that the X-ray characteristic time, τ_{xc} , decreases with increasing X-ray energy. Similar observations motivated a complex theoretical investigation of the dependence of X-ray fall time on energy, assuming a source distribution of nonthermal electrons in a trap of nonuniform density

(Brown 1972). It should be noted, however, that in a wide variety of models the hard X-ray spectrum evolves with a soft-hard-soft time behavior (hardest near the time of maximum flux) so that the events exhibit a decline in characteristic time with energy. A power-law dependence of the event duration with energy is, therefore, not a sensitive test for a trap model. To illustrate this, we briefly consider one of many possible models with soft-hard-soft spectral evolution resulting in a power-law dependence of characteristic time on energy: adiabatic compression. In our example, the hard X-ray emitting plasma is heated at a constant rate from 10 to 60 keV in 5 seconds and the emission measure reaches a peak of 10^{45} cm^{-3} . The process is then reversed. In Figure 44 we show the fraction of maximum flux ($I(t)/I_{\text{max}}$) versus time for five photon energies in the HXRBS range. The characteristic times, τ_{xc} , also plotted in Figure 44 are determined by the same method as in our analysis of these 13 events (see Equation (4)). It is obvious from Figure 44 that τ_{xc} is shorter, the higher the energy. Comparing Fig. 44 with 29, we see that the observed energy dependence of τ_{xc} is simply a soft-hard-soft spectral behavior. All of these events do exhibit a soft-hard-soft spectral evolution. This could result from a variety of properties of the heating or acceleration mechanism, and does not point unambiguously to a trap model.

7.2 Model-dependent Results

In §5.1 we derived source parameters for the 6 events for which a single-temperature interpretation of the X-ray spectrum was possible, obtaining values which are reasonable for the active region corona. Nonuniformities in B, which would then be needed to explain the full microwave spectra, were ignored, and only f_{peak} and $S(f_{\text{peak}})$ were used in the derivation. In one instance (Event 12) the derived source area was available from a direct meas-

urement of the source size. In the time interval from 0658:52 to 0659:02 UT which included $t_{\mu\text{max}}$, t_{xmax} and t_{xh} , an image of the region was obtained at X-ray energies from 17 to 40 keV with the SXT instrument onboard the Hinotori spacecraft. Ohki et al. (1982) reported that the X-rays originated in a single elliptical source with dimensions of approximately 10 arc sec by 30 arc sec. The area within the 40% peak flux contour is $1.2 \times 10^{18} \text{ cm}^2$. This is consistent with our prediction of $1.3 \times 10^{18} \text{ cm}^2$ for the source size at peak emission. This successful prediction of the source area from observations with no spatial resolution lends support to the hypothesis that there are impulsive flares in which a common single-temperature source produces both microwaves and hard X-rays.

The correlations of ED (equation 11), n and A_{peak} (equation 7) with g_{x} (equation 31) also suggest that the single-temperature interpretation is physically significant for the flares involved. Smaller values of $|g_{\text{x}}|$, indicating that the X-ray spectrum was relatively hard for a relatively long portion of the burst, are associated with relatively high values of energy density, ED, and vice versa.

Both the multi-thermal model of DD and the diverging loop model developed in §5.4 were consistent with the properties of some events. Both models require changes in source size with frequency which can be investigated in future multi-frequency imaging observations. The effects of the geometry and nonuniformities of the magnetic field configuration on the spectra will be crucial to understanding flares.

8. CONCLUSION

Our study of 13 Great Microwave Bursts and associated hard X-ray events has led to the following conclusions:

- Eight of the observed microwave spectra have a constant power-law index from the peak frequency down to 1 GHz or less. One spectrum extends to < 0.4 GHz.
- A microwave spectral index of less than 2 below the peak frequency was observed for most of the events, implying nonuniformities in the sources.
- The time of the hardest X-ray spectrum is delayed for most of the events relative to the time of maximum X-ray flux. So is the time of maximum microwave flux.
- The low-frequency microwave spectrum is explained in less than one third of the events by the simple hemispherical geometry of Dulk and Dennis (1982).
- The temporal parameters characterizing the high-frequency microwave time histories are correlated with each other and with the corresponding hard X-ray parameters.
- The low-frequency microwave temporal parameters are not correlated either with the corresponding high-frequency microwave parameters or with the hard X-ray parameters.
- For 6 events in which a single-temperature interpretation of the X-ray spectrum was possible, the derived source density and energy density were found to be correlated with the independent measured parameter g_x (equation 31).

- The source area derived using a single-temperature model is in good agreement with the observed area obtained for the one event for which a spatially resolved hard X-ray image is available.
- In thermal models, complex source structures are required to explain the complete microwave spectrum, both above and below the peak frequency.
- Correlation of the microwave peak frequency with the best fit X-ray spectral index implies that the bulk of microwave and hard X-ray emission is attributable to a single distribution of electrons.

9. ACKNOWLEDGMENTS

It is a pleasure to thank G. Wharen for typing the often chaotic and constantly changing manuscript. We appreciate the help of H.E. Dennis, A.K. Tolbert, B.E. Gibson, G.S. Kennard, and A.J. Kiplinger in the data reduction. We thank H.E. Coffey, NOAA, and D.J. Forrest, University of New Hampshire, for additional data, and G.A. Dulk, University of Colorado, and A. Magun, University of Berne, for helpful discussions. This research was carried out while one of the authors (HJW) was a visiting scientist at the Laboratory for Astronomy and Solar Physics of the NASA Goddard Space Flight Center with a fellowship from the Swiss National Science Foundation. The hospitality of C.J. Crannell and K.J. Frost, SMM Project Scientist, is gratefully acknowledged.

REFERENCES

- Batchelor, D.A., Benz, A.O., and Wiehl, H.J. 1983, in preparation.
- Bevington, P.R. 1969, *Data Reduction and Error Analysis for the Physical Sciences* (New York: McGraw-Hill).
- Brown, J.C. 1971, *Solar Phys.*, 18, 489.
- Brown, J.C. 1972, *Solar Phys.*, 25, 158-77.
- Brown, J.C. 1974, in *Coronal Disturbances*, G. Newkirk, ed., *IAU Symp.* 57, 395.
- Brown, J.C. 1975, in *Solar Gamma, X-, and EUV Radiation*, S.R. Kane, ed., *IAU Symp.* 68, p. 245.
- Brown, J.C., Melrose, D.B., and Spicer, D.S. 1979, *Ap.J.*, 228, 592.
- Brown, J.C., Craig, I.J.D., and Karpen, J.T. 1980, *Solar Phys.*, 67, 143.
- Chubb, T.A., Kreplin, R.W., and Friedman, H. 1966, *J. Geophys. Res.*, 71, 3611.
- Coffey, H. 1980, *SGD Comp.* 433; 1980, *SGD Comp.* 436; 1981, *SGD Comp.* 437.
- Coffey, H. 1981, *SGD Comp.* 441; 1981, *SGD Comp.* 446; 1982, *SGD Comp.* 450; 1982, *SGD Comp.* 454.
- Coffey, H. 1982, *SGD Prompt.*, 455.
- Colgate, S. 1978, *Ap.J.*, 221, 1068.
- Crannell, C., Frost, K., Matzler, C., Ohki, K., Saba, J. 1978, *Ap.J.*, 223, 620-37.
- Datlowe, D.W. 1975, *Space Sci. Inst.*, 1, 389.
- Datlowe, D.W. 1977, *Nuc. Inst. & Meth.*, 145, 365.
- Dennis, B.R., Frost, K.J., Orwig, L.E., Kiplinger, A., Dennis, H.E., Gibson, B.E., Kennard, G.S., and Tolbert, A.K. 1983, *NASA Tech Memo.* 84998.
- Duijveman, A., Hoyng, P., and Machado, M.E. 1982, *Solar Phys.*, 81, 137.
- Dulk, G. and Marsh, K. 1982, *Ap.J.*, 259, 350-8.
- Dulk, G. and Dennis, B. 1982, *Ap.J.*, 260, 875-84.
- Elcan, M. 1978, *Ap.J.*, 226, L99.
- Frost, K.J. 1969, *Ap.J.*, 158, L159.

- Ginzburg, V.L. and Syrovatskii, S.I. 1965, Ann. Rev. Astron. Astrophys., 297.
- Groenschild, E.H.B.M. and Mewe, R. 1978, Astron. Astrophys. Suppl., Ser. 32, 283.
- Guidice, D. and Castelli, J. 1975, Solar Phys., 44, 155-72.
- Hachenberg, O. and Wallis, G. 1961, Z. Astrophys., 52, 42.
- Holt, S. and Ramaty, R. 1969, Sol. Phys., 8, 119.
- Hoyng, P., Machado, M.E., Duijveman, A., Boelee, A., de Jager, C., Fryer, R., Galama, M., Hoekstra, R., Imhof, J., Lafleur, H., Maseland, H.V.A.M., Mels, W.A., Schadee, A., Schrijver, J., Simnett, G.M., Svestka, Z., van Beek, H.F., van Tend, W., van der Laan, J.J.M., van Rens, P., Werkhoven, F., Willmore, A.P., Wilson, J.W.G., and Zandee, W. 1981a, Ap.J., 244, L153.
- Hoyng, P., Duijveman, A., Machado, M.E., Rust, D.M., Svestka, Z., Boelee, A., de Jager, C., Frost, K.J., Lafleur, H., Simnett, G.M., van Beek, H.F. and Woodgate, B.E. 1981b, Ap.J., 246, L155.
- Hoyng, P., Marsh, K.A., Zirin, H., and Dennis B.R. 1983, Ap.J., 268, 865.
- Kane, S. and Anderson, A.K. 1970, Ap.J., 162, 1003.
- Kane, S.: 1972, Space Sci. Rev., 13, 822.
- Kane, S.R., Crannell, C.J., Datlowe, D., Feldman, U., Gabriel, A., Hudson, H.S., Kundu, M.R., Matzler, C., Neidig, D., Petrosian, V., Sheeley, N.R., Jr. 1980, Solar Flares, P.A. Sturrock, Ed.
- Kane, S., 1982 Proceedings of the Hinotori Symp. on Solar Flares, 89-91, Jan. 27-29, Japan
- Kaplan, S.A., Pikel'ner, S.B., and Tsytovich, V.N. 1974, Phys. Reports C, 15(1), 1.
- Kawabata, K., Ogawa, H., Takakura, T., Tsuneta, S., Ohki, K., Yoshimori, M., Okudaira, K., Hirashima, Y., Kondo, I. 1982, Proceedings of the Hinotori Symp. on Solar Flares, 168-185, Jan. 27-29, Japan.
- Kundu, M.R. 1961, J. Geophys. Res., 66, 4308.
- Kundu, M.R., Schmahl, E.J., and Velusamy, T. 1982, Ap.J., 253, 963.
- Kundu, M.R. and Vlahos, L., 1982, Space Sci. Rev., 32, 405.
- McKenzie, D. 1972, Ap.J., 175, 481-92.
- Magun, A., Fuhrer, M., Kampfer, N., Stahli, M., Schochlin, W., Wiehl, H. 1981, Solar Observations Report No. 46, University of Berne.

- Marsh, K.A., Hurford, G.J., Zirin, H., Dulk, G.A., Dennis, B.R., Frost, K.J., Orwig, L.E., 1981, Ap.J., 251, 797.
- Marsh, K. and Hurford, G. 1982, Ann. Rev. Astron. Astrophys., 497.
- Matteson, J.L. 1971, Ph. D. Thesis, UCSD, San Diego, CA.
- Matzler, C., Bai, T., Crannell, C., Frost, K. 1978, Ap.J., 223, 1058-71.
- Matzler, C. 1978, Astron. Astrophys., 70, 181-88.
- Ohki, K., Tsuneta, S., Takakura, T., Nitta, N., Makishima, K., Murakami, T., Ogawara, Y., Oda, M., Miyamoto, S. 1982, Proceedings of the Hinotori Symp. on Solar Flares, 102-119, Jan. 27-29, Japan.
- Orwig, L.E., Frost, K.J. and Dennis, B.R. 1980, Solar Phys., 65, 25.
- Peterson, L.E. and Winkler, J.R. 1959, J. Geophys. Res., 64, 697.
- Ramaty, R., Petrosian, V. 1972, Ap.J., 178, 241.
- Rust, D.M., Nelson, J.J., Pryor, L.H., Frank, Z.A., and Boggess, A.E. 1982, Solar Maximum Year Flare List, SMM Data Analysis Center Document.
- Schochlin, W. and Magun, A. 1979, Solar Phys., 64, 349.
- Smith, D. and Lilliequist, C. 1979, Ap.J., 232, 582-9.
- Smith, D. 1980, Solar Phys., 66, 135.
- Spicer, D. and Brown, J. 1981, in The Sun as a Star, S. Jordan (ed.), NASA SP-450.
- Spruit, H.C. 1981, in The Sun as a Star, S. Jordan, (ed.), NASA SP-450.
- SGD, Explanation of data reports Feb. 1982, No. 450 Supplement.
- Takakura, T. 1972, Solar Phys., 26, 151.
- Takakura, T. and Kai, K. 1966, Publ. Astron. Soc. Japan, 18, 57.
- Takakura, T.: 1975, Solar Gamma-X, and EUV Radiation, S.R. Kane, (ed.), IAU Symp. 68, p. 245.
- Takakura, T., Ohki, K., Tsuneta, S., Nitta, N., Makishima, K., Murakami, T., Ogawara, Y., and Oda, M. 1982, Proceedings of the Hinotori Symp. on Solar Flares, 142-161, Jan. 27-29, Japan.
- Tsuneta, S., Ohki, K., Takakura, T., Nitta, N., Makishima, K., Murakami, T., Ogawara, Y., Odo, M., and Kondo, I. 1982, Proceedings of the Hinotori Symp. on Solar Flares, 142-161, Jan 27-29, Japan.

Wiehl, H. 1980, Dissertation, University of Berne.

Wiehl, H., Schochlin, W., Magun, A. 1980, Astron. & Astrophys., 92, 260-66.

Wiehl, H. and Desai, U. 1983, to appear in July Ap.J.

Wiehl, H. and Matzler, C. 1980, Astron. Astrophys., 82, 93.

Zolcinski, M.C., Forrest, D.J., Ryan, J.M., Chupp, E.L., Kanbach, G., Reppin, C.,
Rieger, E., and Share, G.E. 1982, presented at the 24th Plenary Meeting of
COSPAR, Ottawa, Canada.

NAMES AND ADDRESSES OF AUTHORS

D.A. Batchelor, C.J. Crannell, B.R. Dennis, and P.N. Price
Code 684,
NASA Goddard Space Flight Center
Greenbelt, MD 20771.

H.J. Wiehl
Institute for Astronomy
ETH
8092 Zurich
Switzerland

FIGURE CAPTIONS

Figures 1 to 13

Time histories of the Great Microwave Bursts at three microwave frequencies, of the X-ray bursts at two energies and of the best fit temperature, computed from the X-ray spectra.

Figure 14

Microwave characteristic times as a function of frequency for all 13 events. Straight lines indicate cases in which a power-law approximation is acceptable. The numbers designate the individual events.

Figures 15 to 27

Microwave spectra at the time of maximum microwave emission. Open circles indicate Berne data while closed circles are additional data from SGD Comprehensive Reports (Coffey, 1980-82).

Figure 28

Polarization as a function of frequency as observed with the Berne instruments. L and R indicate left handed and right handed polarization, respectively. The numbers next to the points designate the individual events.

Figure 29

Hard X-ray characteristic times as a function of energy, determined using channels 1 to 9. Straight lines indicate acceptable power-law fits. The numbers designate the individual events. Data points and fits for events 3, 8 and 12 are multiplied by factors of 100, 10 and 0.1, respectively, to separate them from the results of other events.

Figures 30 to 42

Hard X-ray spectra at the time of maximum microwave intensity for both power-law and thermal assumptions of the incident spectra. Horizontal bars through the points in these plots indicate the channel widths and vertical bars indicate the statistical uncertainties.

Figure 43

Correlation diagrams between emission measure (EM) and temperature (T) for four events. The dashed dotted lines indicate the general behaviour of the correlation. In each case the event begins at the point with the lowest temperature.

Figure 44

Plots of the rising part of the X-ray time profile computed for several different energies assuming adiabatic compression. The time history for each energy is normalized to its peak value. The following part of the time history is the reverse of the rising part for a reversible adiabatic process. The inset shows the characteristic times, τ_{XC} , computed from the indicated time profiles plotted as a function of energy in the HXRBS range.

Figure 1

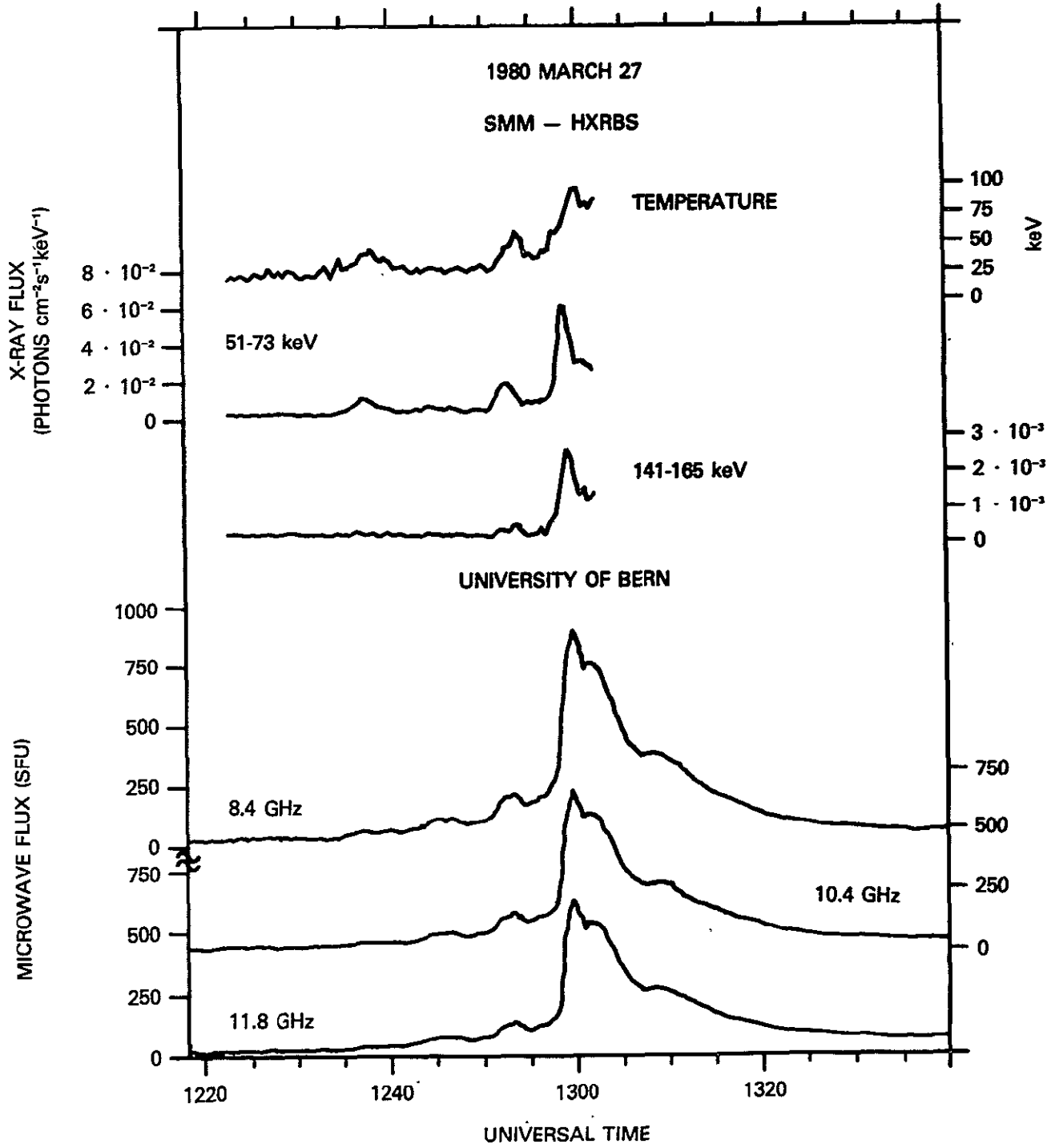


Figure 2

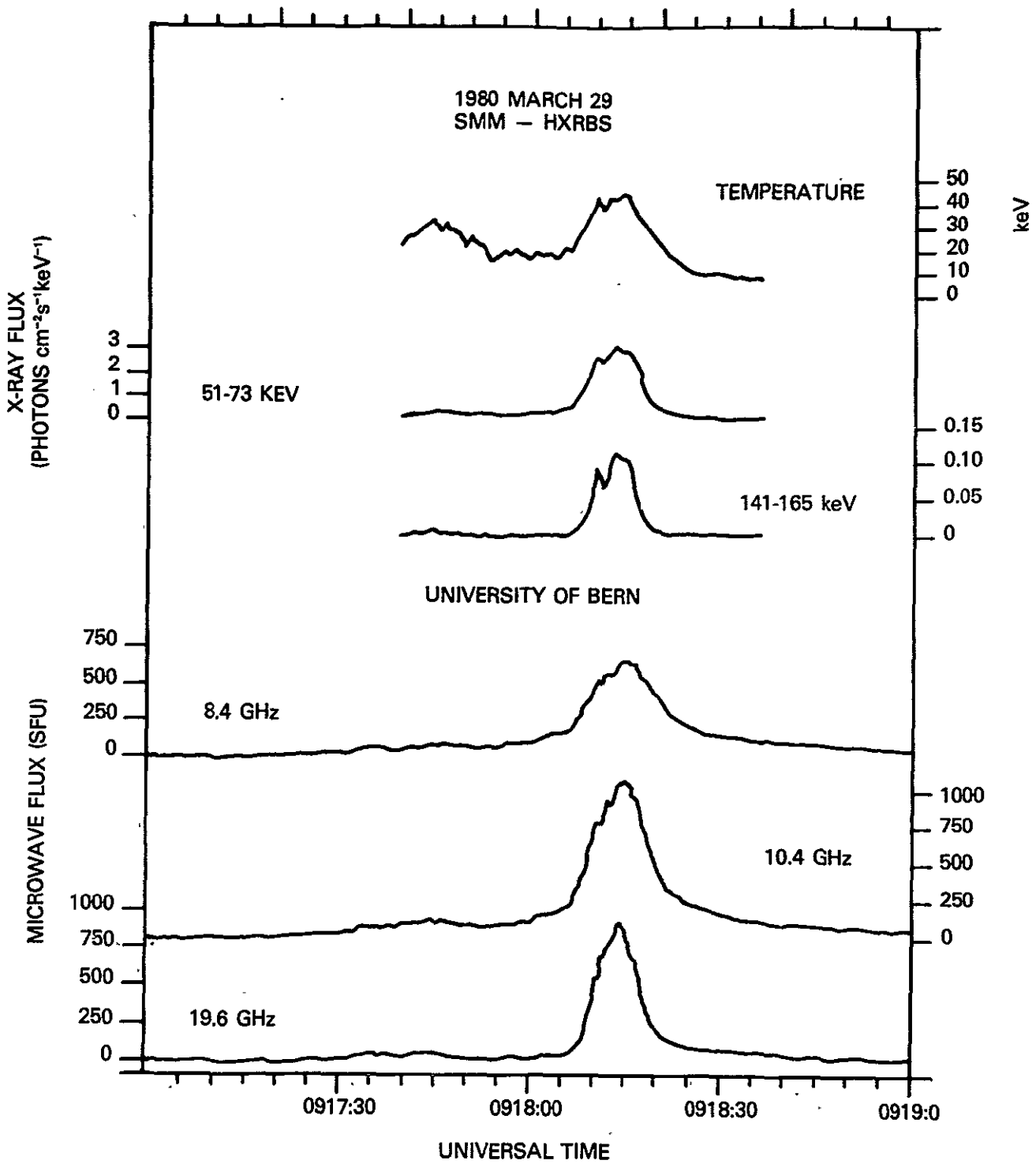


Figure 3

ORIGINAL PAGE IS
OF POOR QUALITY

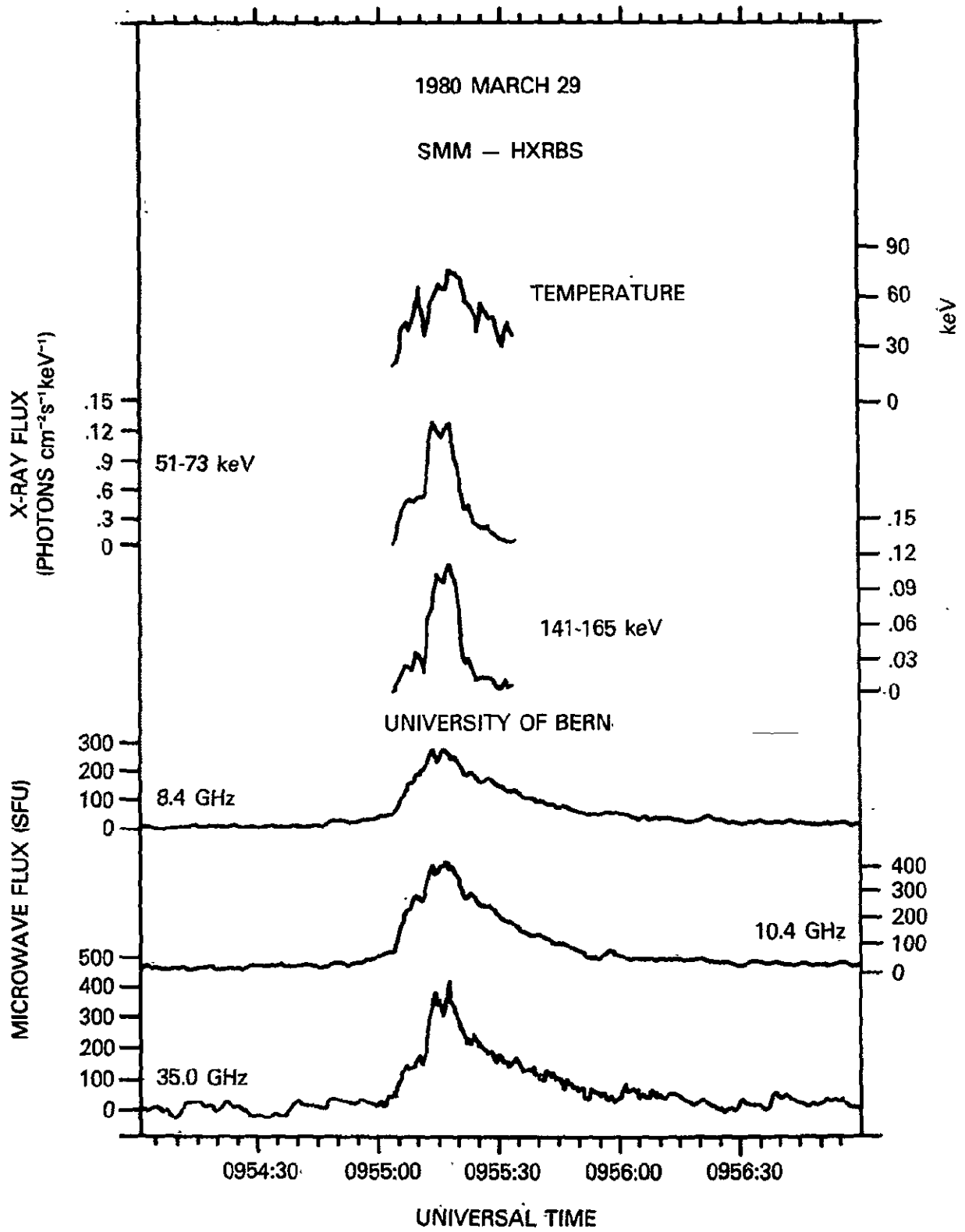


Figure 4

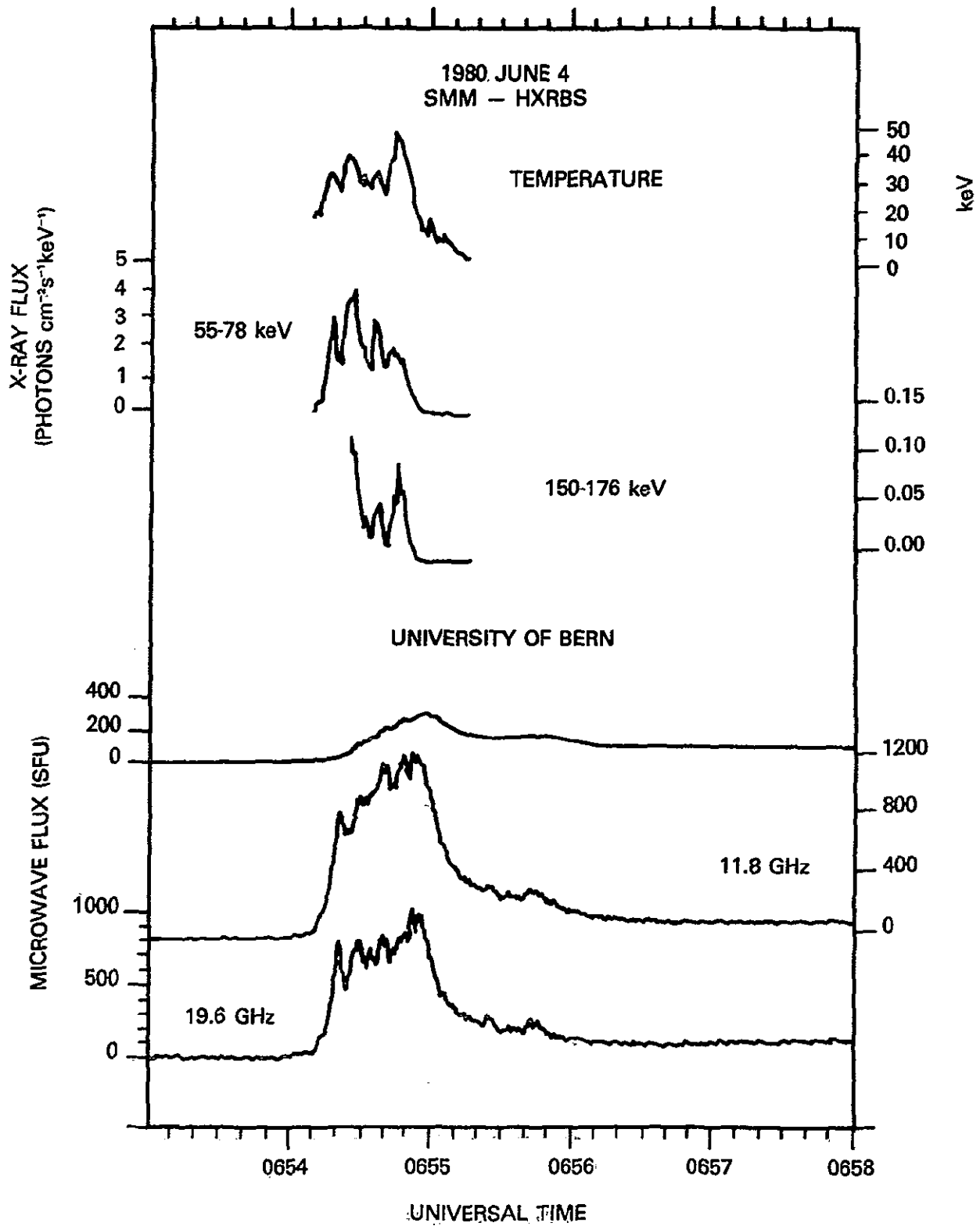


Figure 5

ORIGINAL PAGE IS
OF POOR QUALITY

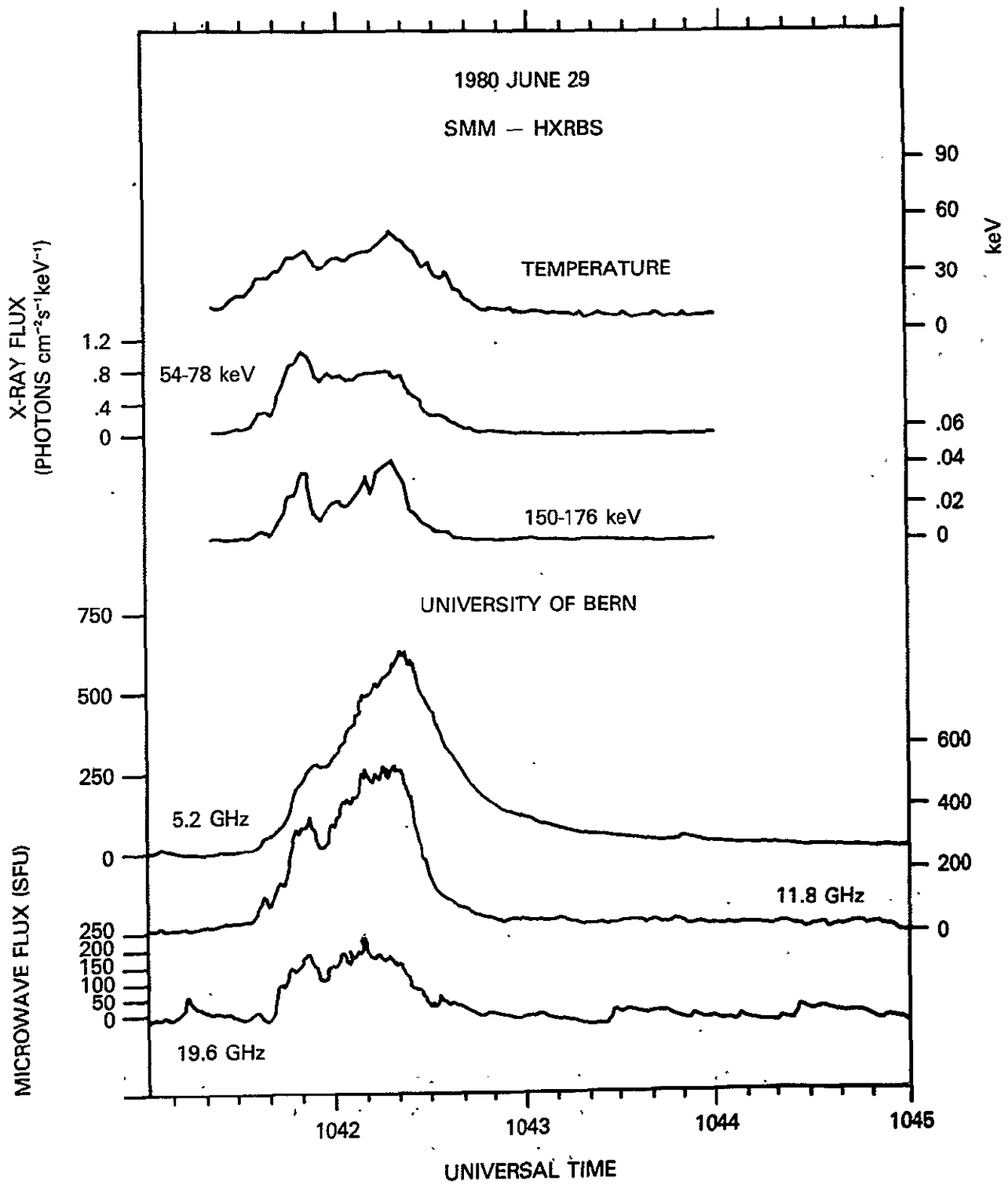


Figure 6

ORIGINAL PAGE IS
OF POOR QUALITY

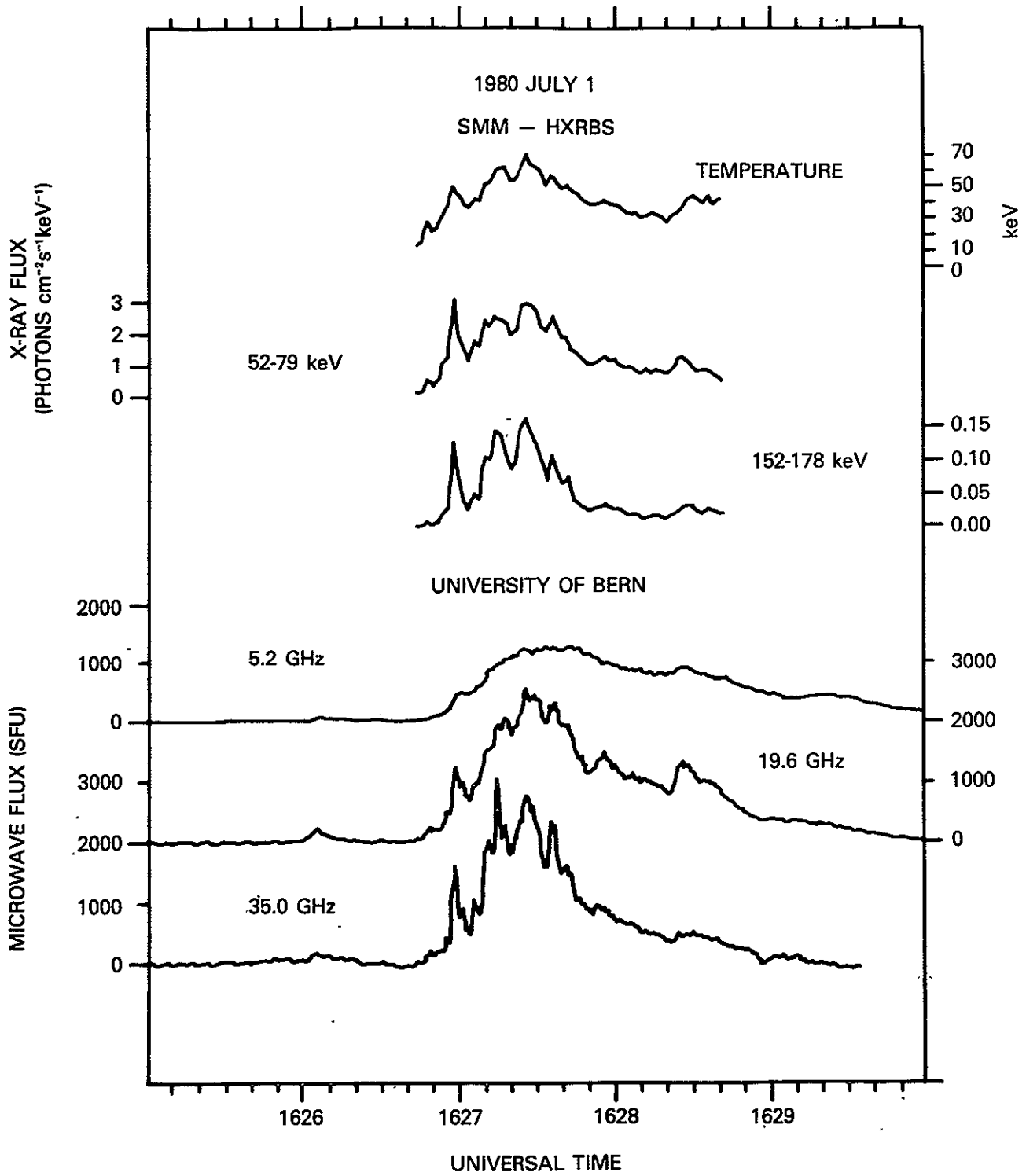


Figure 7

ORIGINAL PAGE IS
OF POOR QUALITY

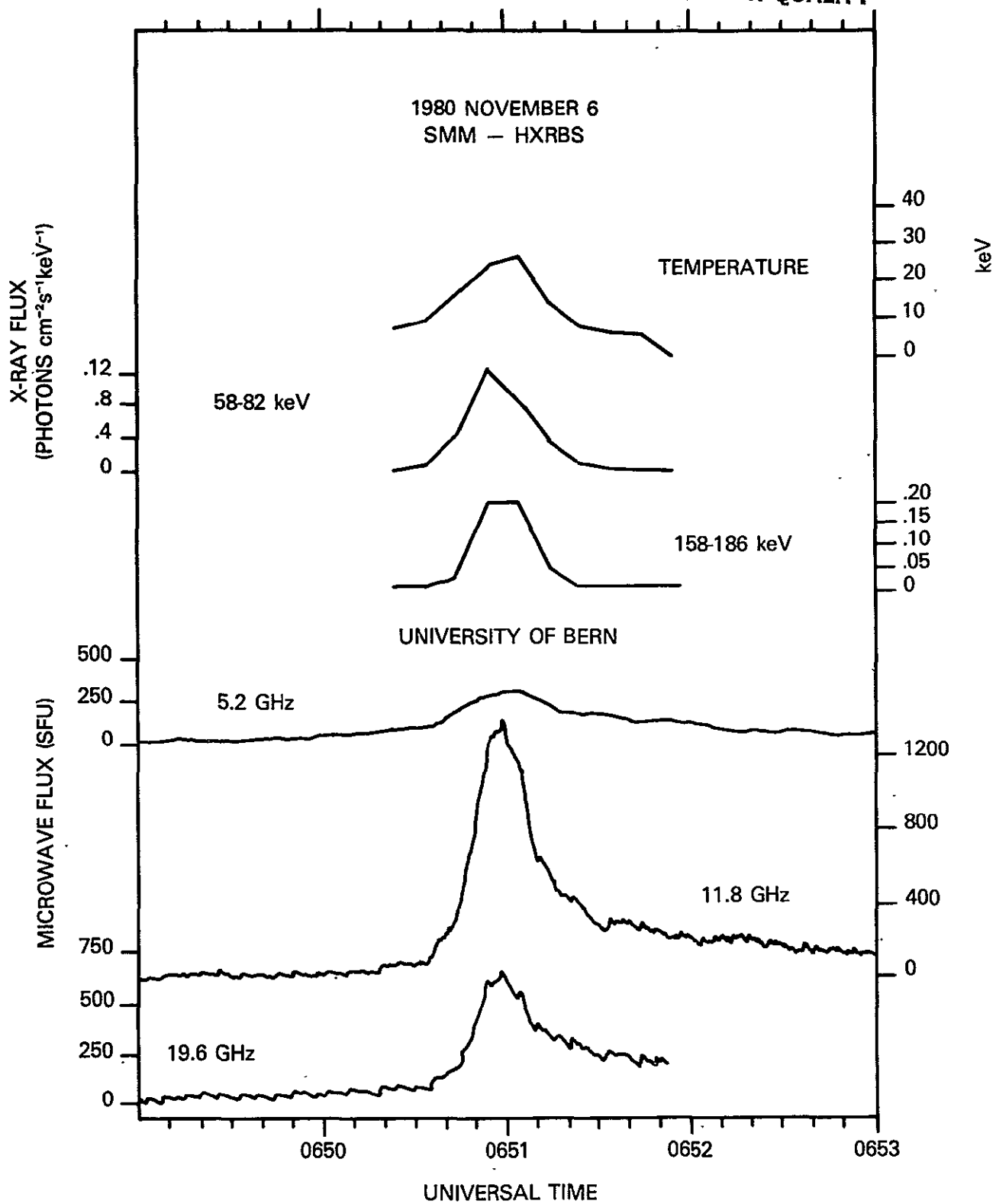


Figure 8 ORIGINAL PAGE IS OF POOR QUALITY

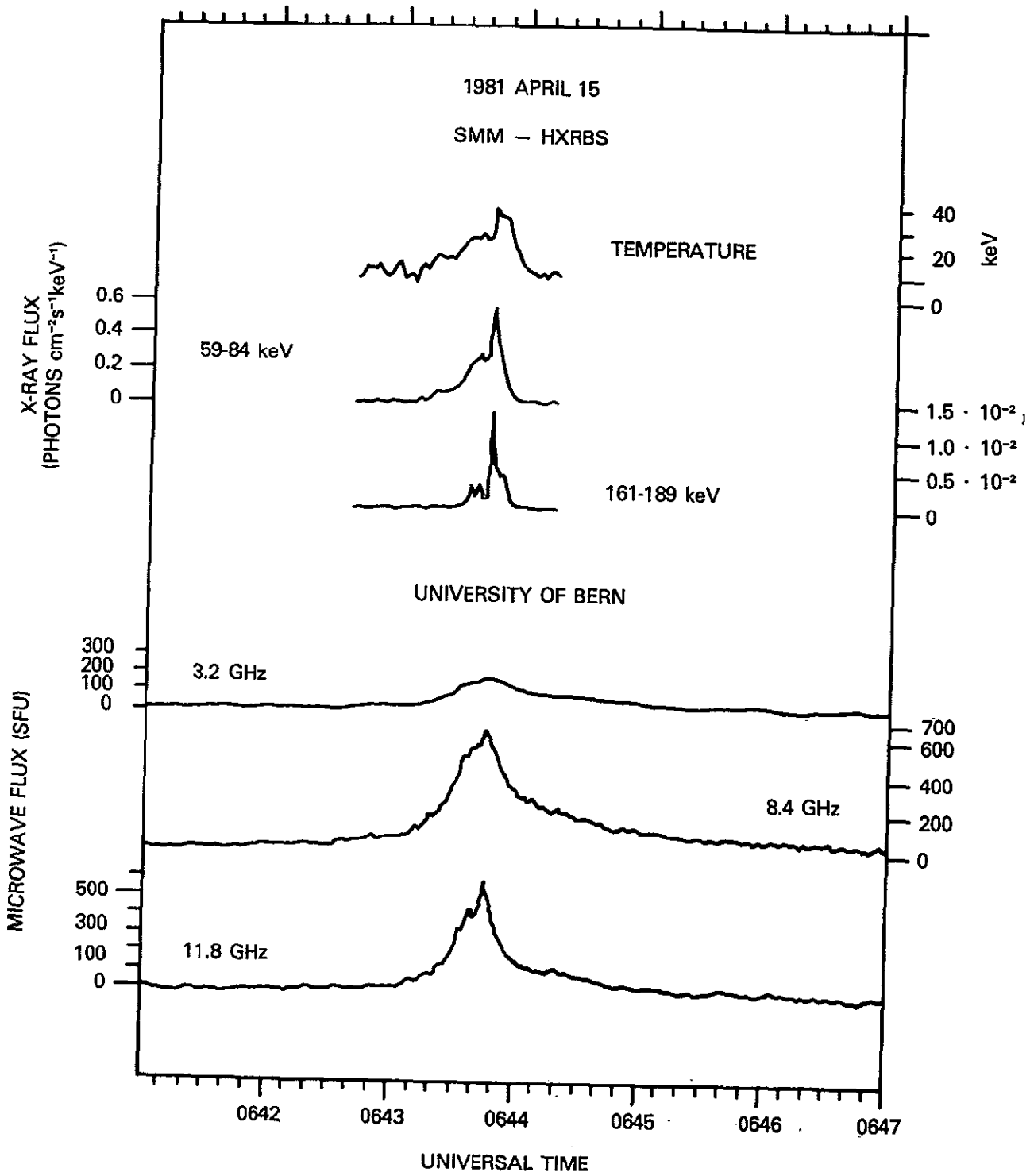


Figure 9

ORIGINAL PAGE IS
OF POOR QUALITY

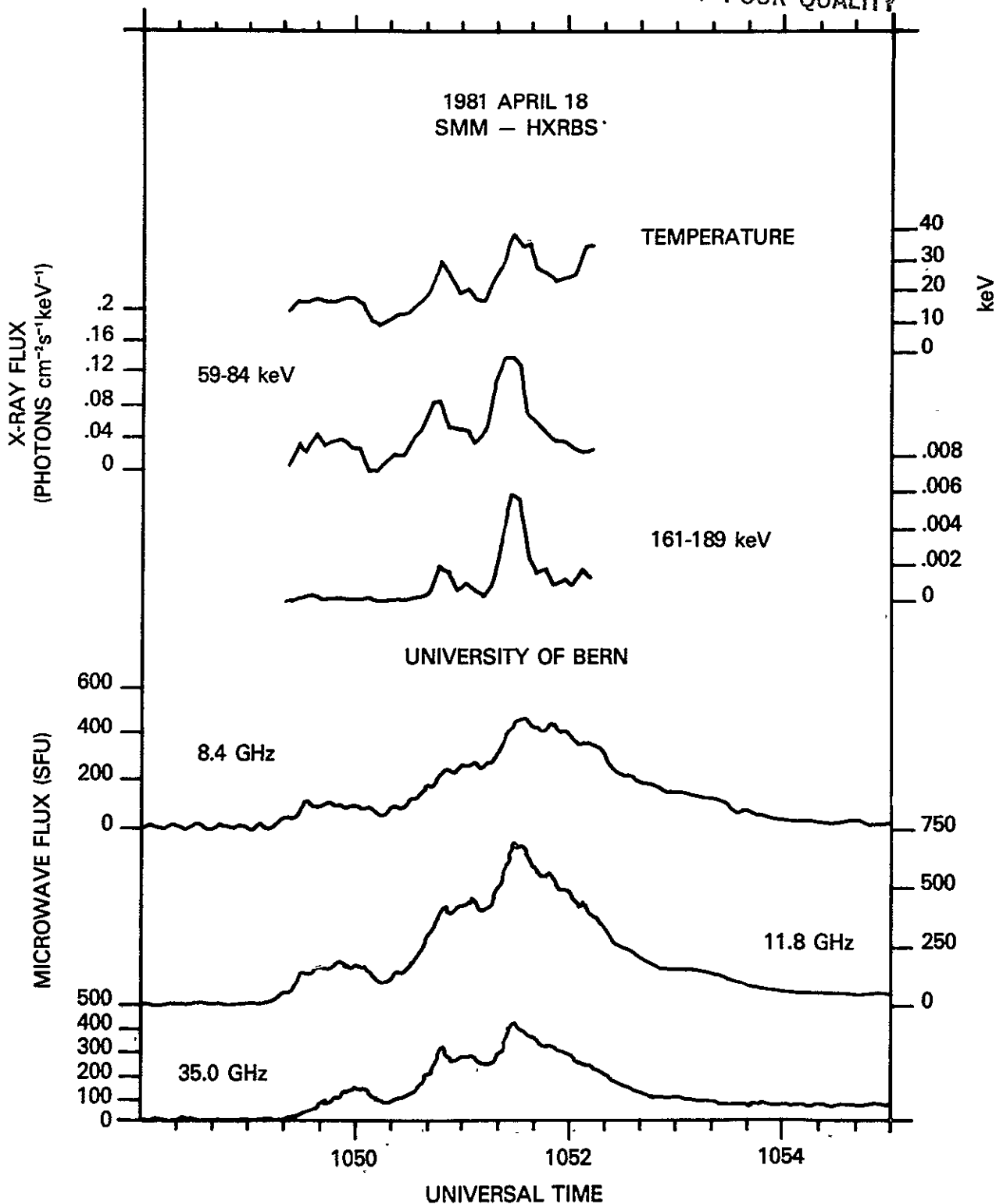


Figure 10

ORIGINAL PAGE IS
OF POOR QUALITY

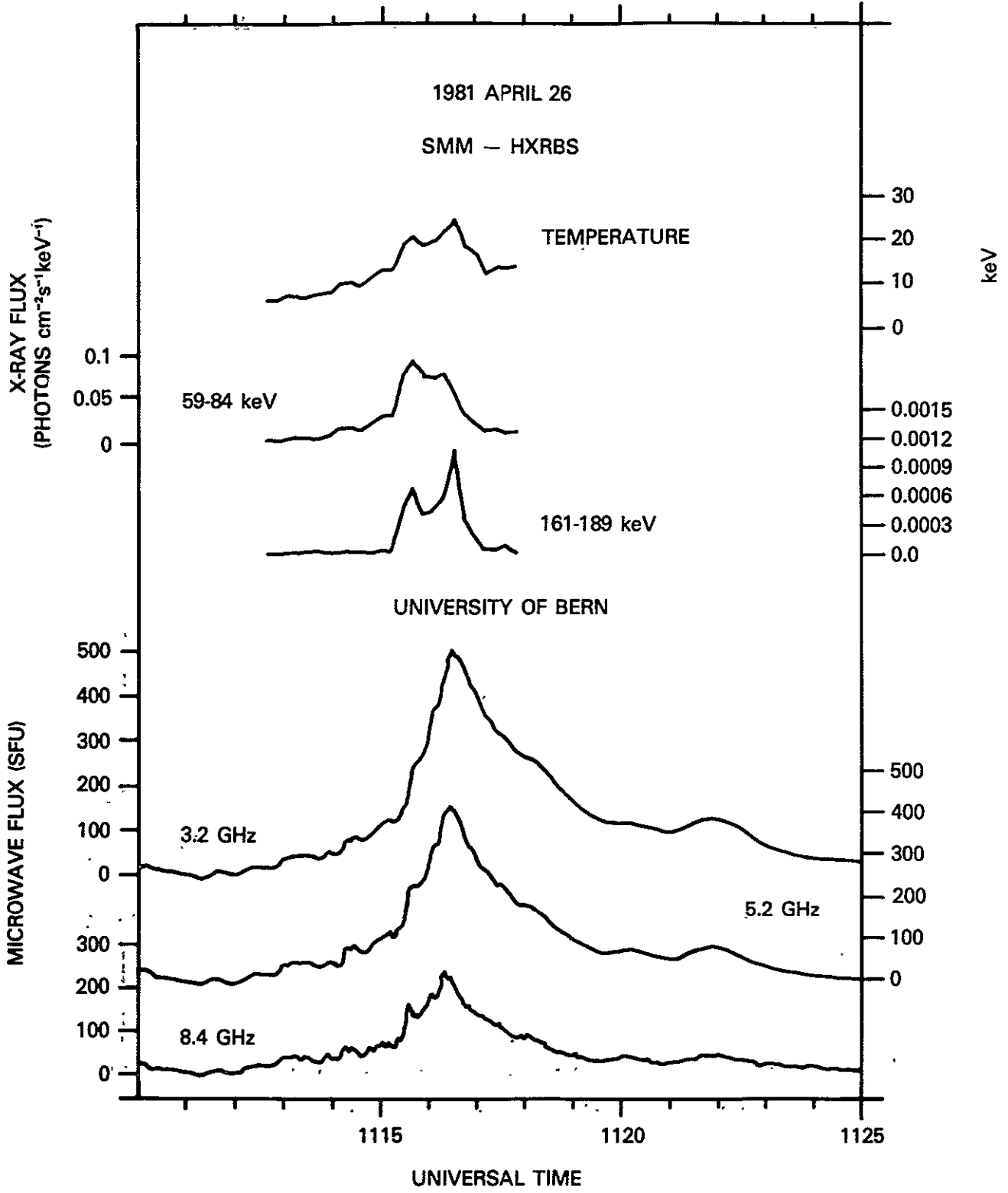


Figure 11

ORIGINAL PAGE IS
OF POOR QUALITY

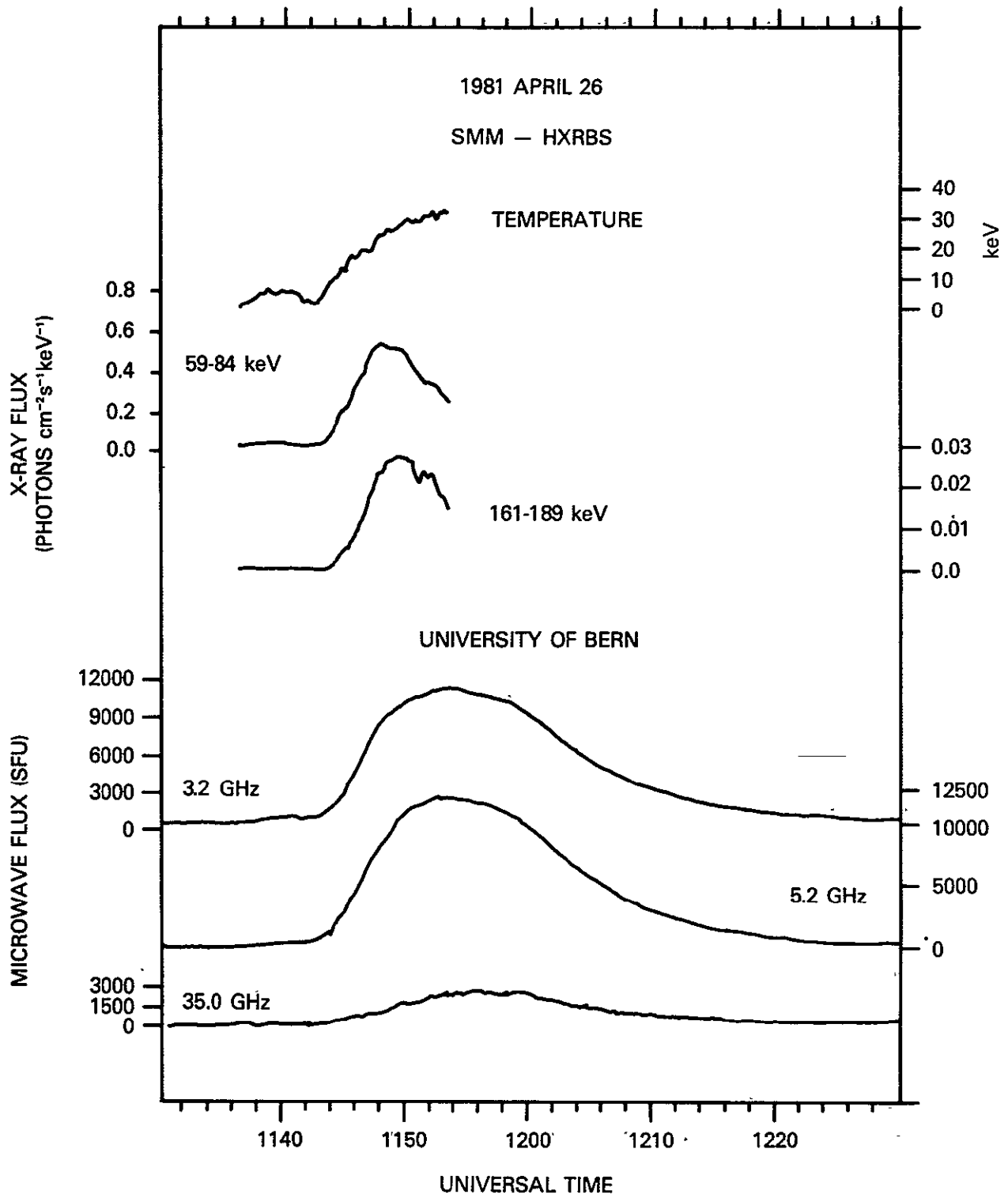


Figure 12

ORIGINAL PAGE IS
OF POOR QUALITY

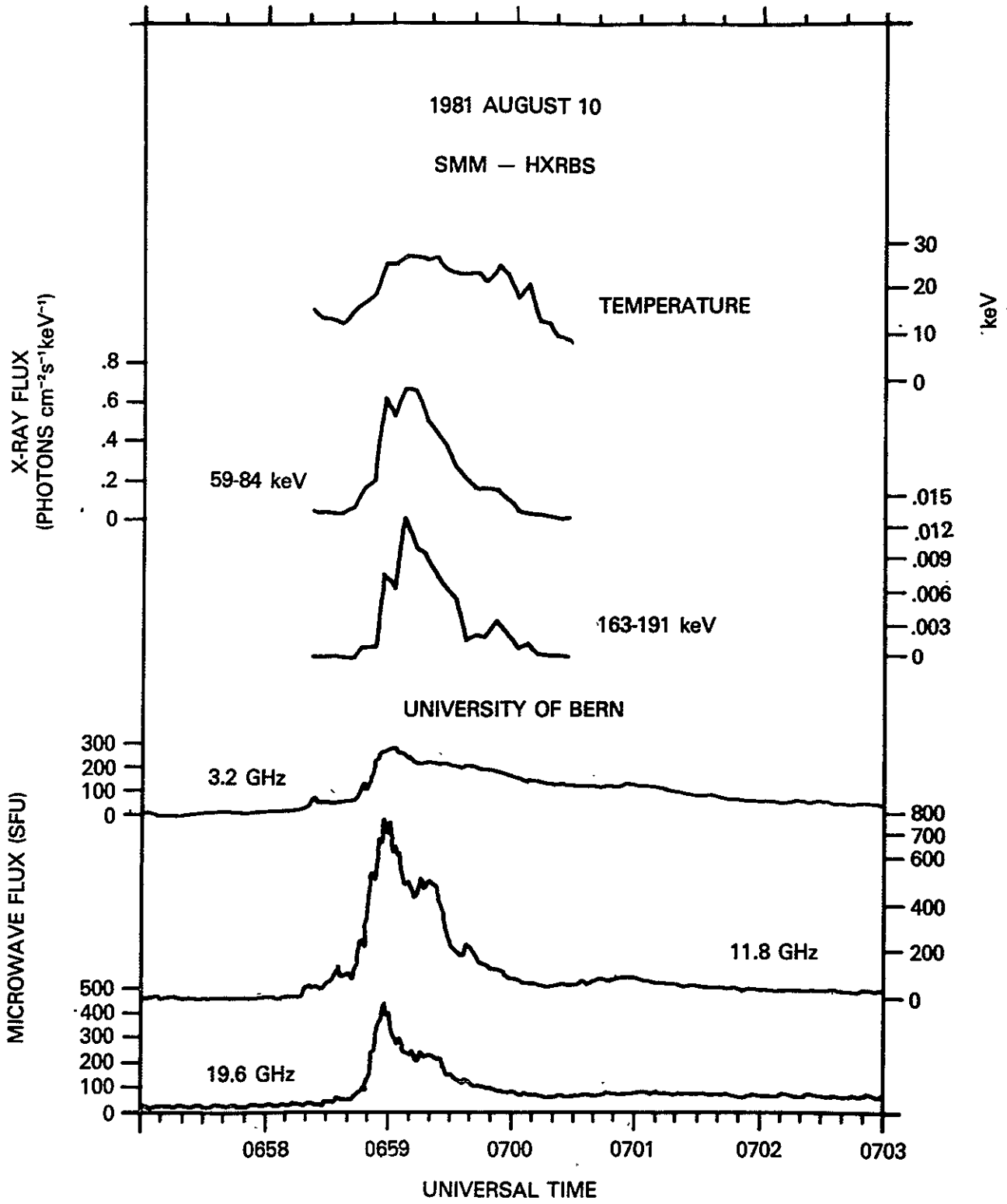
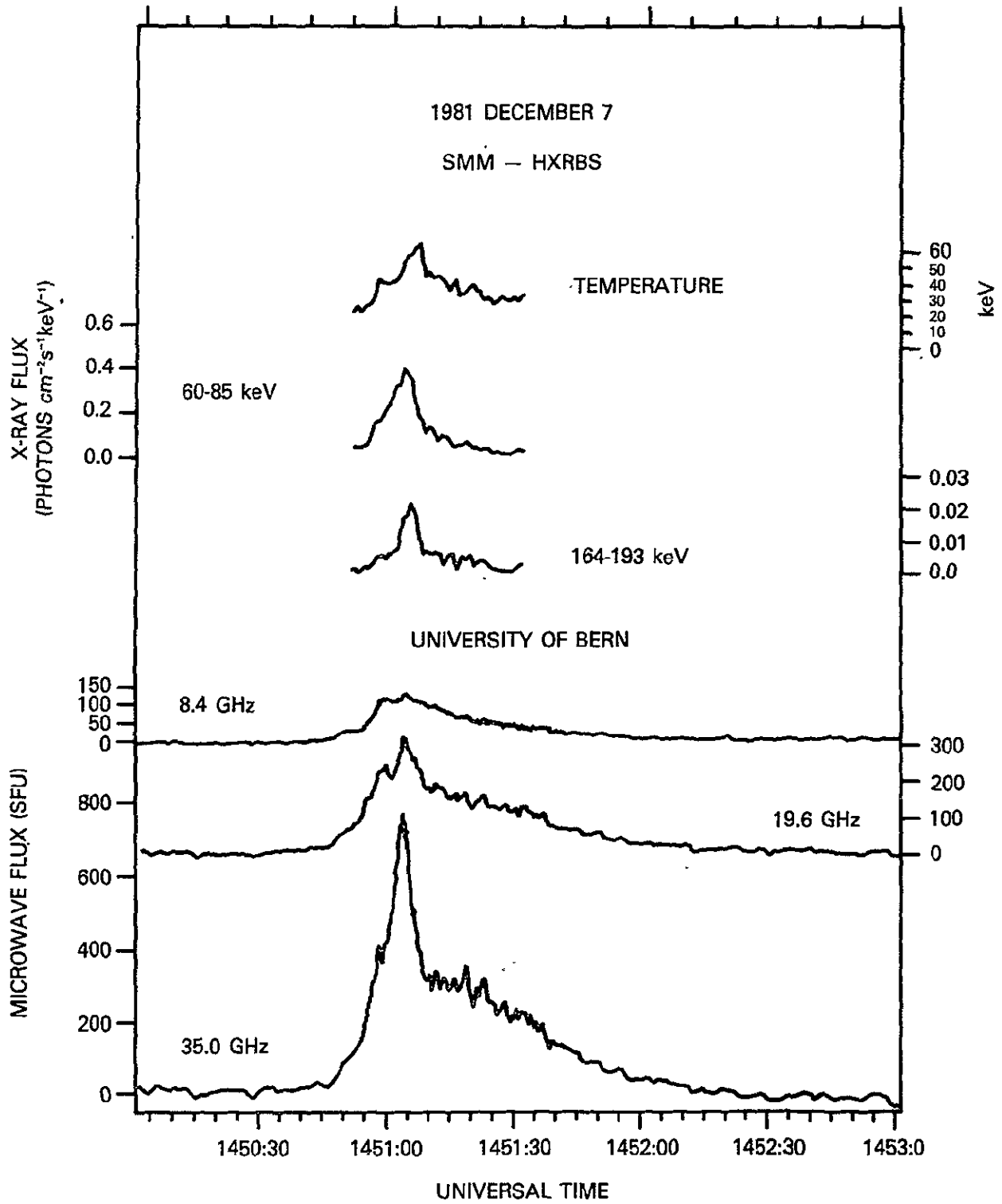


Figure 13

ORIGINAL PAGE IS
OF POOR QUALITY



MICROWAVE CHARACTERISTIC TIME

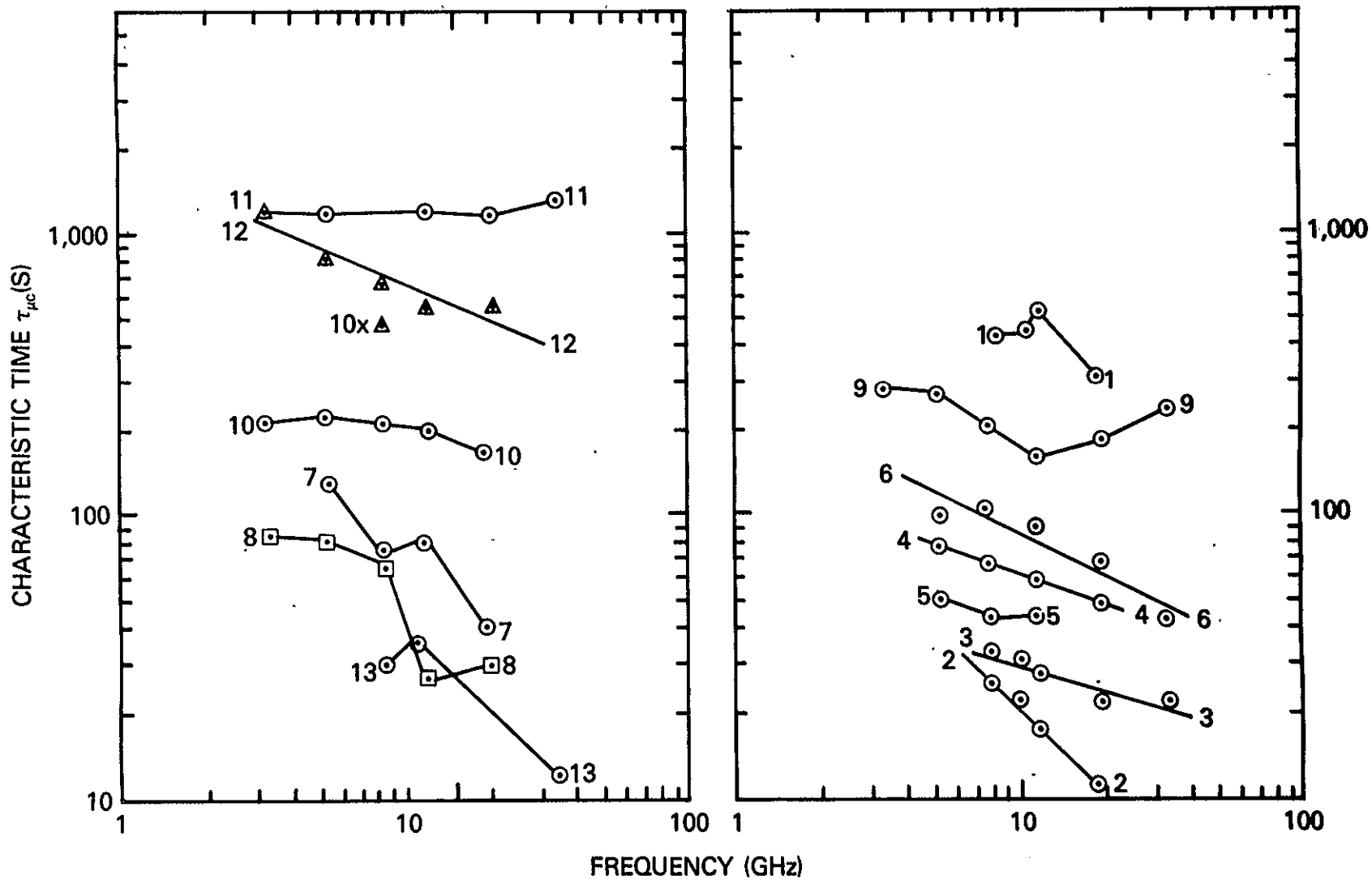


Figure 14

ORIGINAL PAGE IS
OF POOR QUALITY

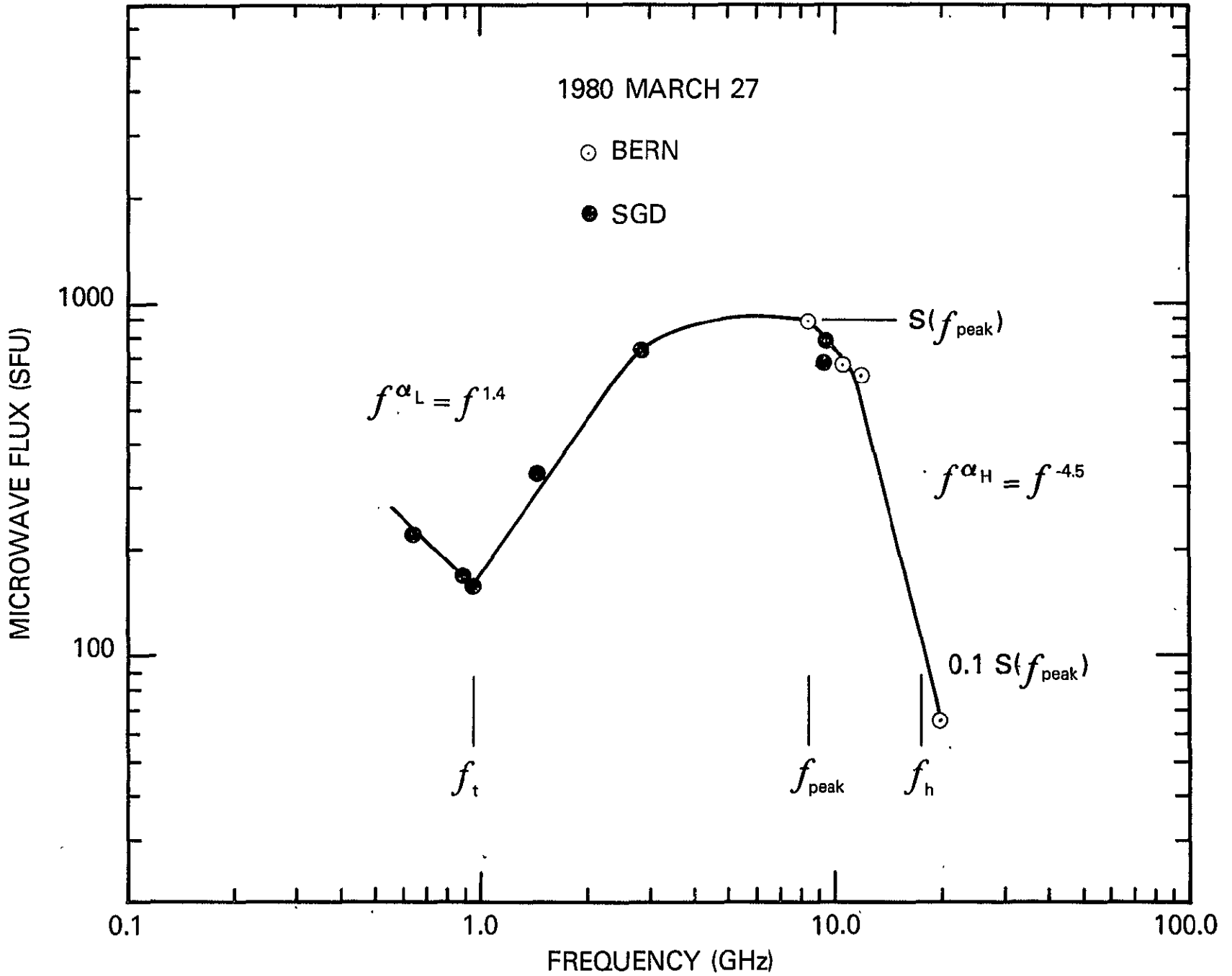


Figure 15

ORIGINAL PAGE IS
OF POOR QUALITY

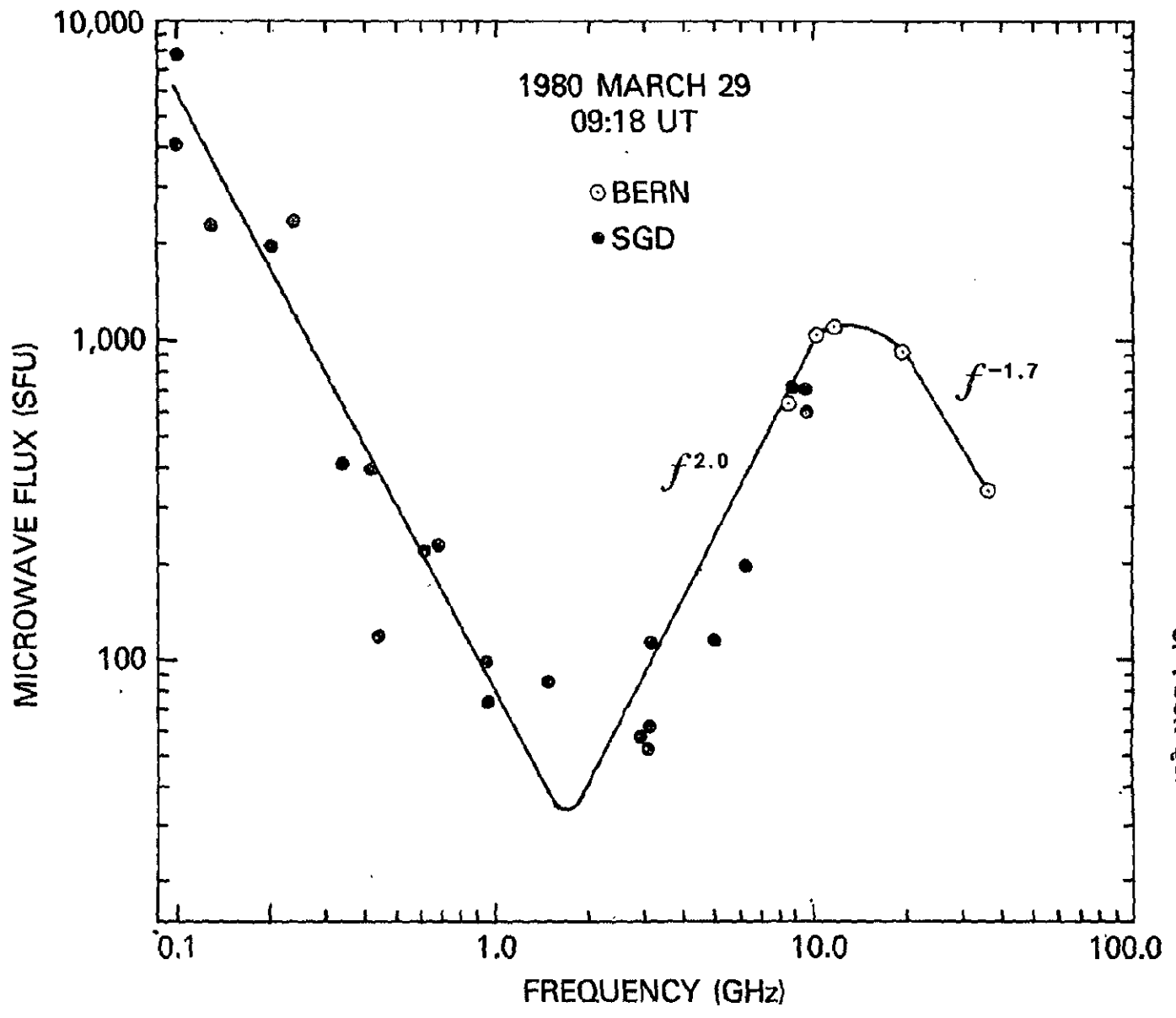


Figure 16
ORIGINAL PAGE IS
OF POOR QUALITY

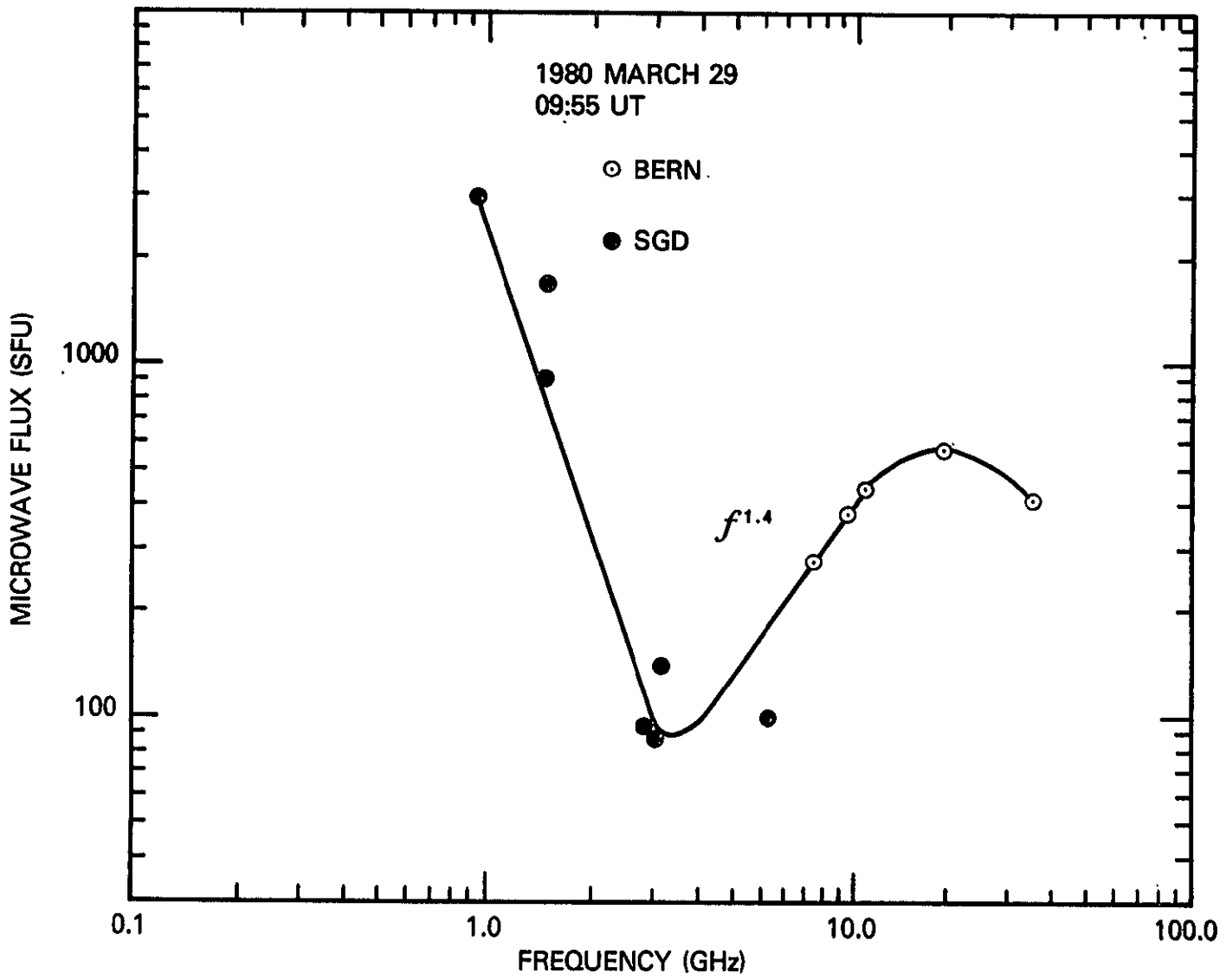


Figure 17

ORIGINAL PAGE IS
OF POOR QUALITY

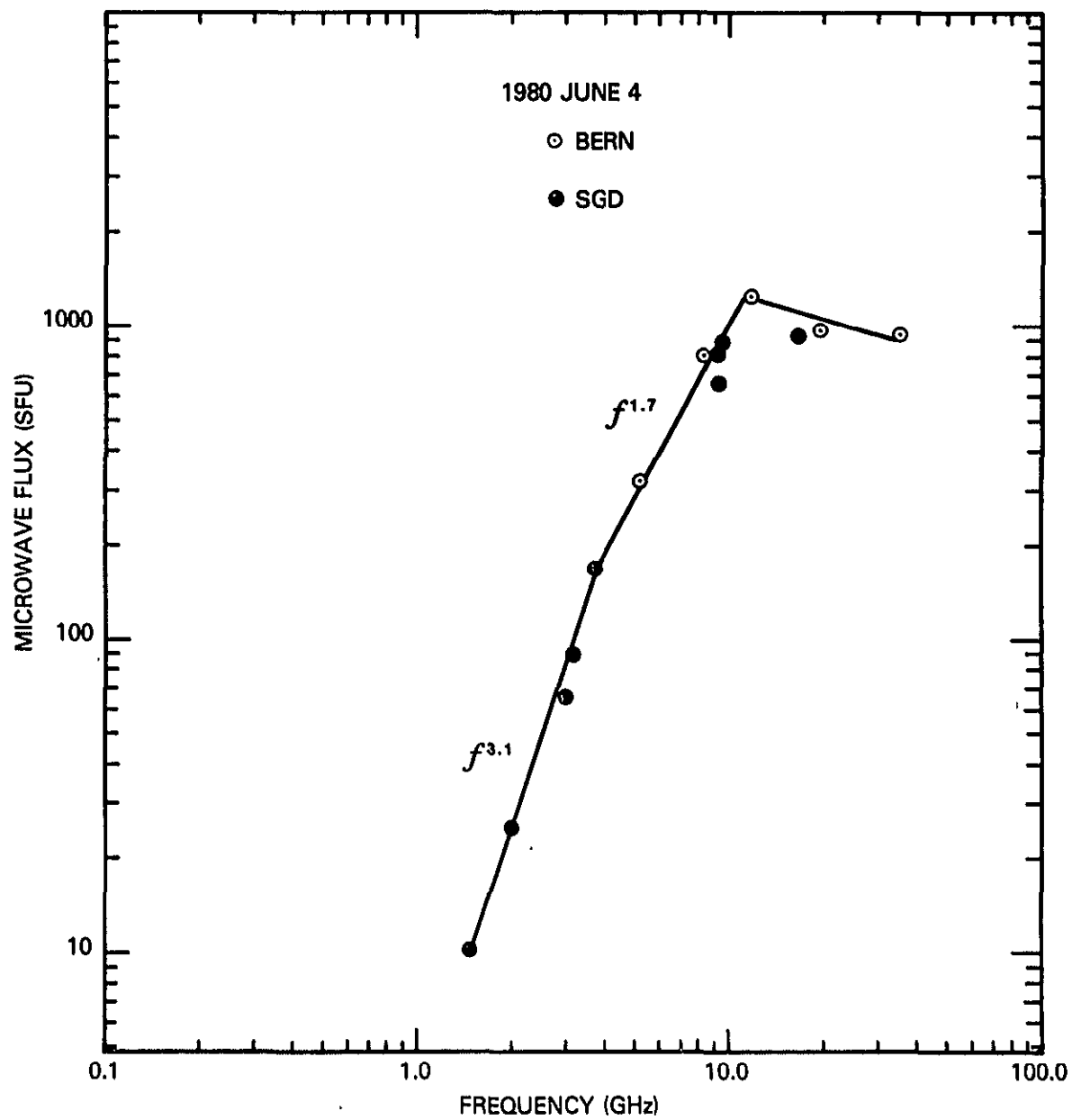


Figure 18

ORIGINAL PAGE IS
OF POOR QUALITY

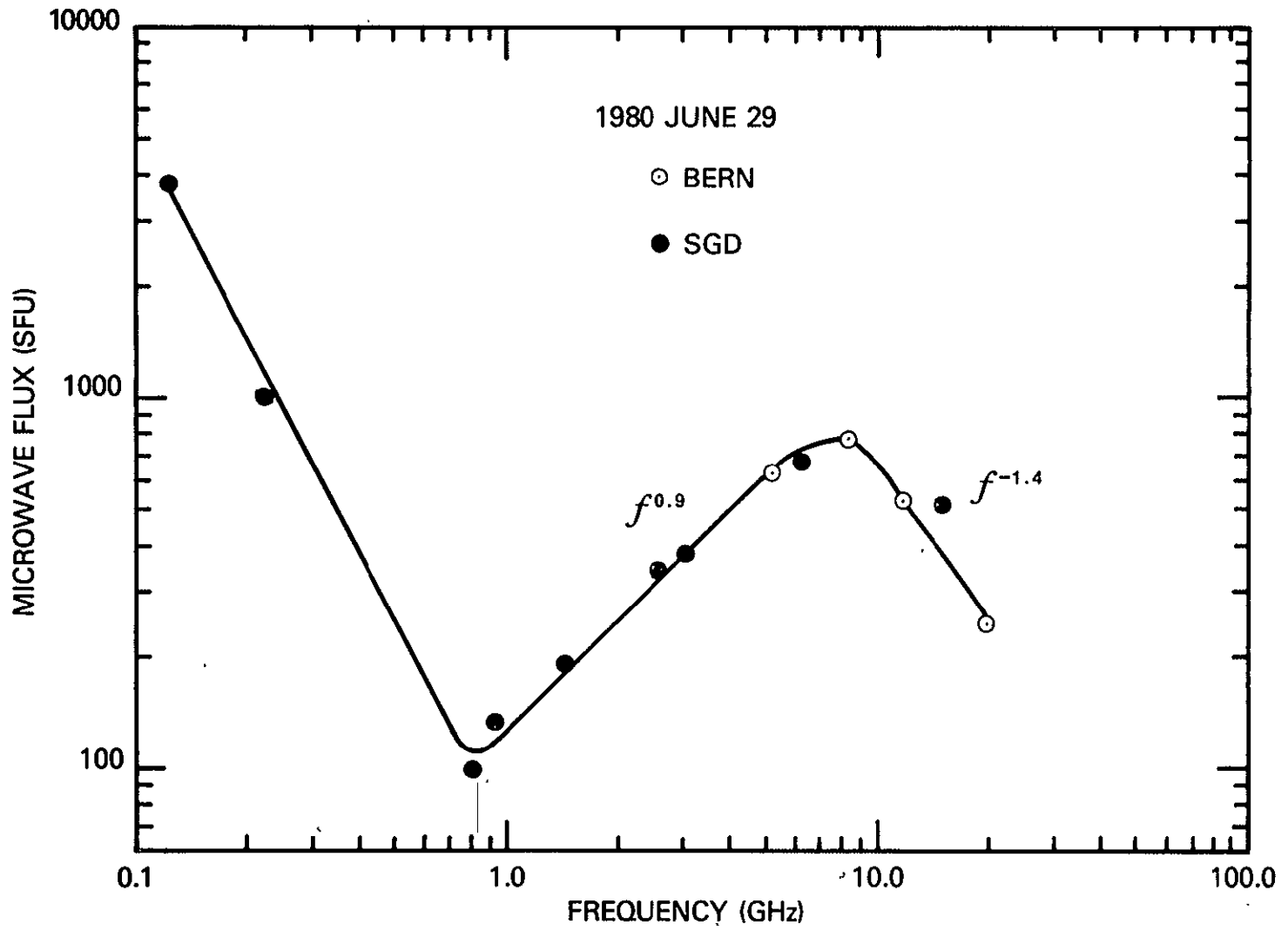


Figure 19
ORIGINAL PAGE IS
OF POOR QUALITY

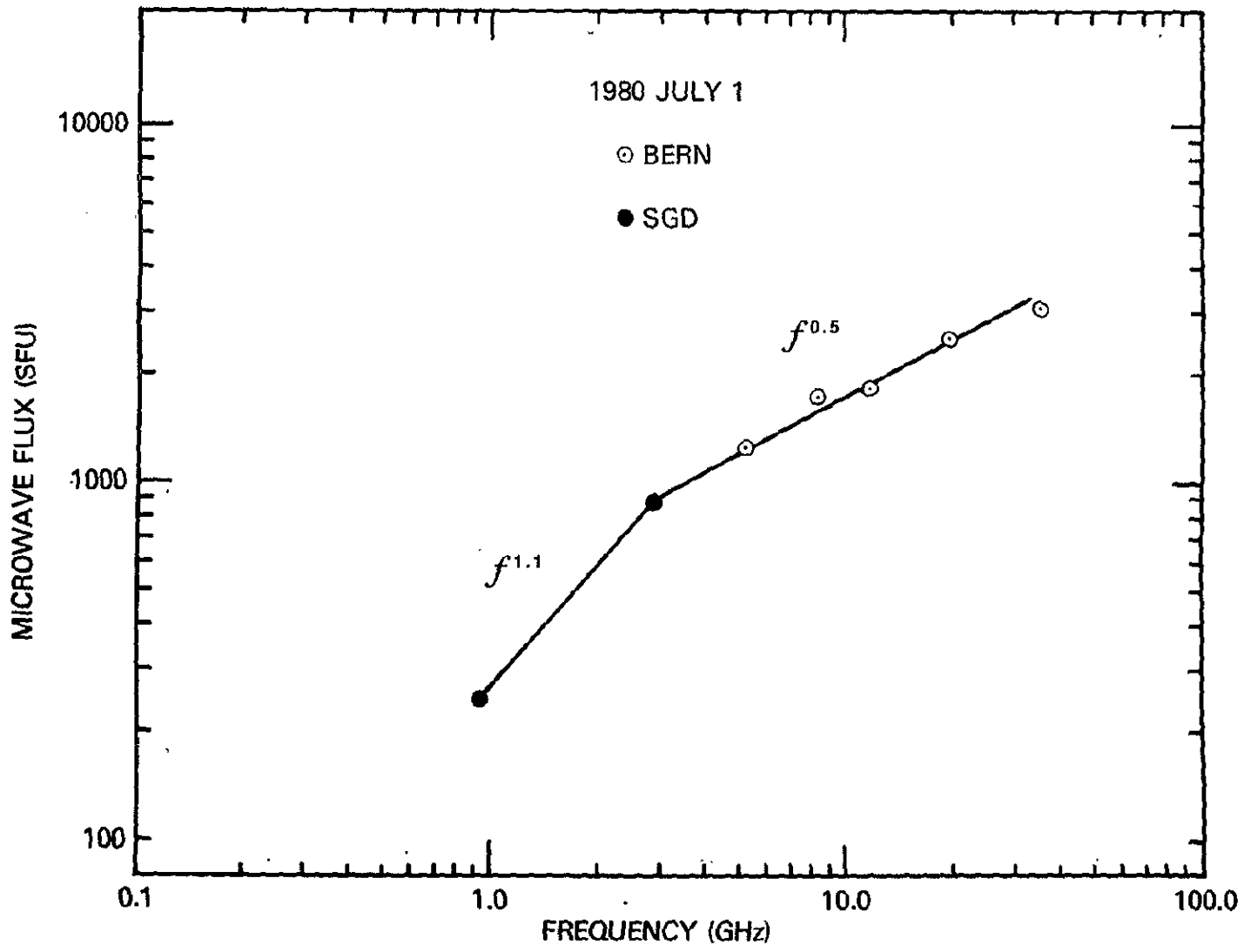
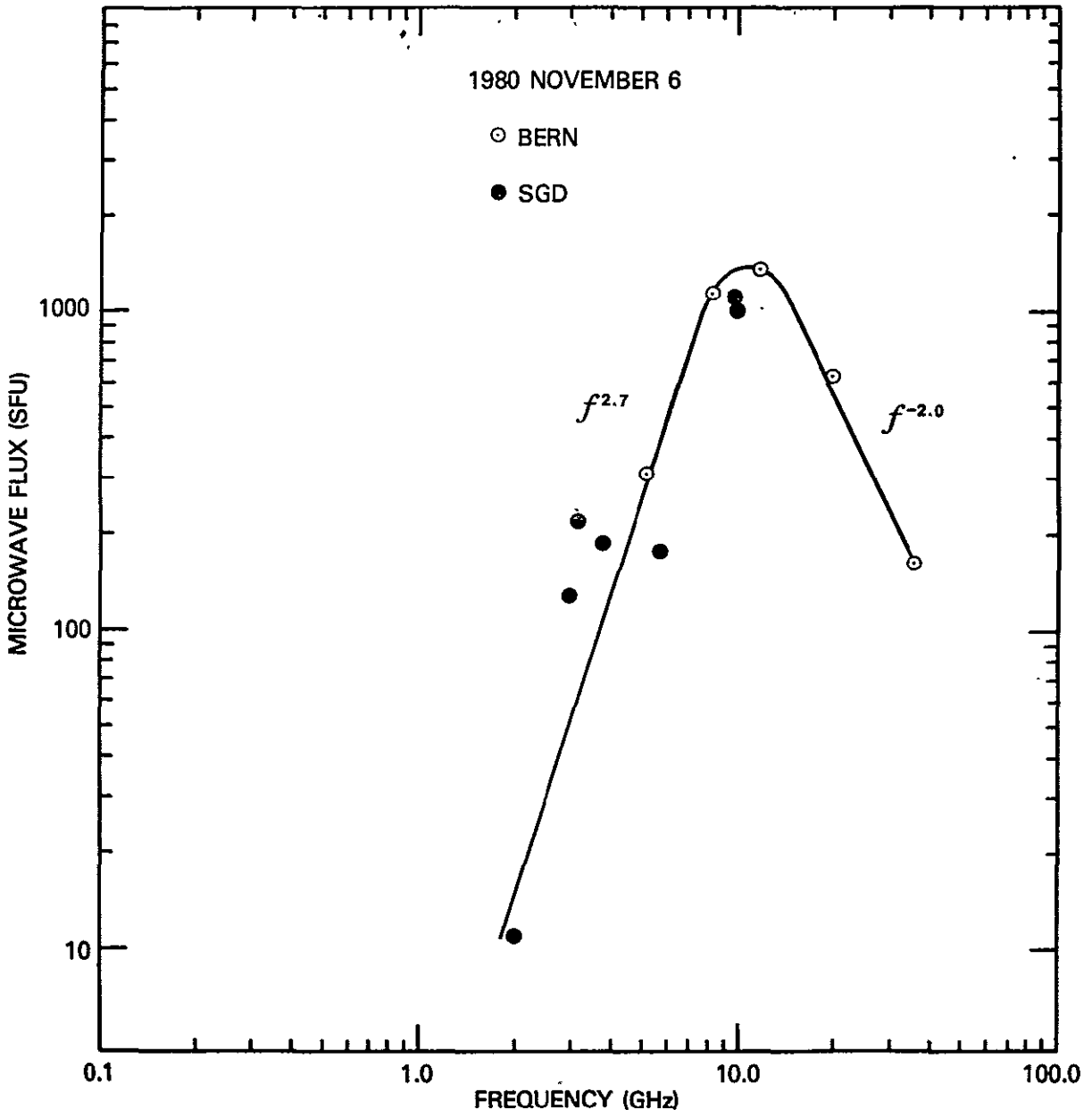


Figure 20

ORIGINAL PAGE IS
OF POOR QUALITY

Figure 21

ORIGINAL PAGE IS
OF POOR QUALITY



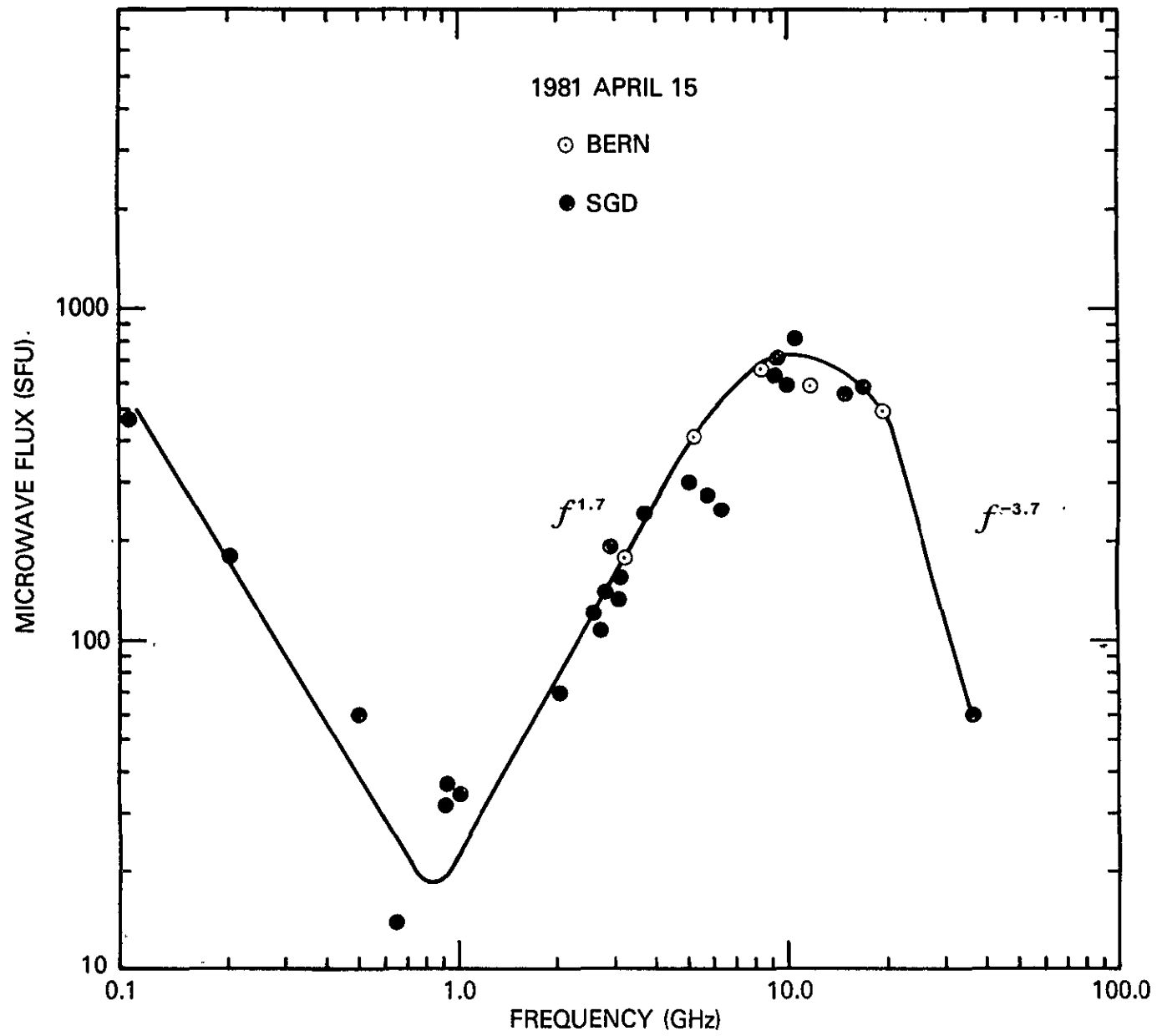


Figure 22

ORIGINAL PAGE IS
OF POOR QUALITY

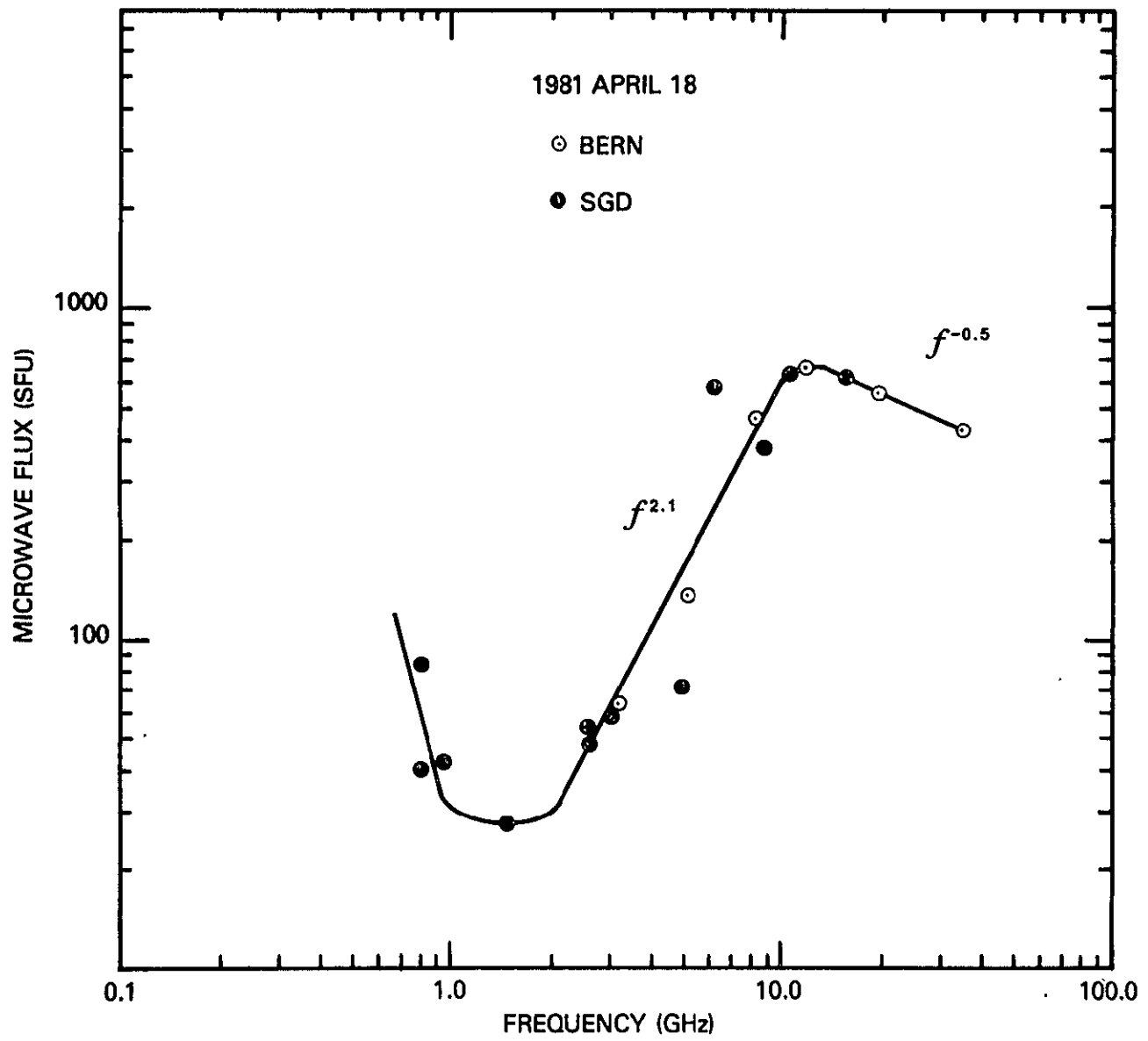


Figure 23

ORIGINAL PAGE IS
OF POOR QUALITY

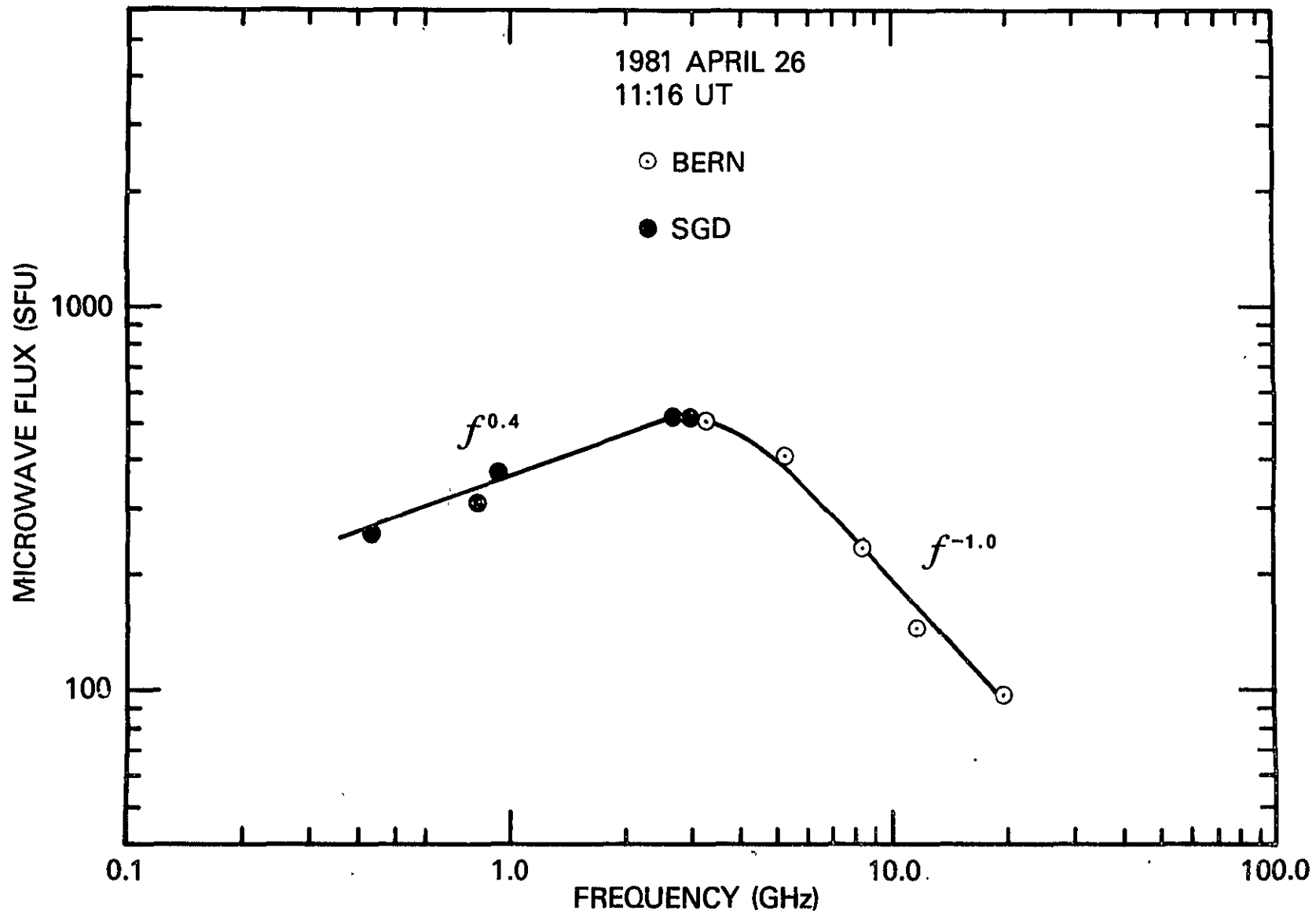


Figure. 24

ORIGINAL PAGE IS
OF POOR QUALITY

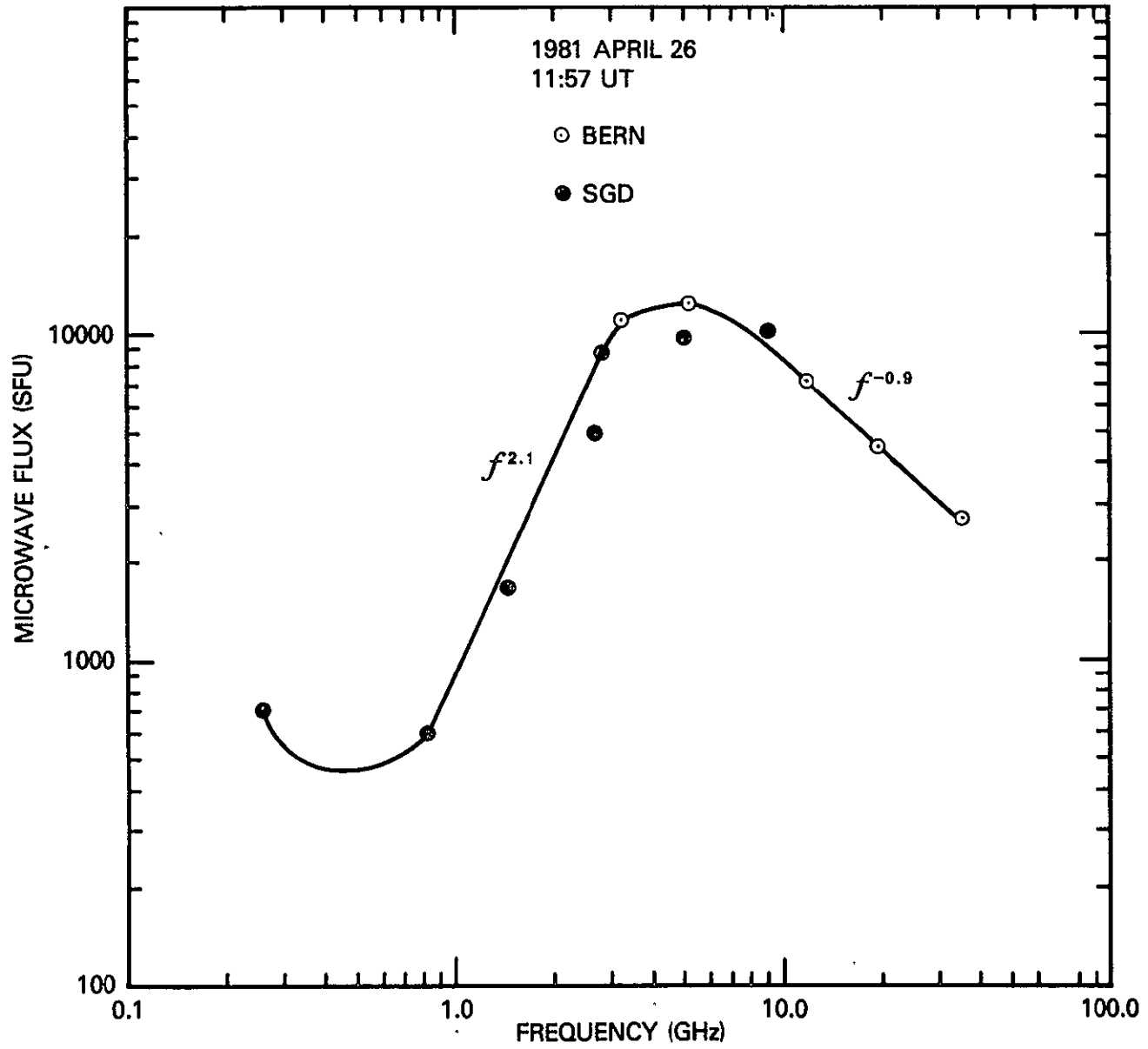


Figure 25

ORIGINAL PAGE IS
OF POOR QUALITY.

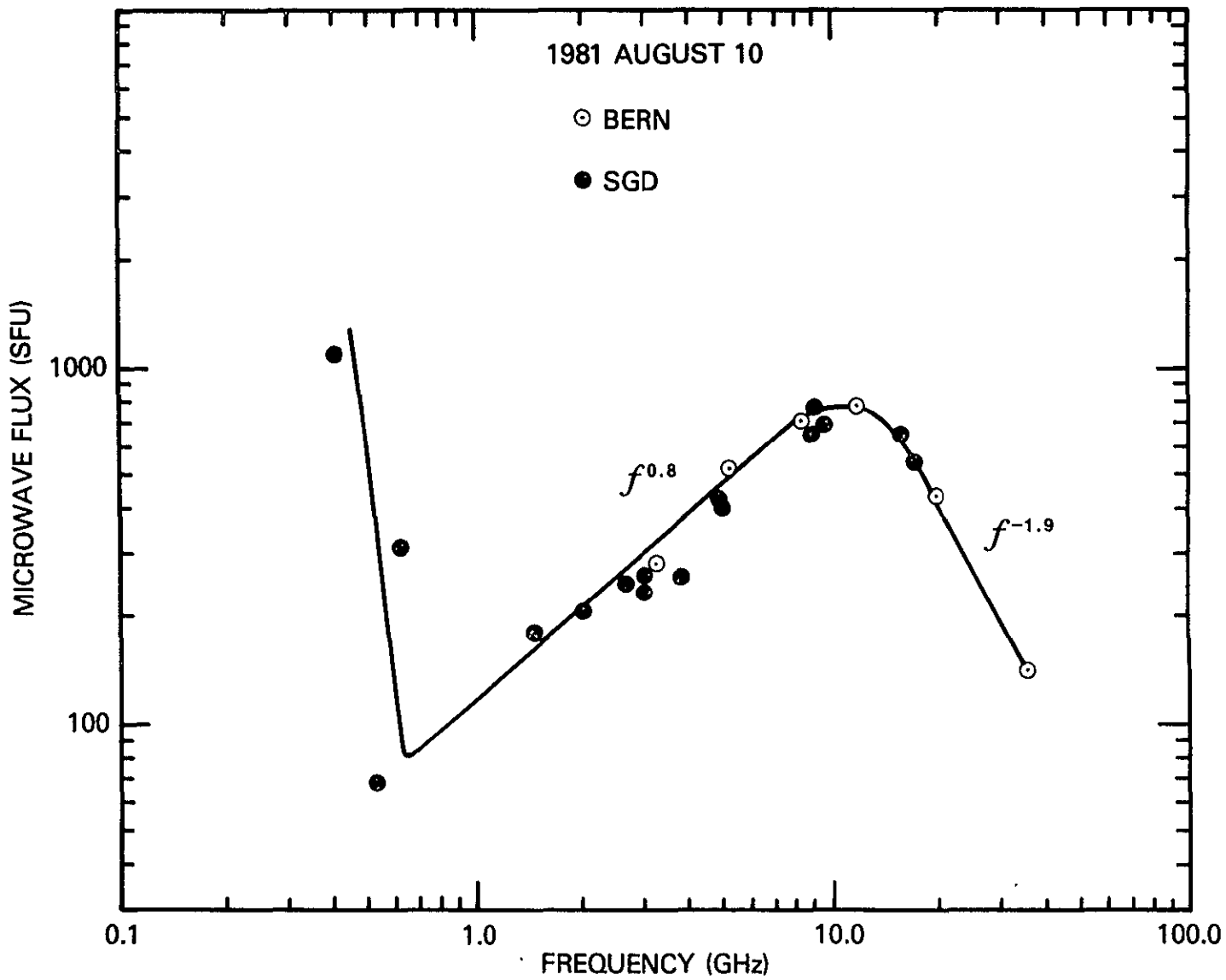


Figure 26

ORIGINAL PAGE IS
OF POOR QUALITY

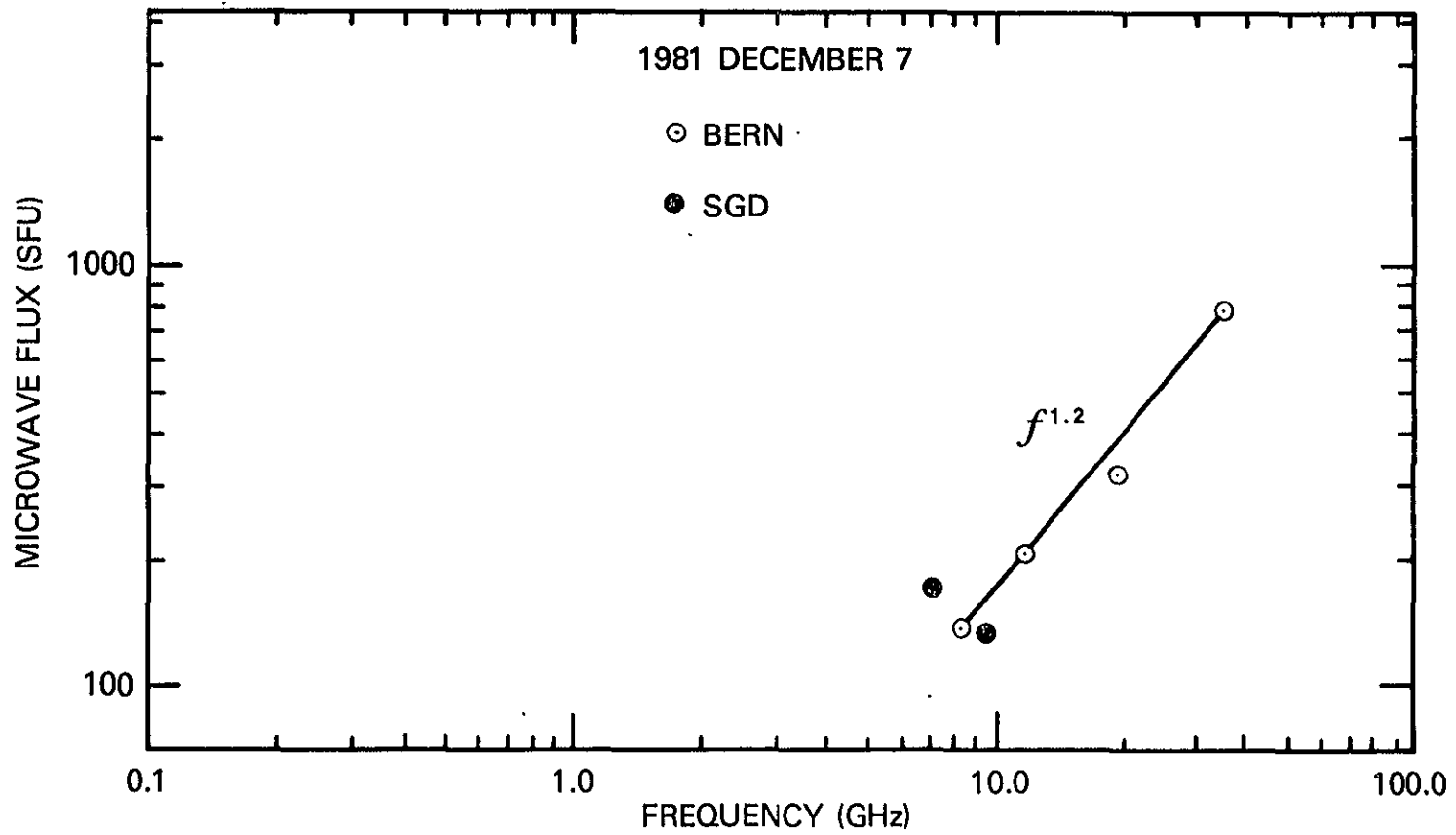


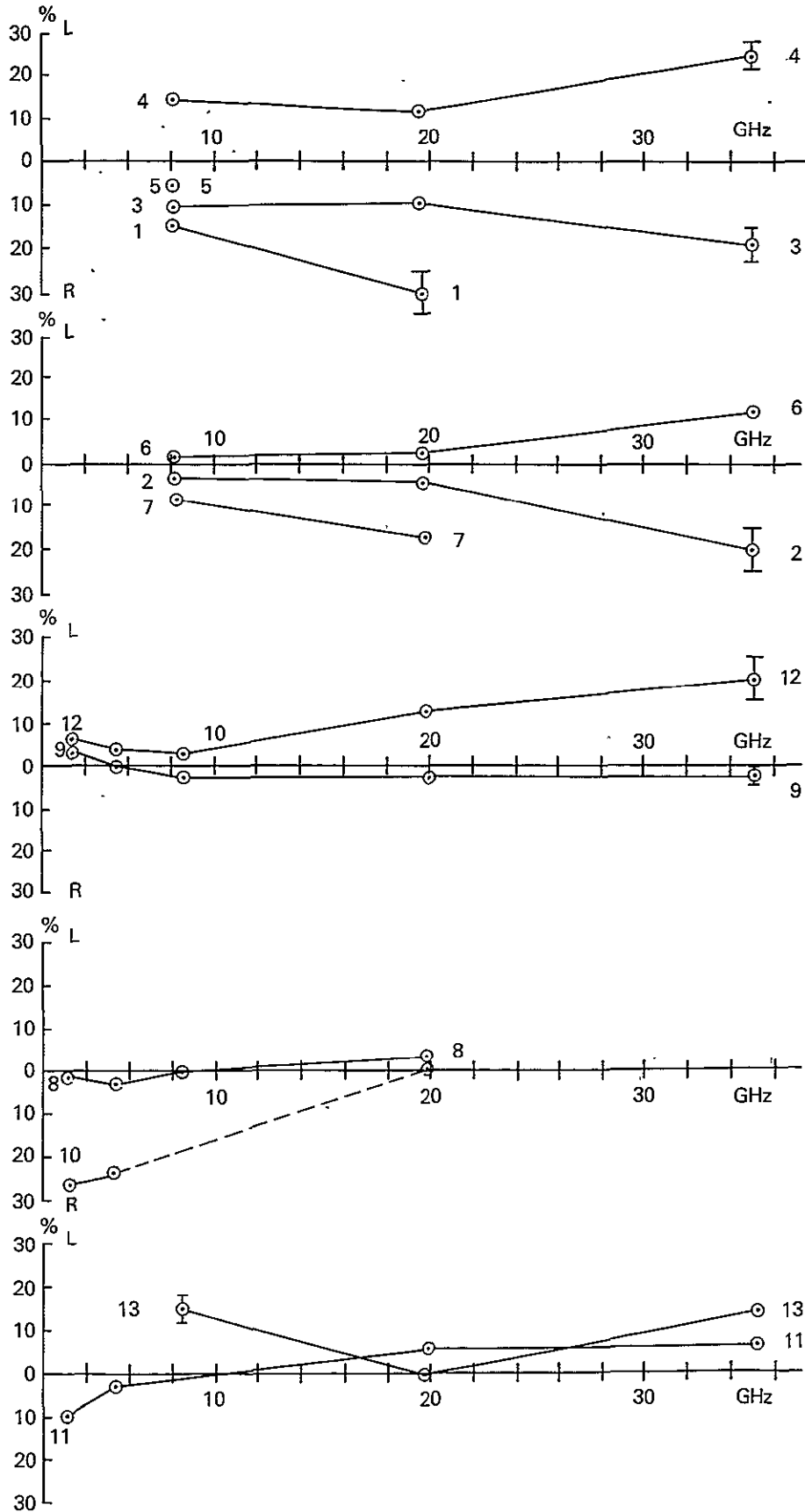
Figure 27

ORIGINAL PAGE IS
OF POOR QUALITY

Figure 28

ORIGINAL PAGE IS
OF POOR QUALITY

MICROWAVE POLARIZATION



HARD X-RAY CHARACTERISTIC TIMES

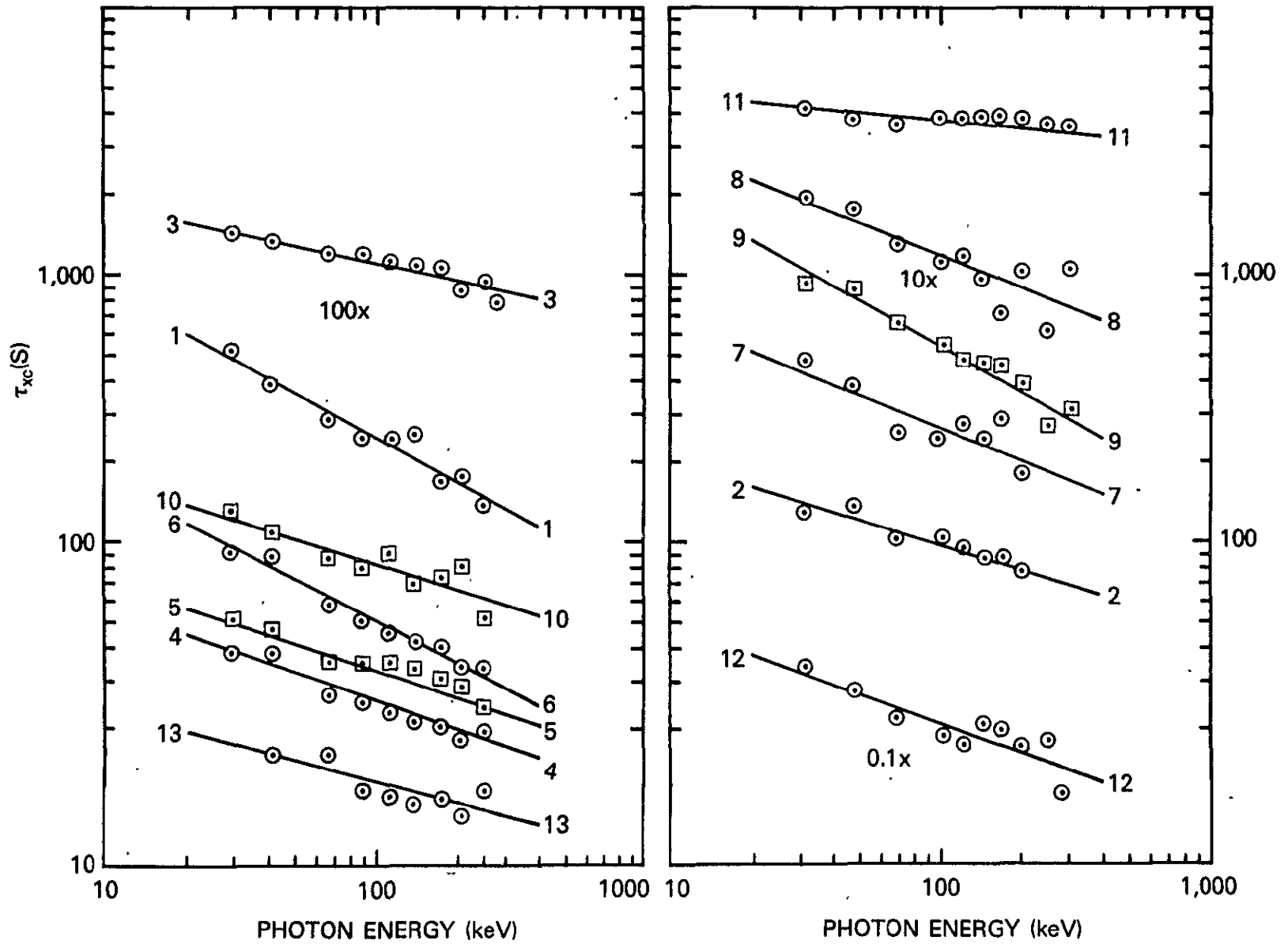


Figure 29

ORIGINAL PAGE IS
OF POOR QUALITY

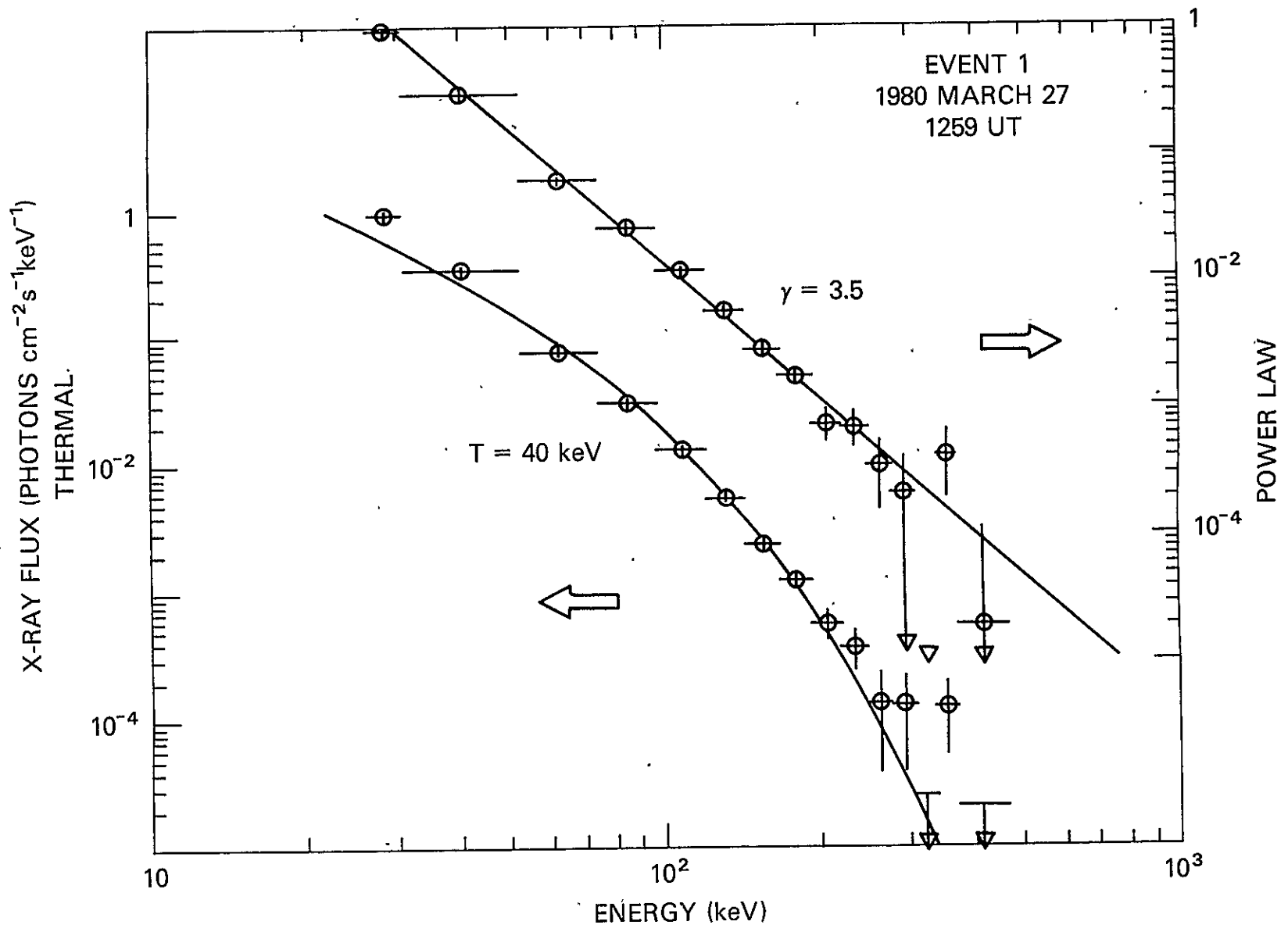


Figure 30

ORIGINAL PAGE IS
OF POOR QUALITY

C-2

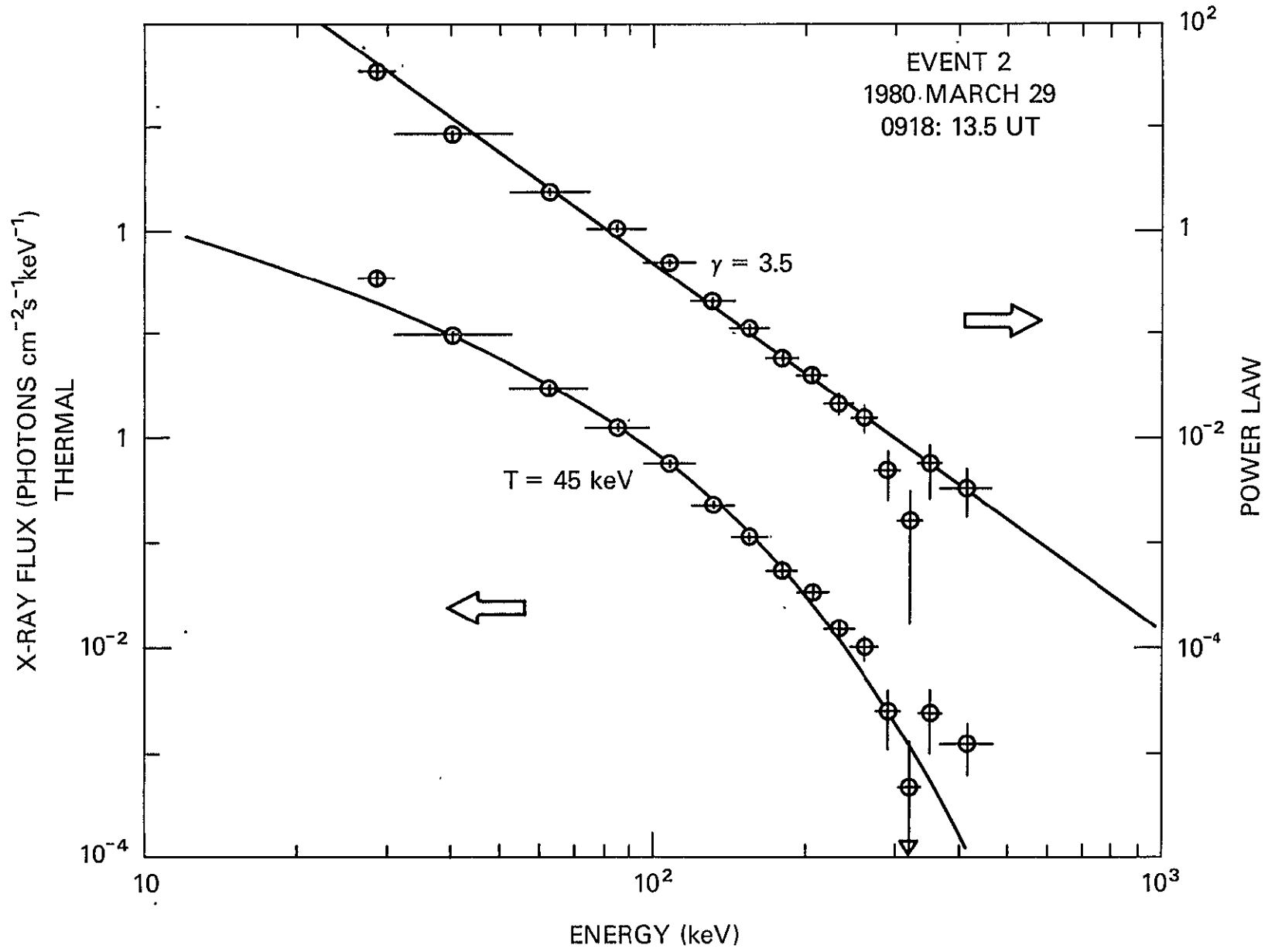


Figure 31 ORIGINAL PAGE IS OF POOR QUALITY

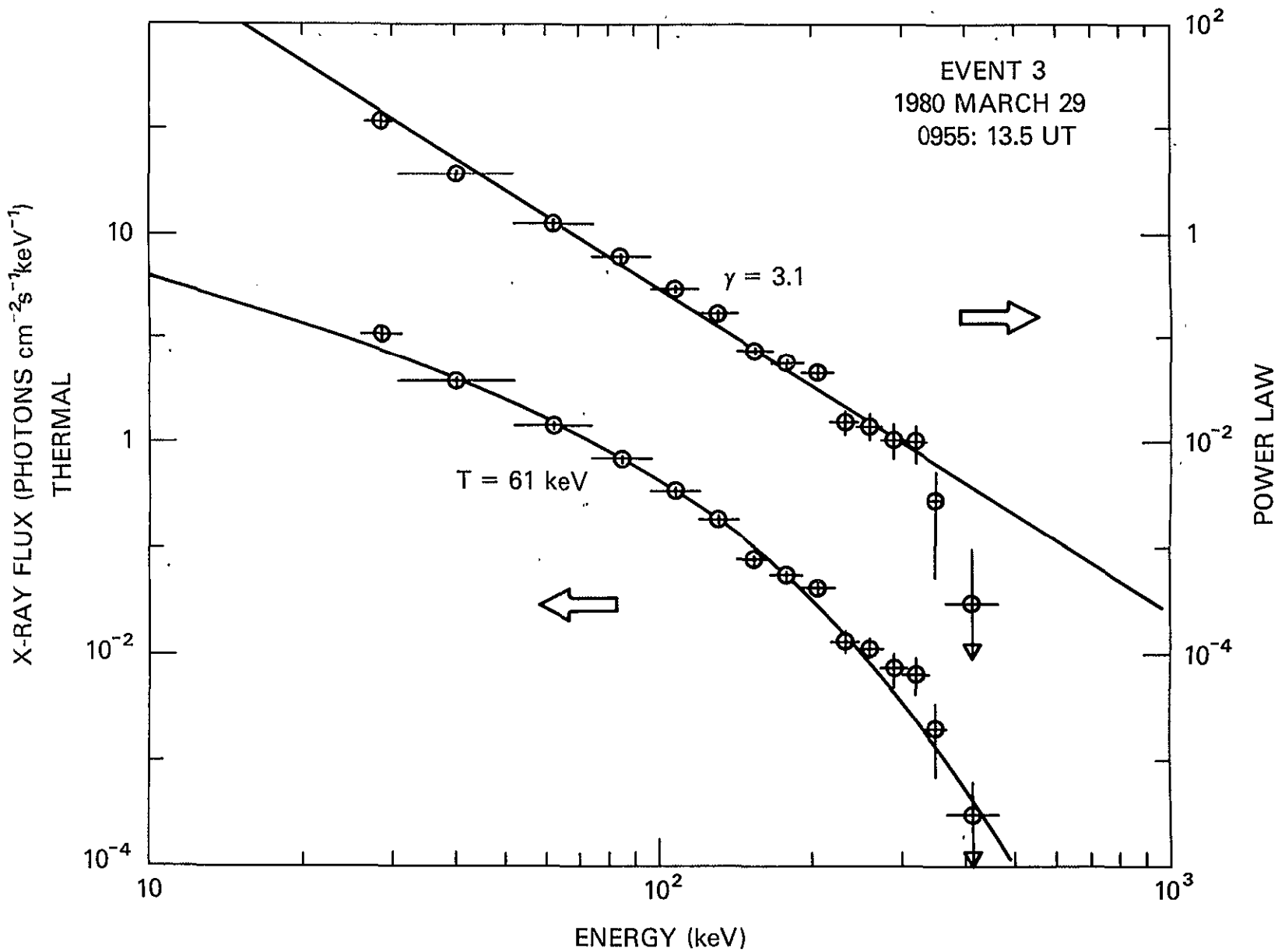
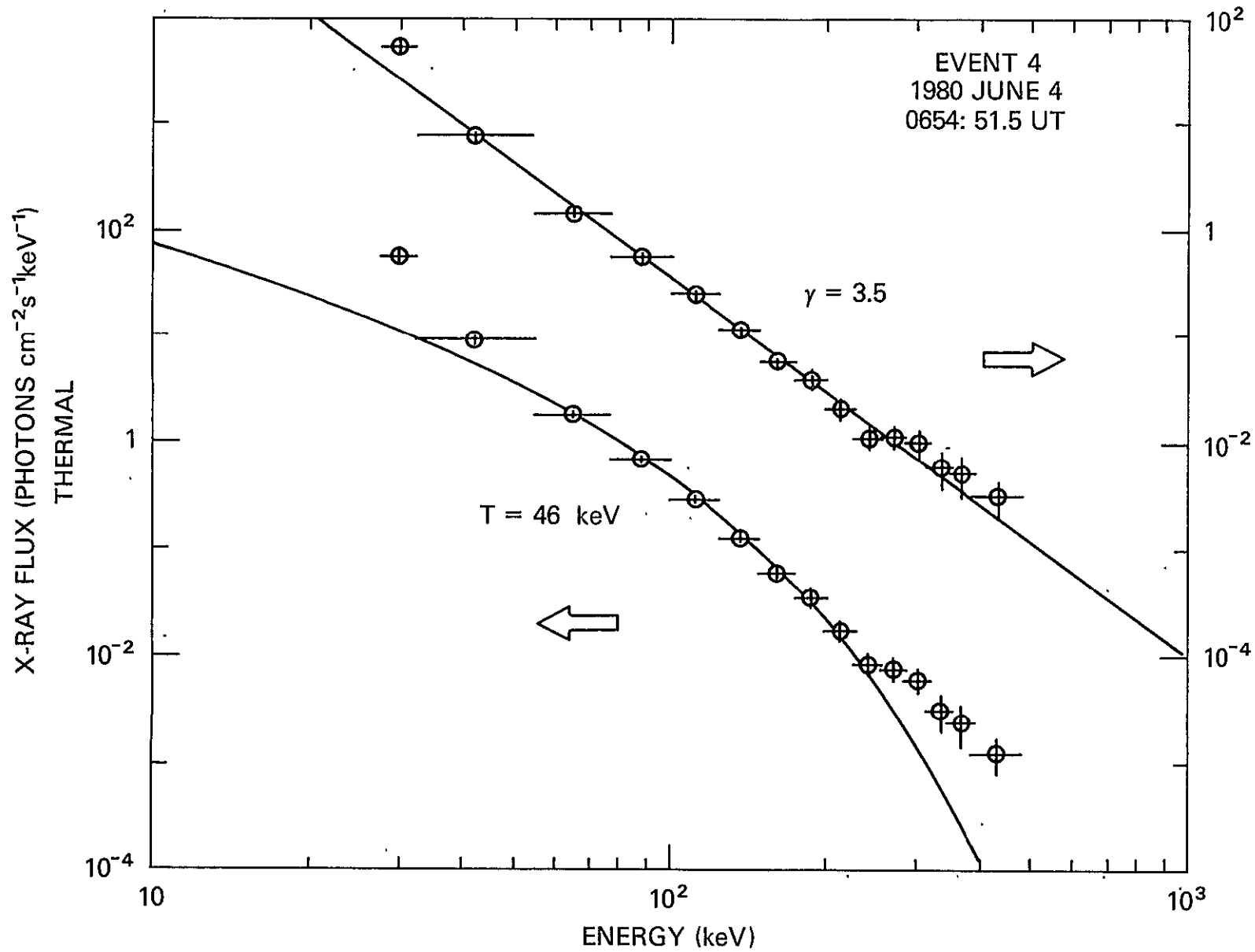


Figure 32

ORIGINAL PAGE IS
OF POOR QUALITY



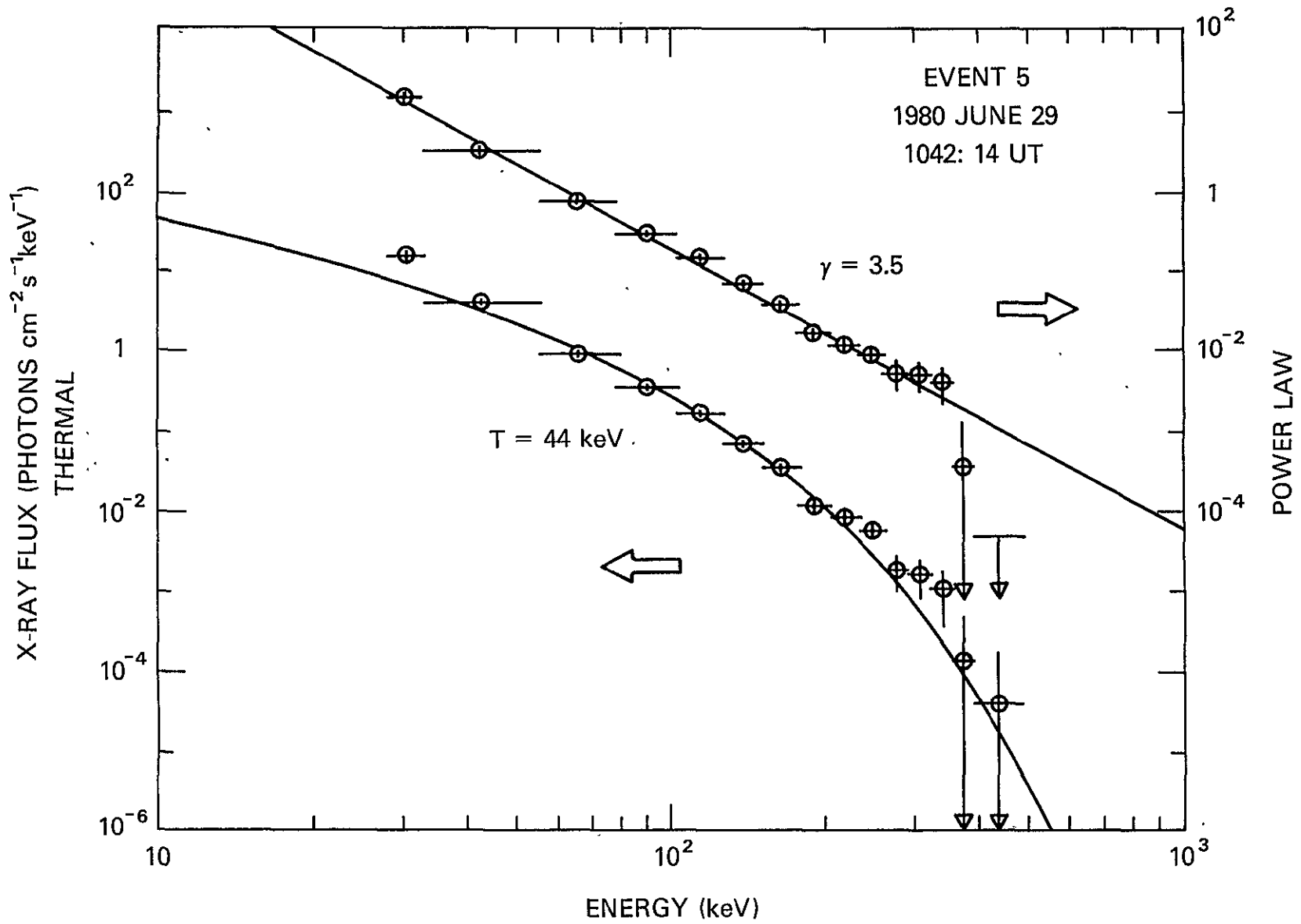


Figure 34

ORIGINAL PAGE IS
OF POOR QUALITY

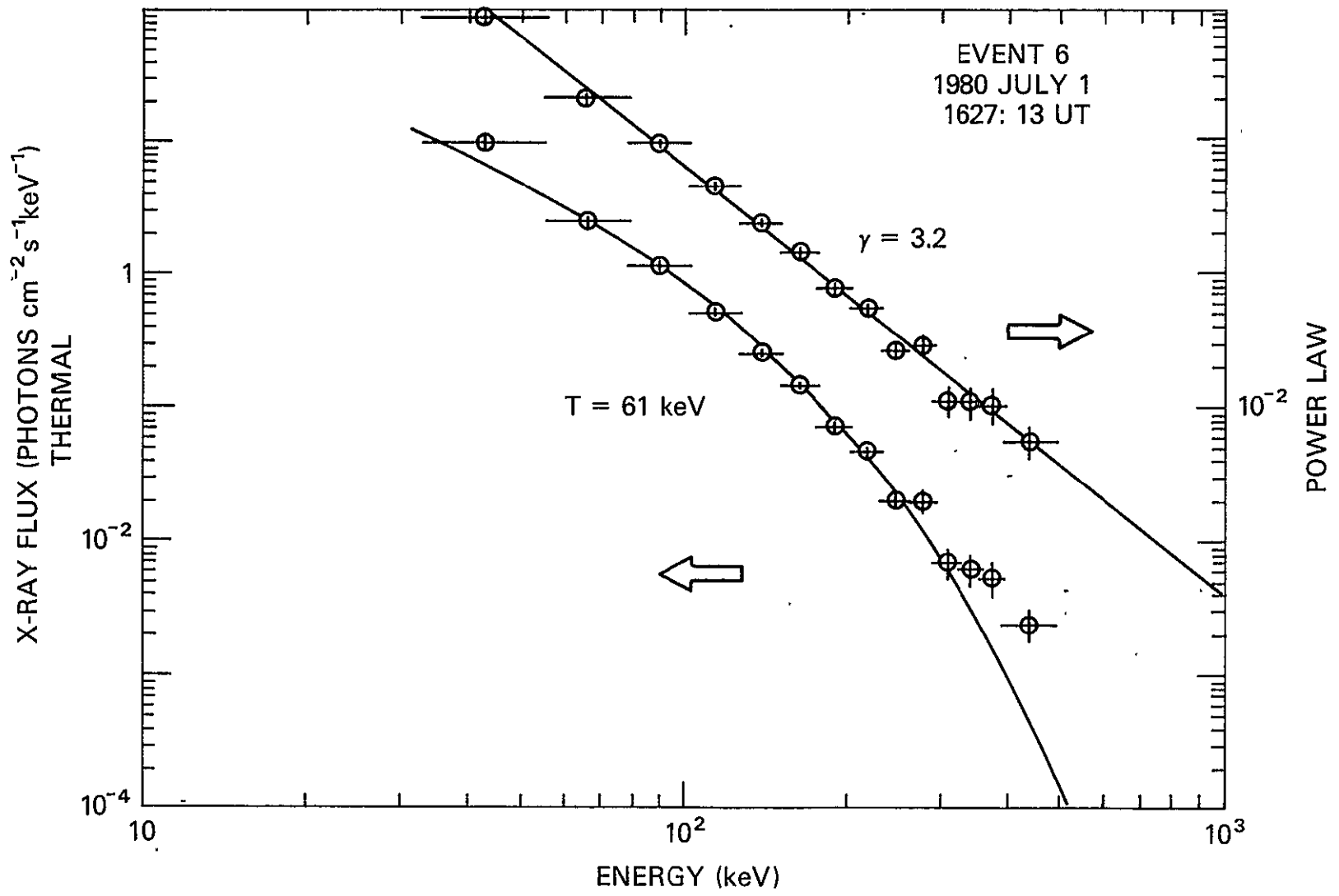


Figure 35

ORIGINAL PAGE IS
OF POOR QUALITY

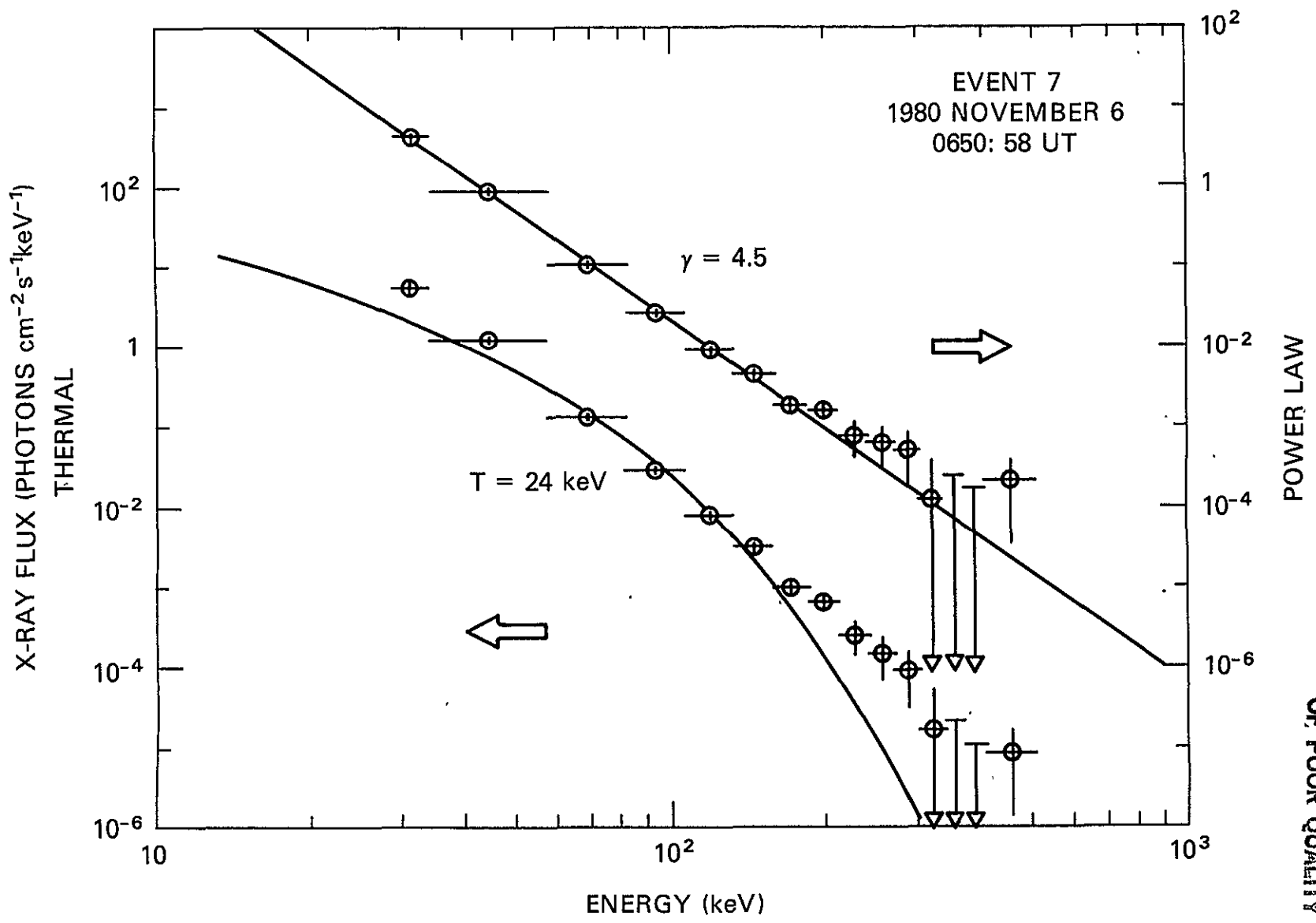


Figure 36

ORIGINAL PAGE IS
OF POOR QUALITY

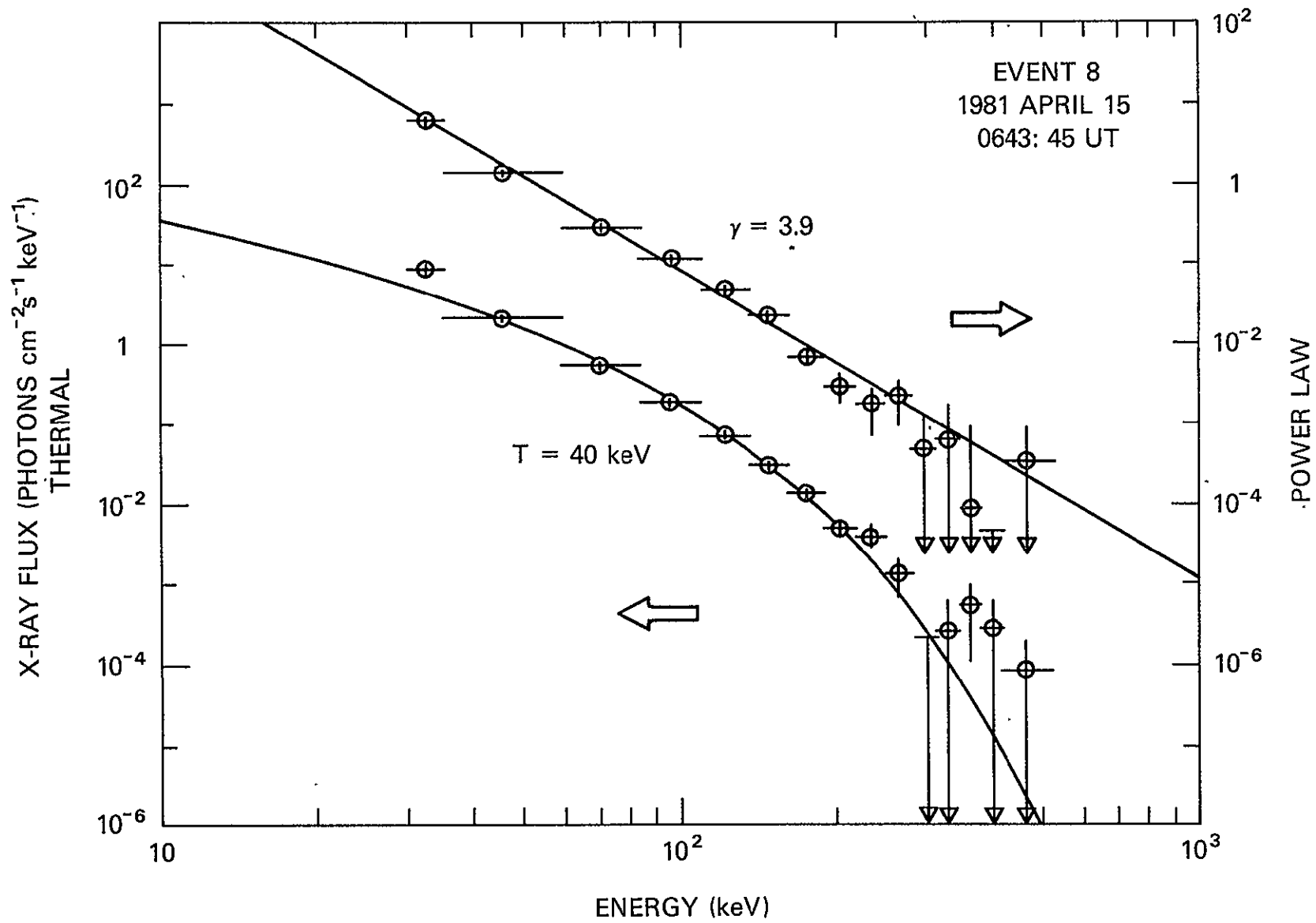


Figure 37

ORIGINAL PAGE IS
OF POOR QUALITY

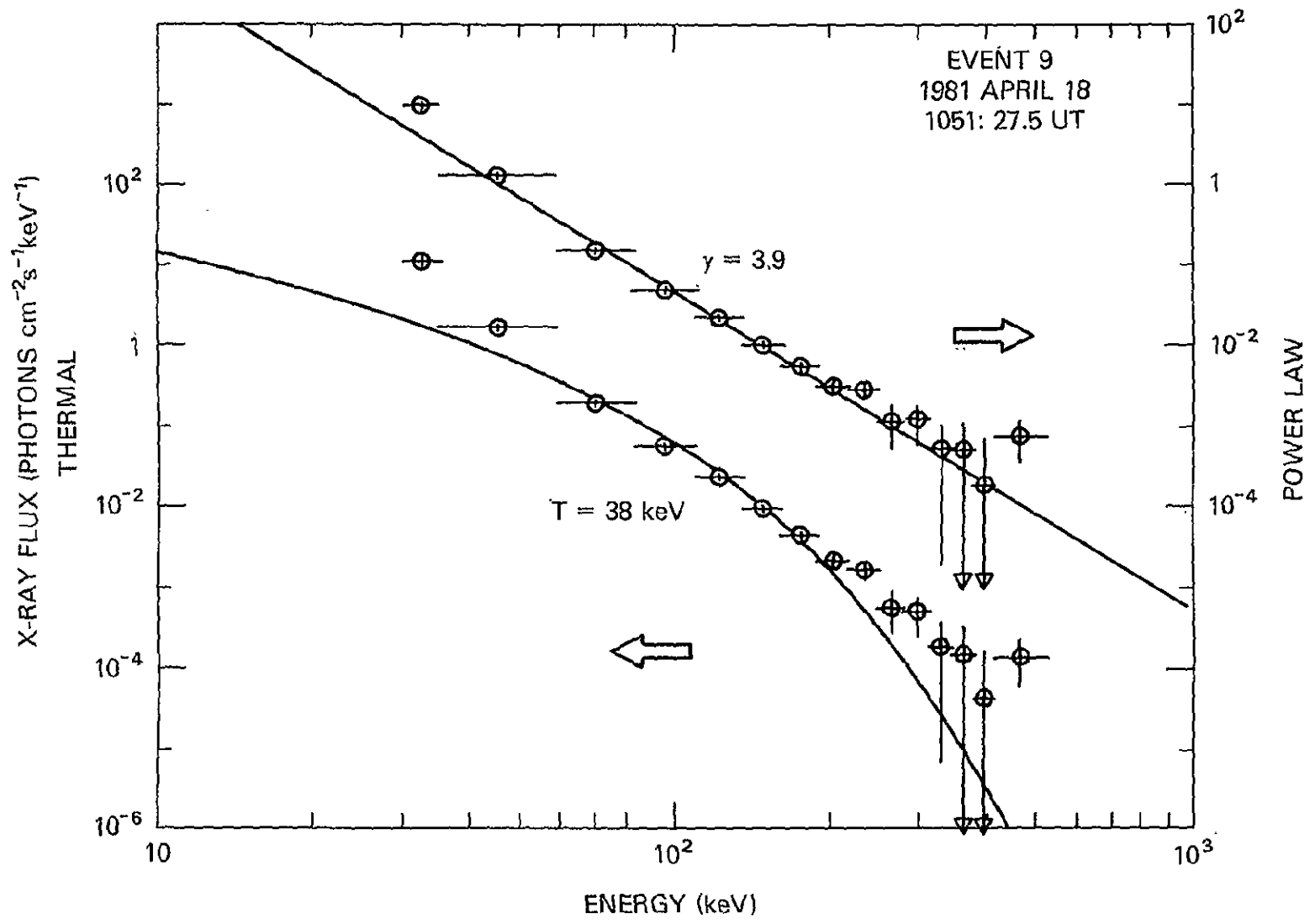


Figure 38

ORIGINAL PAGE IS
OF POOR QUALITY

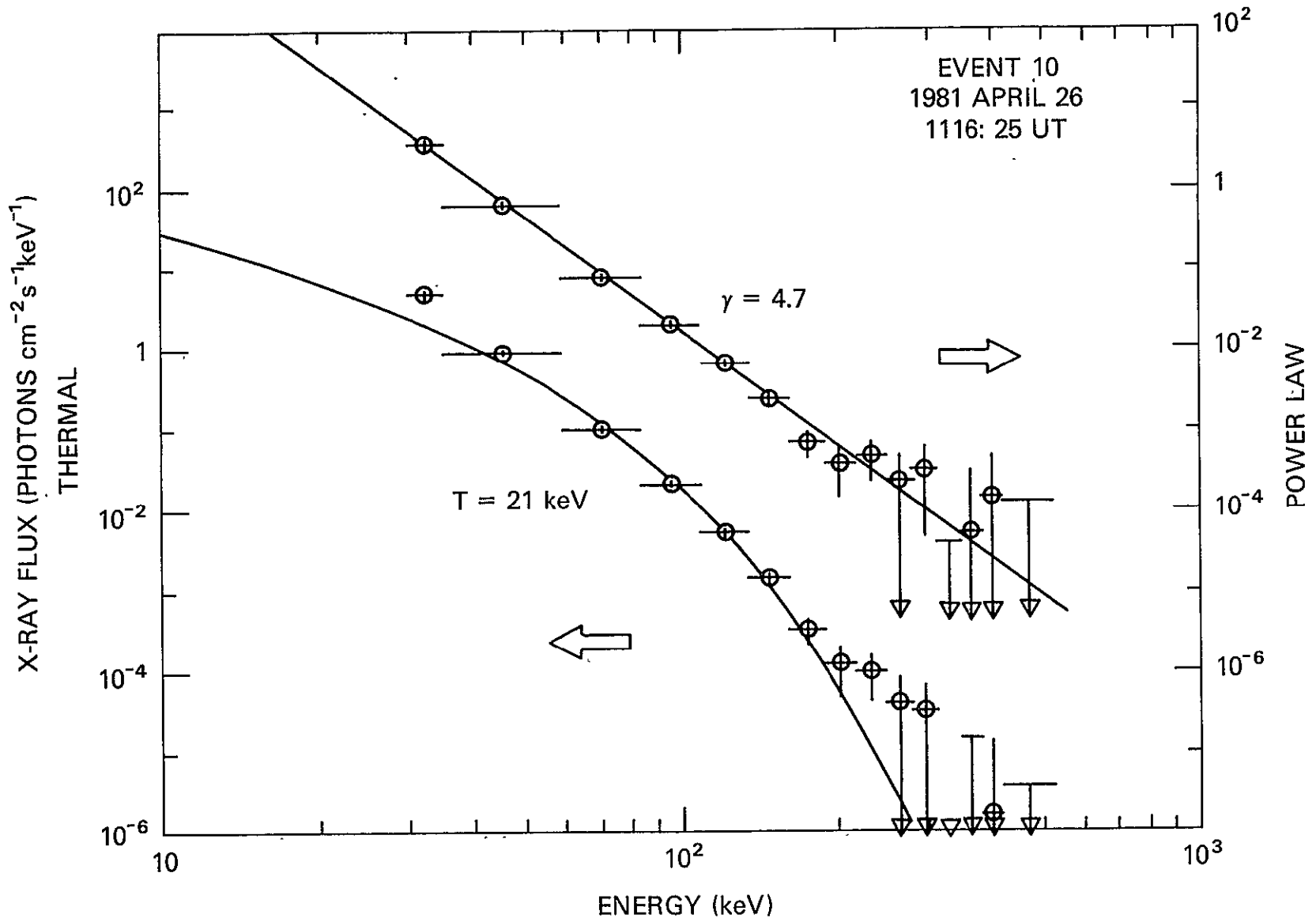


Figure 39
 ORIGINAL PAGE IS
 OF POOR QUALITY

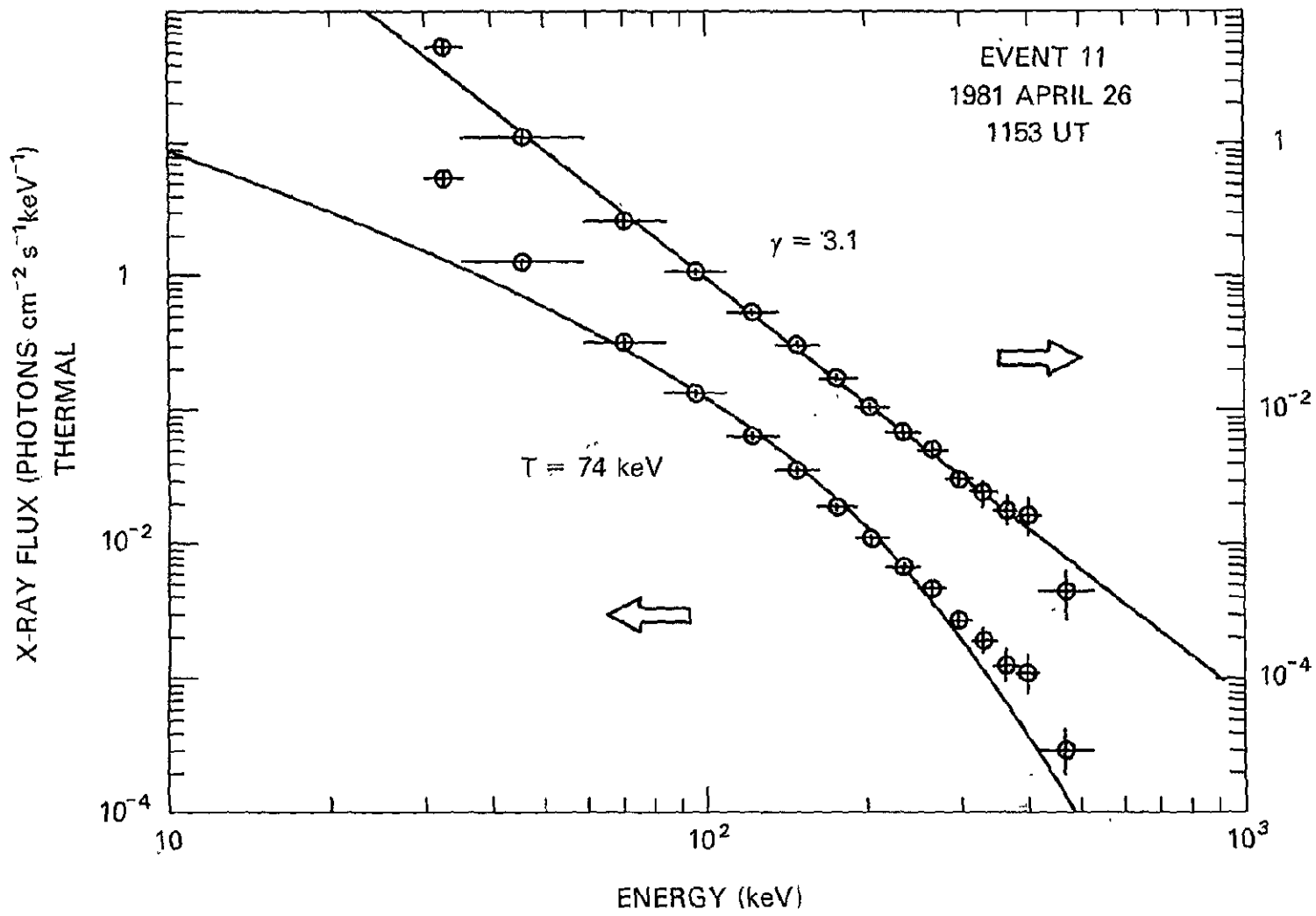


Figure 40
 ORIGINAL PAGE IS
 OF POOR QUALITY

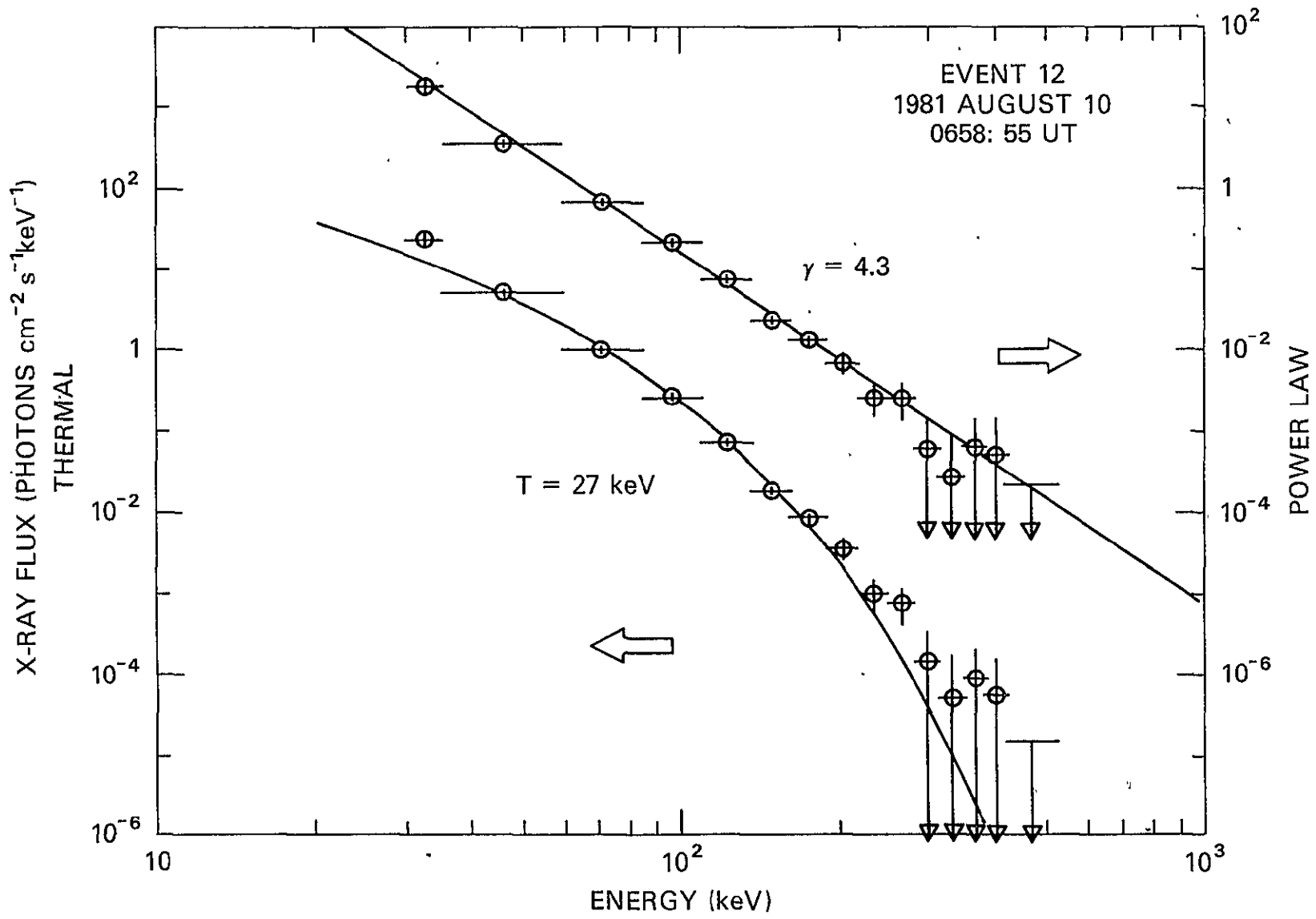


Figure 41

ORIGINAL PAGE IS
OF POOR QUALITY

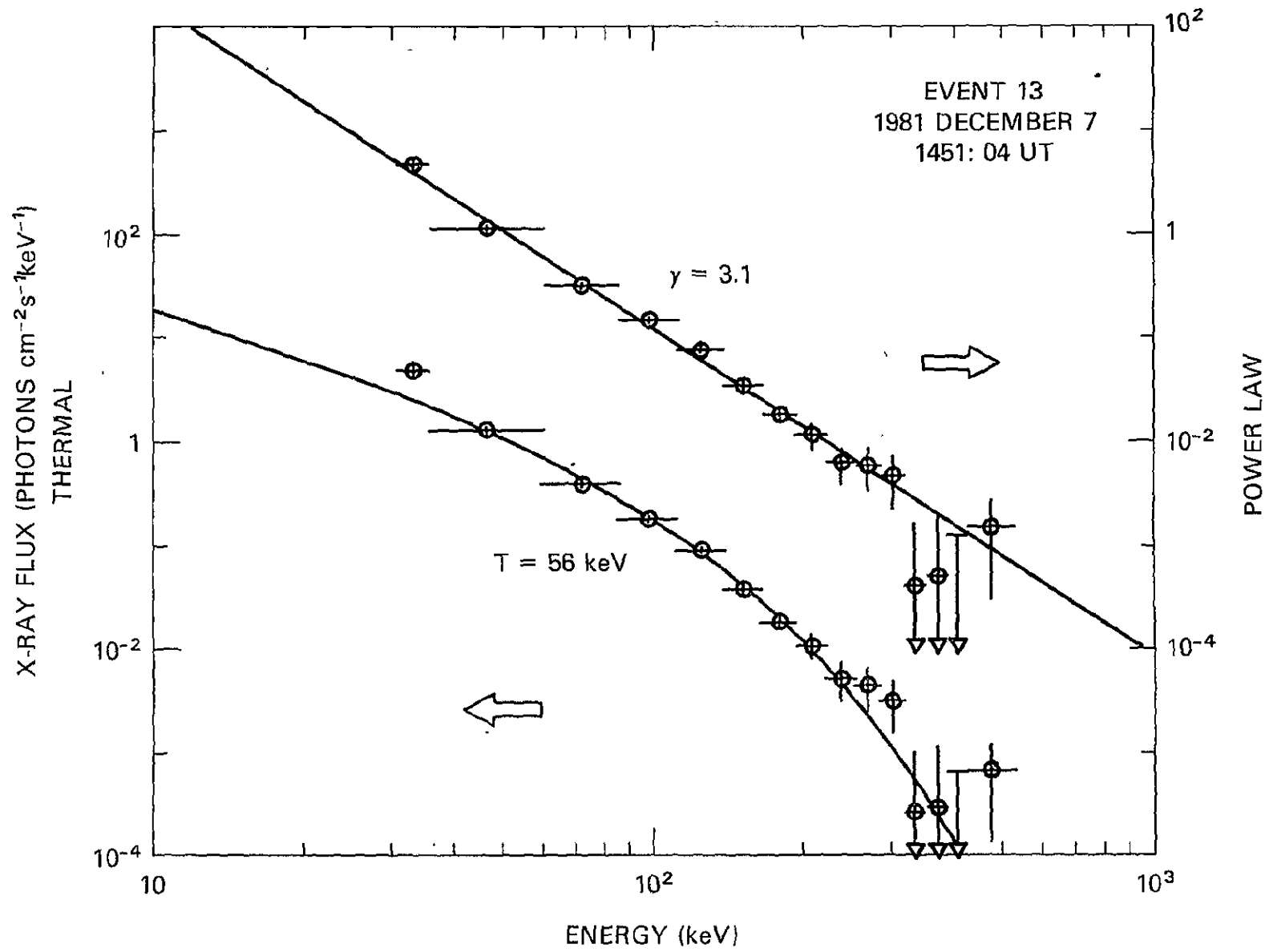


Figure 42 . ORIGINAL PAGE IS OF POOR QUALITY

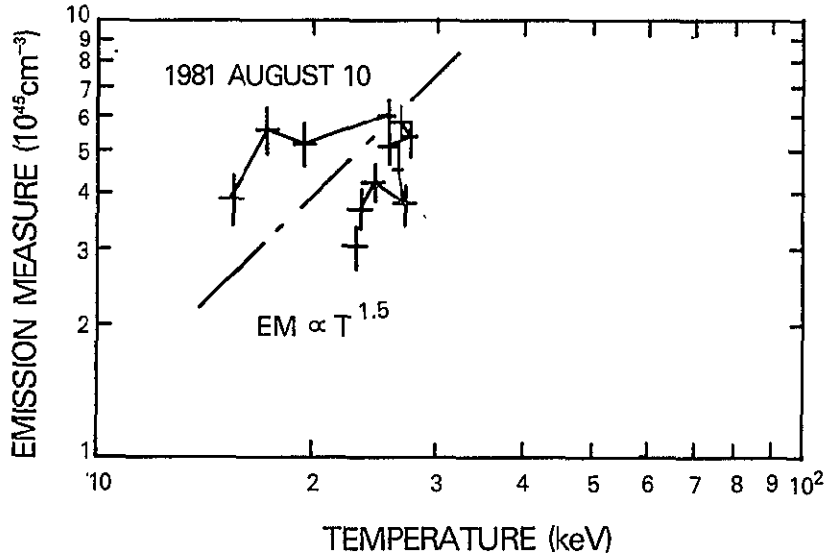
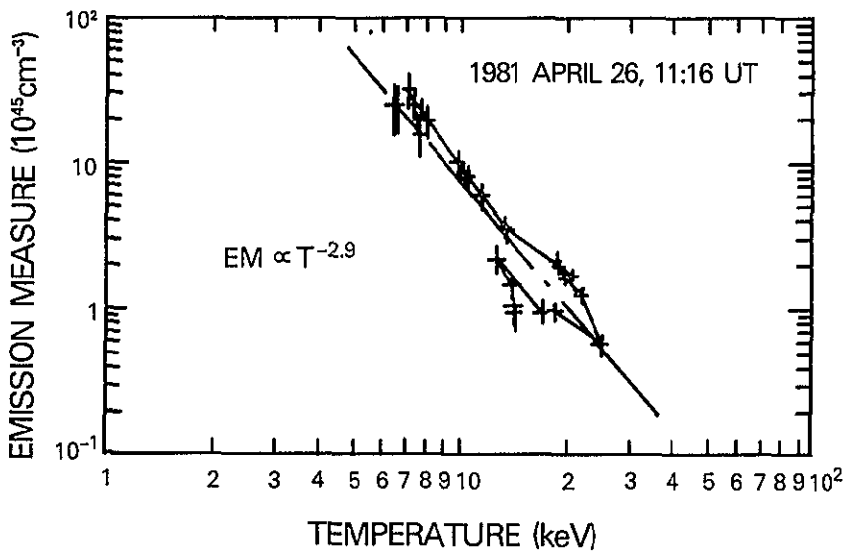
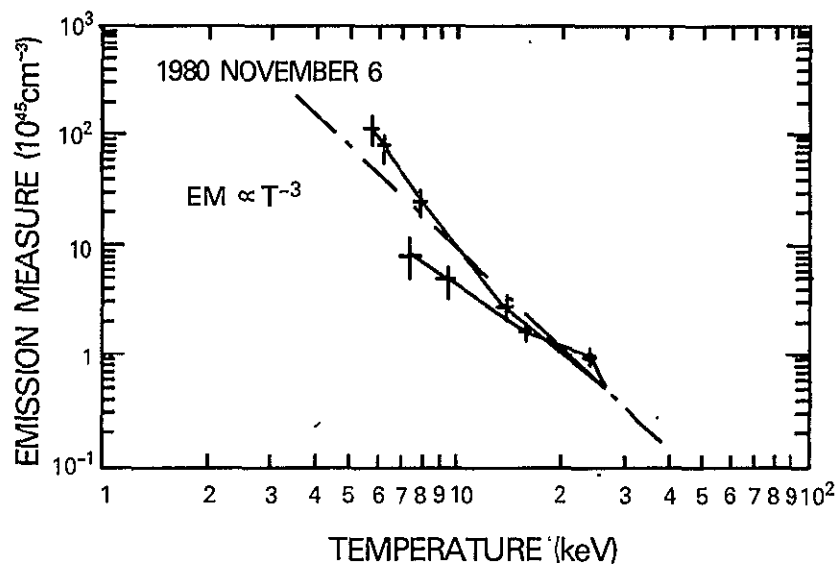
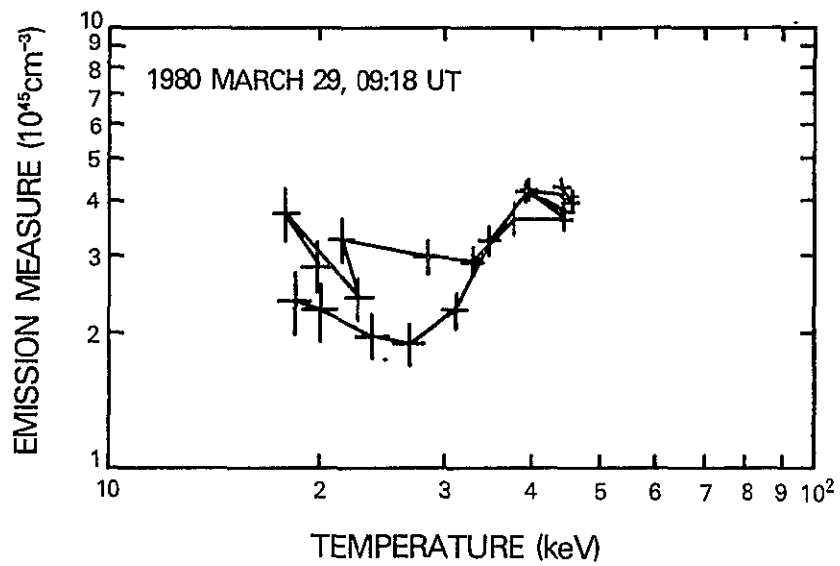


Figure 43

ORIGINAL PAGE IS
OF POOR QUALITY

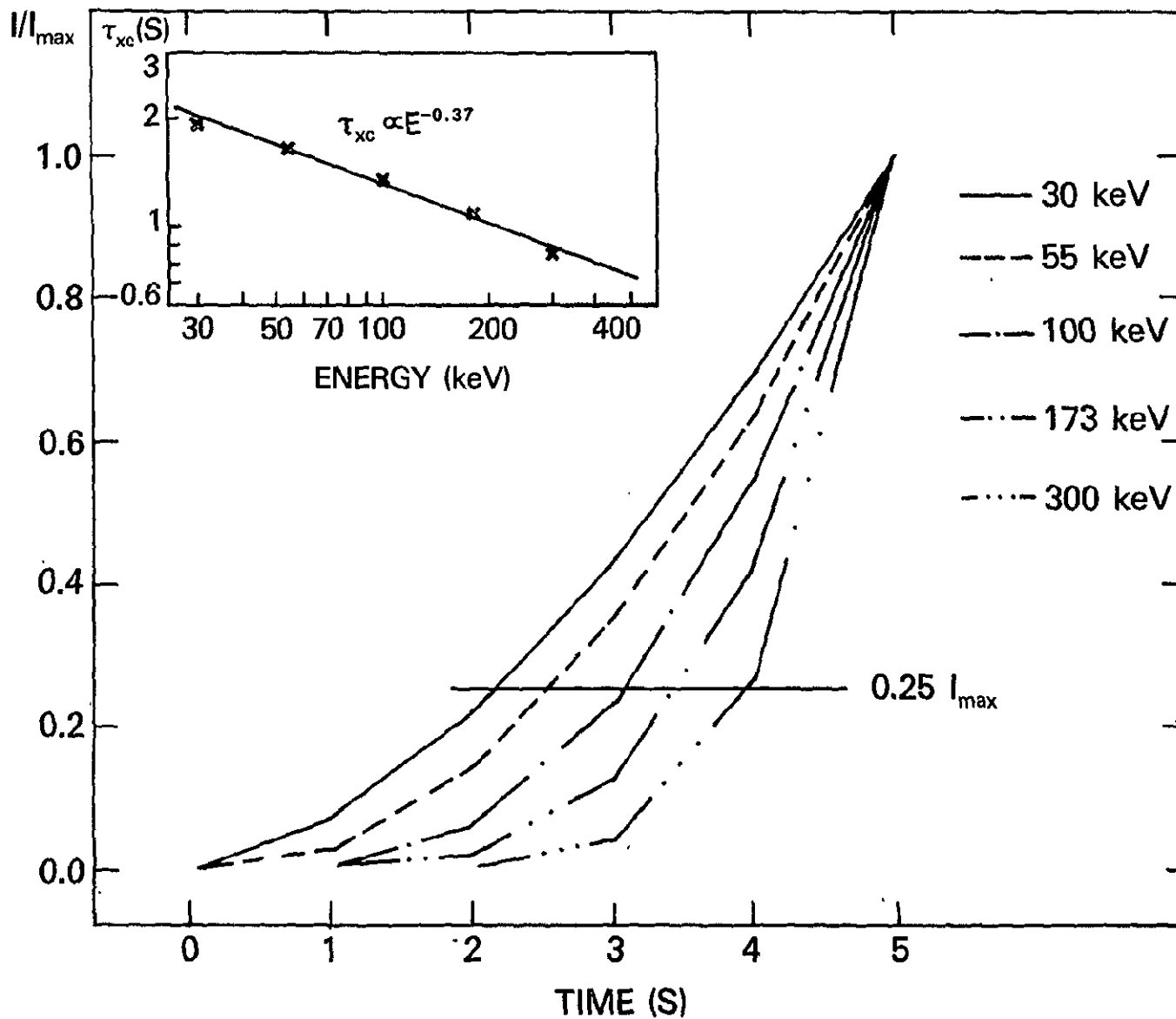


Figure 44

ORIGINAL PAGE IS
OF POOR QUALITY

BIBLIOGRAPHIC DATA SHEET

1. Report No. TM 85052	2. Government Accession No.	3. Recipient's Catalog No.	
4. Title and Subtitle Great Microwave Bursts and Hard X Rays from Solar Flares		5. Report Date June 1983	
		6. Performing Organization Code 684	
7. Author(s) H. J. Wiehl, D. A. Batchelor, C. J. Crannell, B. R. Dennis and Phillip N. Price		8. Performing Organization Report No.	
9. Performing Organization Name and Address NASA-Goddard Space Flight Center Greenbelt, Maryland 20771		10. Work Unit No.	
		11. Contract or Grant No.	
		13. Type of Report and Period Covered	
12. Sponsoring Agency Name and Address		14. Sponsoring Agency Code	
		15. Supplementary Notes	
16. Abstract The microwave and hard X-ray characteristics of 13 solar flares that produced microwave fluxes greater than 500 Solar Flux Units have been analyzed. These Great Microwave Bursts were observed in the frequency range from 3 to 35 GHz at <u>Berne</u> , and simultaneous hard X-ray observations were made in the energy range from 30 to 500 keV with the Hard X-Ray Burst Spectrometer on the <u>Solar Maximum Mission</u> spacecraft. The principal aim of this analysis is to determine whether or not the same distribution of energetic electrons can explain both emissions. Correlations were found between respective temporal characteristics and, for the first time, between microwave and hard X-ray spectral characteristics. A single-temperature and a multi-temperature model from the literature were tested for consistency with the coincident X-ray and microwave spectra at microwave burst maximum. Four events are inconsistent with both of the models tested, and neither of the models attempts to explain the high-frequency part of the microwave spectrum. We propose a model in which the emissions above and below the peak frequency originate in two different parts of a diverging magnetic loop. With this model we explain the entire microwave spectrum of all but 1 of the events.			
17. Key Words (Selected by Author(s)) Plasmas - Sun: Bursts - Sun: Microwaves - Sun: X-Rays		18. Distribution Statement <div style="border: 1px solid black; padding: 5px; width: fit-content; margin: 10px auto;">UNLIMITED</div>	
19. Security Classif. (of this report) <div style="border: 1px solid black; padding: 2px; width: fit-content; margin: 5px auto;">UNCLASSIFIED</div>	20. Security Classif. (of this page) <div style="border: 1px solid black; padding: 2px; width: fit-content; margin: 5px auto;">UNCLASSIFIED</div>	21. No. of Pages	22. Price*